

NASA CONTRACTOR REPORT

NASA CR-137474

# STUDY OF RADAR PULSE COMPRESSION

(NASA-CR-137474) STUDY OF RADAR PULSE COMPRESSION FOR HIGH RESOLUTION SATELLITE ALTIMETRY Final Report, Oct. 1972 - May 1973 (Technology Service Corp., Silver Spring, Md.) 176 p HC \$7.00 CSDL 171	N75-14013  Unclas. G3/32 06504
--	---

## FOR

## HIGH RESOLUTION

## SATELLITE ALTIMETRY

## FINAL REPORT

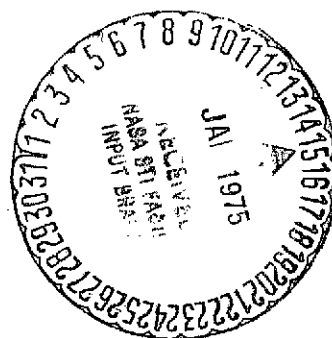
Report No. TSC-WO-111

Prepared Under Contract No. NAS6-2241 by

Technology Service Corporation

Washington Division

Silver Spring, Maryland 20910



Prepared for

NATIONAL AERONAUTICS AND SPACE ADMINISTRATION

WALLOPS FLIGHT CENTER

WALLOPS ISLAND, VIRGINIA 23337

December 1974



NATIONAL AERONAUTICS AND SPACE ADMINISTRATION  
Wallops Flight Center  
Wallops Island, Virginia 23337



REPLY TO  
ATTN OF: TL (A-13)

JAN 1 3 1975

NASA Scientific and Technical  
Information Facility  
Attn: Acquisitions Branch  
Post Office Box 33  
College Park, MD 20740

Subject: Document Release for NASA CR-137474

Document Release Authorization Form FF 427 and two (2) copies  
of the following report are forwarded:

NASA CR-137474 Study of Radar Pulse Compression for  
High Resolution Satellite Altimetry

We are forwarding, under separate cover, thirty (30) additional  
copies of NASA CR-137474 as requested by you for your use.

*James C. Floyd*

James C. Floyd  
Head, Administrative Management Branch

Enclosures

1. Report No. NASA CR-137474	2. Government Accession No.	3. Recipient's Catalog No.	
4. Title and Subtitle Study of Radar Pulse Compression for High Resolution Satellite Altimetry		5. Report Date December 1974	6. Performing Organization Code
		8. Performing Organization Report No. TSC-WO-111	
7. Author(s) R. P. Dooley, F. E. Nathanson, and L. W. Brooks		10. Work Unit No.	11. Contract or Grant No. Contract No. NAS6-2241
9. Performing Organization Name and Address Technology Service Corporation 8555 Sixteenth Street Silver Spring, MD 20910		13. Type of Report and Period Covered Contractor Report October 1972 to May 1973	
		14. Sponsoring Agency Code	
12. Sponsoring Agency Name and Address National Aeronautics and Space Administration Wallops Flight Center Directorate of Applied Science Wallops Island, VA 23337		15. Supplementary Notes  This is a final report	
16. Abstract  A study is made of pulse compression techniques applicable to a satellite altimeter having a topographic resolution of + 10 cm. A systematic design procedure is used to determine the system parameters. The performance of an optimum, maximum likelihood, processor is analysed in a supporting study and provides the basis for modifying the standard split-gate tracker to achieve improved performance. Bandwidth considerations lead to the recommendation of a full deramp STRETCH pulse compression technique followed by an analog filter bank to separate range returns. The implementation of the recommended technique is examined in detail.			
17. Key Words (Suggested by Author(s)) Radar Radar Altimetry High Resolution Pulse Compression STRETCH Split-Gate Tracker		18. Distribution Statement  Unclassified - Unlimited  Cat. 43	
19. Security Classif. (of this report) Unclassified	20. Security Classif. (of this page) Unclassified	21. No. of Pages 176	22. Price*

## FOREWORD

This report contains the results of the Study of Radar Pulse Compression for High Resolution Satellite Altimetry awarded Technology Service Corporation under Contract No. NAS6-2241 by the National Aeronautics and Space Administration Wallops Station, Wallops Island, Virginia. The study was conducted by Technology Service Corporation under the direction of Mr. Fred Nathanson as Program Manager with Dr. Richard P. Dooley as Assistant Program Manager.

Successful implementation of this effort was due primarily to Mr. William Townsend, NASA/Wallops Program Manager, who provided considerable guidance and direction during the course of this program.

A major contributor to this study was Dr. Lowell Brooks, Senior Scientist of Washington Operations, who performed the analysis of improved range tracking algorithms. The concept of a maximum likelihood processor, which has a significant impact on the results of this study, was originally suggested by Dr. Peter Swerling, President, Technology Service Corporation. Other researchers who contributed to this effort included Mr. James Bucknam who performed much of the system design calculations and analysis, Dr. Peter Tong who performed the study of binary phase code with digital processing, Dr. Glen Gray for the analysis of the linear FM generation requirements, Mr. Alexander Mac Mullen who developed the system implementation, and Dr. August Rihaczek who acted in an advisory and review capacity during the course of this program.

## ABSTRACT

A study is made of pulse compression techniques applicable to a satellite altimeter having a topographic resolution of  $\pm 10$  cm. A systematic design procedure is used to determine the system parameters. The performance of an optimum, maximum likelihood, processor is analysed in a supporting study and provides the basis for modifying the standard split-gate tracker to achieve improved performance. Bandwidth considerations lead to the recommendation of a full deramp STRETCH pulse compression technique followed by an analog filter bank to separate range returns. The implementation of the recommended technique is examined in detail.

TABLE OF CONTENTS

	<u>Page</u>
<b>PART I SYSTEM DESIGN</b>	
1.0 INTRODUCTION AND SUMMARY . . . . .	1
2.0 SYSTEM PARAMETERS . . . . .	6
2.1 Systematic Design Procedure . . . . .	7
2.2 Parameter Calculations . . . . .	20
3.0 SELECTION OF PULSE COMPRESSION TECHNIQUE . . . . .	40
3.1 Summary of Candidates . . . . .	40
3.2 Binary Phase Coding . . . . .	42
3.3 Linear FM Techniques . . . . .	47
3.4 Hybrid Pulse Compression Techniques . . . . .	60
3.5 Stretch-ALCOR Techniques . . . . .	64
4.0 IMPLEMENTATION . . . . .	73
4.1 Recommended Approach for FM Generation . . . . .	73
4.2 Range Processing . . . . .	74
4.3 Ramp/De-Ramp Generation Requirements . . . . .	77
<b>PART II SUPPORTING STUDIES</b>	
1.0 INTRODUCTION AND SUMMARY . . . . .	86
2.0 IMPROVED ALTITUDE TRACKING ALGORITHMS . . . . .	88
2.1 Introduction and Summary . . . . .	88
2.2 Optimum Processing . . . . .	90
2.3 Split-Gate Trackers . . . . .	112
2.4 Comparison of Tracker Performances . . . . .	131
3.0 BINARY PHASE CODE WITH DIGITAL PROCESSING . . . . .	135
3.1 Summary . . . . .	135

TABLE OF CONTENTS (CONT'D)

	<u>Page</u>
3.2 Problem Description . . . . .	135
3.3 Basic Assumptions . . . . .	137
3.4 Digital Compressor Output Power . . . . .	141
3.5 Hardlimiting Digital Processor . . . . .	147
3.6 Multibit Digital Processor . . . . .	155
3.7 Beam Limited Case . . . . .	158
3.8 Conclusion . . . . .	159
4.0 COMPARISON OF SEA SURFACE CROSS SECTION MEASUREMENTS AT NORMAL INCIDENCE WITH BARRICK'S MODEL . . . . .	161
4.1 Effect on Tracker Performance . . . . .	169
5.0 AIRCRAFT SYSTEM PARAMETERS . . . . .	172
5.1 Beam Width and Tracker Gate Widths . . . . .	173
5.2 Compressed Pulse Length . . . . .	175
5.3 PRF . . . . .	176
5.4 Pulse Averaged by Loop Filter . . . . .	176
5.5 Peak Transmitter Power . . . . .	176

PART I  
SYSTEM DESIGN

1.0      INTRODUCTION AND SUMMARY

The design of a high resolution satellite altimeter is described in this part of the report. The resulting design achieves all specified performance requirements. These performance requirements are given in Table 1.1 and the system design is summarized in Table 1.2.

Section 2 describes a systematic design procedure for determining the system parameters. This procedure clearly identifies the tradeoffs among alternate designs and as such, provides a basis for the selection of a design which can be achieved in the most efficient and economical manner. The dependencies between the various system parameters and performance requirements are examined in detail. It is shown that the results of the improved altitude tracking algorithms investigation, Part II, have a significant impact on the selection of the nominal system parameters. The form of the optimum (maximum likelihood estimate) processor led to modifications of the simple split-gate tracker which enable the performance requirement of 10 cm resolution at 10 meter wave height to be achieved with onboard processing.

Section 3 examines the types of pulse compression considered for the satellite altimetry experiment. Utilizing the set of required system parameters, the feasibility of each technique is examined in detail. Bandwidth considerations led to the selection of a full deramp STRETCH followed by an analog filter bank to separate range returns as the recommended technique. The state-of-the-art in the generation of linear FM signals, an essential part of the selected STRETCH technique, is examined in detail.



Recommendations concerning the implementation of the selected pulse compression technique are given in Section 4. While the reflective array compressor (RAC) is the preferred method for the generation of the 360 MHz 2.8  $\mu$ sec linear FM signal, procurement would be required from MIT Lincoln Lab since there are presently no established vendors of the RAC line, and if obtained from industry this approach would involve some development risk. Instead, a configuration using a lower bandwidth (60 MHz) delay line followed by frequency multiplication (x6) is recommended for the "baseline design". While TSC would prefer to see the implementation using RAC, perpendicular diffraction grating delay line (PPDL), and conventional surface waves in that order, all approaches are capable of meeting the easier specification of the "baseline design". An analysis of the accuracy with which the ramp and deramp linear FM signals must be generated provides a linearity requirement of 0.2% and peak allowable frequency deviations of < 25 KHz (for one cycle of variation across the pulse). The implementation of the analog filter band for range processing is examined in detail.

Table 1.1 SYSTEM PERFORMANCE REQUIREMENTS

I.	Geodetic Accuracy	50 cm
II.	Topographic Resolution	10 cm rms (7 cm allocated to system error)
III.	Wave Height Range:	1-10 m crest-to-trough
	Accuracy:	25%
IV.	Correlation between pulses	< 1/e
V.	Oceanographic phenomena of interest (maximum spatial frequency)	.25 Hz

Table 1.2 DESIGN SUMMARY

I. Orbit Parameters

a)	Height	556 km
b)	Inclination	90° retrograde
c)	Eccentricity	.0064 maximum

II. Radar Parameters:

a)	Antenna Beamwidth	3° (24 inch dish)
b)	Pointing Accuracy	$\sigma_{\theta} = 1/2^{\circ}$
c)	Antenna Gain	Peak
		Average
		34.9 dB
		34.25 dB
d)	Peak Power	2 KW
e)	System Losses (other than processing losses in pulse compressor)	5 dB
f)	Noise Figure	5.5 dB
g)	Frequency	13.9 GHz
h)	Uncompressed Pulse Width	2.8 $\mu$ sec
i)	Pulse Bandwidth	360 MHz
j)	Compressed Pulse Width	3.0 nsec
k)	Compression ratio	1000:1
l)	PRF <sub>max</sub> (Uncorrelated returns)	1.8 KHz
m)	PRF	$\geq 1.4$ KHz
n)	S/N (Single Pulse)	10 dB
o)	Ocean Backscatter Coefficient ( $\sigma_0$ )	+6 dB

Table 1.2 DESIGN SUMMARY (Continued)

p) * Receiver Weighting	-26 dB Modified Taylor
q) * Pulse compression processing loss	.55 dB
r) * Main lobe broadening due to tapering	23%

---

\* Included in the design but considered optional.

III. Tracker Configuration

Type	Modified Split-Gate
Tracks	Quarter power point of leading edge
Early Gate Width	3.0 nsec
Late Gate Width	48 nsec
Gate Separation	$\geq 70$ nsec
Bandwidth	1.0 Hz

IV. Pulse Compression

Type	Full Deramp STRETCH
Range Processing	Analog Filter Bank
Filter Bank	Discrete Passive
Number of Filters	30
Frequency Range	9.2 to 20.8 MHz
Filter Bandwidth	385 KHz (3 nsec resolution)
Output Data Form	Two TTL parallel words A. Range Bin Number, 5-bits B. Range Bin Amplitude, 6-bits
Time required for full sampling	450 microseconds, max.
A/D Sampling Frequency	< 1 MHz

Table 1.2 DESIGN SUMMARY (Continued)

V. Linear FM Generation

** Type	Surface Wave
Bandwidth	.60 MHz
Multiplier Chain	X6
Pulse Length	2.8 $\mu$ sec
Linearity of FM	$\leq 0.2\%$
Peak Frequency Deviation (one cycle of variation across pulse)	< 25 KHz

---

\*\* One device used for both transmit and receive.

VI. Wave Height and Return Shape Processing

Type	Averaged Samples of Power Return
Averaging Time	.1 sec
Number of Samples	30
Sample Interval	3.0 nsec

In this section, a nominal set of system parameters are determined for achieving the performance requirements of the satellite altimeter. The approach to this task is a systematic design procedure which clearly identifies the tradeoffs among alternate designs and as such, provides a basis for the selection of a design which can be achieved in the most efficient and economical manner. Obviously, the systematic design procedure was not employed until the final stage of the selection process. In fact, a major portion of the effort involved a detailed examination of the dependencies between the various system parameters and performance requirements.

These studies produced two results which have a significant impact on the selection of the nominal system parameters.

First, the effect of wave height on system resolution (RMS tracking error) has been determined. Previous expressions for RMS tracking error have assumed a smooth sea surface. It was found that, for a given resolution and signal-to-noise ratio, going from the smooth sea case (say 1 meter wave height) to a 10 meter wave height resulted in a factor of 100 increase in required PRF. This result is quite significant since the performance requirement of 10 cm resolution at 10 meter wave height requires considerable improvement in tracker performance compared to that originally envisioned for the smooth sea case.

Second, a study of improved range tracking algorithms has shown that the performance of a split-gate tracker could be improved considerably by widening the width of the late gate and having the early gate positioned well below the half power point of the return signal. These modifications to the simple split-gate tracker were indicated after a detailed examination of the form of

the optimum (maximum likelihood estimate) processor. Without this result, the performance requirement of 10 cm resolution at 10 meter wave height could not be achieved with onboard processing. The recommended tracker is a "modified split-gate" that tracks the  $\frac{1}{2}$  power point of the return signal. The width of the early gate is  $\tau$  and that of the late gate is  $16\tau$ , where  $\tau$  is the compressed pulse width.

The selected set of system parameters were presented in Table 1.2 of Section 1.0. The remaining portions of this section provide the rationale for the selection of these parameters. Section 2.1 describes the utilization of the systematic design procedure while the detailed calculations are presented in Section 2.2.

## 2.1 Systematic Design Procedure

In Section 2.2, the dependencies between the various system parameters and performance requirements are described in detail. These efforts are necessary prerequisites for obtaining a system design, but there remains a need for systematically organizing the design procedure to clearly reveal whether or not a particular design has been achieved in the most efficient and economical manner.

In the following, it is shown that the design need not be based on trial and error methods, but can be accomplished with a systematic procedure. The guideline for such a design is to attain the given performance specifications while minimizing equipment complexity. This is, of course, what every designer is attempting to do. The objective here is to provide a method by which this can be done systematically, to yield a design where the selection of every parameter value is justifiable. Moreover, in the process, an under-

standing is obtained of the cost of improving the performance should the specifications be changed, and of the cost of achieving some critical performance parameter.

As described above, the process of system design can be viewed as a multivariate, constrained minimization problem. The problem is multivariate since, in general, several system parameters must be determined by the design procedure, e.g. pulse length, compression ratio, tracker bandwidth, etc. The constraints of the problem are provided by the system performance specifications (e.g. tracking accuracy, resolution, etc). Finally, the quantity to be minimized is the equipment complexity. That is, the best choice of system parameters is the set of parameters which, first, meet all the design goals, and second, can be implemented more simply than any other set of parameters which meet the specifications.

There are at least two basic problems in rigorously solving the above minimization problem. The first is that of quantifying system complexity. This is an extremely difficult task, and it is felt that without a major effort any quantification formula would be, at best, highly controversial and, at worst, useless. Therefore, the judgement as to the system complexity implied by a set of parameters must be left to a competent engineer. The resulting design procedure cannot then be mathematically rigorous (possibly to its advantage).

The second basic problem, and the one which is addressed by the systematic design procedure is that of determining all combinations of system parameters which will satisfy the performance requirements. It is felt that if these "feasible" system solutions are presented in an orderly manner, then the final judgement as to which is simplest can be made fairly easily.

The design process can be summarized in 5 steps.

- 1) Define precisely which parameters are to be determined.

- 2) Define those input and system parameters which have previously been determined from other considerations.
- 3) Determine the various dependencies between the system parameters, the parameters, and the system specifications. Make a precedence table to indicate these dependencies.
- 4) Use a procedure developed by Steward [1], to reorder the precedence matrix and to develop a flow chart which shows the order in which the parameters are to be determined. This yields a systematic procedure for exhaustively examining all feasible sets of system parameters.
- 5) From the flow chart developed in 4), compute and present tables of feasible solutions, and then select the set of parameters which gives minimum complexity.

#### 2.1.1 Application to altimeter design

Step 1. As defined in the work statement [2], and from basic considerations, the parameters which must be determined to define the altimeter are given in Table 2.1.1.



TABLE 2.1.1. Altimeter System Parameters to be Determined

Min	Max	Parameter	Symbol
	✓	Spatial frequency	SF
✓		Number of pulses integrated	N
✓		Signal-to-noise ratio	S/N
	✓	Compressed pulse length	$\tau$
✓		Compression ratio	CR
✓		Tracker bandwidth	$B_T$
✓	✓	Pulse rep. freq.	PRF

In general, all of the parameters would have a range of values which lead to feasible system solutions. However, in many cases only one end of the range will have any impact on the system design. For example, consider the compressed pulse length. Although in principle, there may be a minimum pulse length which will meet the system specifications, this will have little impact on the design. That is, the complexity of the pulse compression system increases rapidly with system bandwidth. Thus the designer will always want to minimize the system bandwidth, or equivalently, use the longest compressed pulse he can. Thus he is only interested in the maximum pulse length which will still meet the system specifications.

By similar arguments, it can be shown that only the maximum spatial frequency and the minimum-number of pulses integrated, signal-to-noise ratio, compression ratio, and tracker bandwidth are of concern from a design standpoint.

In the case of PRF, the minimum PRF is of concern from a system complexity standpoint, however, since the return for a very high PRF becomes correlated, there is an upper limit on the PRF which must be considered.

Step 2. Table 2.1.2 outlines the performance specifications, and system parameters which have been previously determined from other considerations.

Step 3. Table 2.1.3 shows the precedence matrix of interrelations between parameters. This matrix was obtained from the various dependencies outlined in Section 2.2. The dependencies between the parameters can be seen by reading down columns of the matrix, and "X" indicates a dependency. For example, the maximum spatial frequency to be tracked can be computed from tables of the oceanographic phenomena of interest (OPI) and the satellite orbit parameters (OP).

Similarly the minimum compression ratio required (CR) can be found once the input radar parameters (R) and the sea surface crosssection ( $\tau^0$ ) are given, and after the minimum signal-to-noise ratio has been determined.

Step 4. The reordered PTBD precedence matrix using Steward's algorithm is given as Table 2.1.4. The purpose of Steward's algorithm is to put the matrix into block upper triangular form. By reordering the matrix so that the "X's" fall above the diagonal, it becomes immediately apparent which parameters must be determined first. One can then develop a flow chart as in Fig. 2.1.1, which allows a systematic development of all feasible sets of parameters which satisfy the performance constraints.

For example, the max spatial frequency depends only on the input parameters OPI and OP (Table 2.1.3) and not on any other system parameters. Thus it is determined first. From SF and the wave height, the maximum pulse length and the bandwidth of the tracker are determined. Third, from  $\tau$  the  $PRF_{\max}$  is determined.

TABLE 2.1.2 Input Parameters, and Systems Parameters Which Have Been Previously Determined.

A. Requirements from Specification		<u>Symbol</u>	<u>Value</u>
I	Geodetic Accuracy	GA	50 cm
II	Topographic Resolution	TR	10 cm rms (7 cm allocated to system error)
III	Wave Height Range:	WH	1-10 m crest-to-trough
	Accuracy:		25%
IV	Correlation between pulses	$\rho$	$< 1/e$
V	Oceanographic phenomena of interest	OPI	Table 2.2.1
B. System Parameters which have been specified			
I	Radar parameters:	R	
	a) Antenna Beamwidth		$3^\circ$
	b) Pointing Accuracy		$\sigma_\theta = 1/2^\circ$
	c) Antenna Gain		Peak
			Average
	d) Peak Power		2 KW
	e) System losses (other than processing losses in pulse compressor)		5 dB
	f) Noise Figure		5.5 dB
	g) Frequency		13.9 GHz
	h) *Pulse compression processing loss		.55 dB
	i) *Main lobe broadening due to tapering		23%
II	Ocean Backscatter Coefficient	$\sigma^0$	+6dB
III	Orbit Parameters	OP	
	a) Height		556 km
	b) Inclination		$90^\circ$ retrograde
	c) Eccentricity		.0064 maximum

\* For an assumed Modified Taylor weighting, -25.7 dB peak sidelobe.

TABLE 2.1,3 Precedence Matrix

Parameters To Be Determined. (PTBD)

		SF <sub>max</sub>	N <sub>min</sub>	S/N <sub>min</sub>	T <sub>max</sub>	CR <sub>min</sub>	B <sub>T</sub> min	PRF <sub>min</sub>	PRF <sub>max</sub>
I N P U T  P A R A M E T E R S	GA								
	TR		X	X					
	WH		X	X	X				
	ρ								X
	OPI	X			Weak				
	R					X			
	σ°					X			
	OP	X			Weak				X
P. T. B. D.	SF	////			Weak		X	X	
	N		////	X				X	
	S/N		X	////		X			
	τ				////	X			X
	CR					////			
	B <sub>T</sub>						////	X	
	PRF <sub>min</sub>							////	
	PRF <sub>max</sub>								////

TABLE 2.1.4 Re-Order Precedence Matrix

	$SF_{max}$	$\tau_{max}$	$B_T_{min}$	$PRF_{max}$	$N_{min}$	$S/N_{min}$	$CR_{min}$	$PRF_{min}$
SF	////	Weak	X					X
$\tau$		////		X			X	
$B_T$			////					X
$PRF_{max}$				////				
N					////	X		X
S/N					X	////	X	
CR							////	
$PRF_{min}$								////

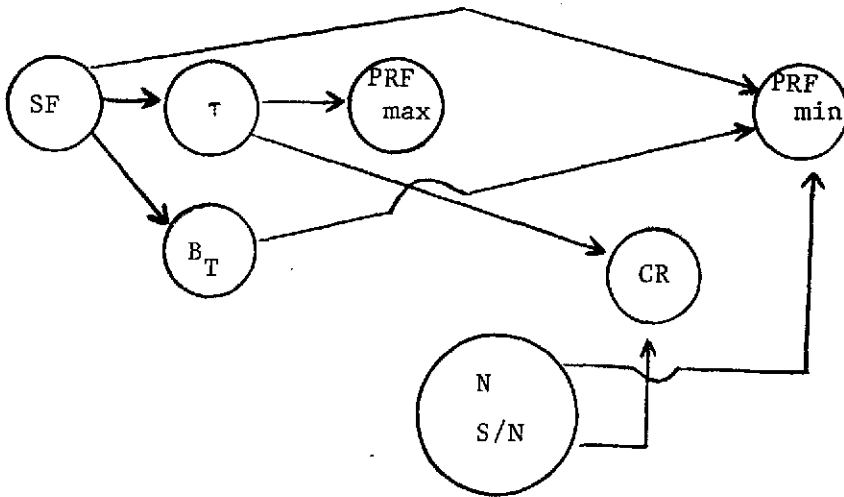


Fig. 2.1.1 Flow chart giving the order in which the parameters must be determined.

Now, in Table 2.1.4, the number of pulses integrated and signal-to-noise ratio occur as a block on the diagonal. Thus, these parameters must be varied simultaneously since they cannot be factored into a precedence order. Having chosen them, the compression ratio is determined next, and the minimum PRF is determined last.

Step 5. From the performance criteria, the first four parameters ( $SF$ ,  $\tau$ ,  $B_T$ ,  $PRF_{max}$ ) are determined almost uniquely. They are given in Table 2.1.5. As noted in that table, the max spatial frequency is determined by the Gulf Stream, and is .75 Hz for an extreme case. The pulse length is determined primarily by the minimum wave height resolution criterion.

Thus in order to measure wave height down to 1 m, the pulse length must be no greater than about .5 m (3 nsec). In order to keep tracking biases down, the min bandwidth of the tracker is made 4 times the max spatial frequency. The max PRF is determined from  $\tau$  to be 1.8 KHz.

The remaining parameters are presented in tabular form since they must be varied simultaneously. Three tables are presented which correspond to three types of epoch tracking systems, i.e. the standard split-gate tracker, the modified split-gate tracker, and the MLE tracker. These systems are ranked in order of increasing complexity.

The system selected based on considerations of system complexity and development risk is boxed in on Table 2.1.7.

TABLE 2.1.5 Parameters Shown to Have Nearly Unique Values

<u>Parameter</u>	<u>Selected Values</u>
max SF	.75 Hz Extreme Gulf Stream .1 -.25 Hz Typical Gulf Stream
max $\tau$	3 nsec
min $B_T$	3 Hz Extreme Gulf Stream 1 Hz Typical Gulf Stream
max PRF	1.8 KHz

TABLE 2.1.6 Half-Power Split-Gate Tracker

$T_{gE} = \tau, T_{gL} = 16\tau$	WH = 10 meters
k = .5 (tracks half-power point)	$\sigma_\tau = 7$ cm.

Continuous model

S/N (dB)	N	CR	PRF <sub>min</sub> @ $B_T = 1$ Hz
0	$19.4 * 10^3$	96	19.4 KHz
5	$6.0 * 10^3$	303	6.0
10	$3.4 * 10^3$	957	3.4
15	$2.7 * 10^3$	3030	2.7
20	$2.5 * 10^3$	9570	2.5

Table 2.1.7 Modified Split-Gate Tracker

$$T_{gE} = \tau, T_{gL} = 16\tau$$

WH = 10 meters

k = .25 (tracks quarter-power point)

$\sigma_r = 7$  cm.

Continuous model

S/N (dB)	N	CR	PRF <sub>min</sub> @ B <sub>T</sub> = 1 Hz
0	$13.5 * 10^3$	96	13.5 KHz
5	$3.0 * 10^3$	303	3.0
10	$1.4 * 10^3$	957	1.4
15	$1.0 * 10^3$	3030	1.0
20	$0.9 * 10^3$	9570	0.9

Table 2.1.8 MLE Tracker

$U_{max} = 16, WH = 10$  meters,  $\sigma_r = 7$  cm.

S/N	N	CR	PRF <sub>min</sub> @ B <sub>T</sub> = 1 Hz	PRF <sub>min</sub> @ B <sub>T</sub> = 3 Hz
0	$1.9 * 10^3$	96	1900	5700
5	600	303	600	1800
10	345	957	345	1050
15	270	3030	270	810
20	240	9570	240	720



A system based on the half-power split-gate tracker is preferred since it is easiest to implement and its characteristics are well understood from the Geos-C program. However, as an examination of Table 2.1.6 shows, a system based on the half-power split-gate tracker does not meet the performance specification unless it operates at PRF's greater than 2.5 kHz. But at this rate, the maximum PRF of 1.8 kHz is exceeded, and the pulses become correlated. Therefore, it is unlikely that the half-power split-gate tracker will meet the specifications.

The modified split-gate tracker brings the PRF down to an acceptable level for S/N greater than 10 dB while the MLE has acceptable PRF's at all S/N greater than about 5 dB.

Note that in both cases, as the S/N increases, the required compression ratio increases rapidly. For compression ratios greater than about 1000, the pulse compression unit becomes a higher risk development item. Thus the sets of feasible solutions are reduced to the portions of Tables 2.1.7 and 2.1.8 corresponding to a modified split-gate tracker operating at about S/N = 10 dB, and a MLE operating in the range of S/N = 5 to 10 dB. Of the two, the MLE places less stringent requirements of the transmitter duty cycle (due to the low PRF). However, from a development standpoint, the higher performance transmitter is thought to be a lower risk item since one which meets the requirements [3] is known to exist. The MLE, however, must be considered as high risk since only theoretical performance calculations have been made, and no development work has been done.

The system chosen is summarized in Table 2.1.9.

The epoch tracker is a modified split-gate tracker which tracks the quarter power point of the return, the early gate width is 3 nsec, and the late gate width is 48 nsec.

TABLE 2.1.9 System Parameters-Determined from The Design Procedure

Parameter	Symbol	Value
Max Spatial Freq.	SF	.25 Hz
Min Number of Pulses	N	1400
Min Signal-to-Noise Ratio	S/N	10 dB
Max. Compressed Pulse Length	$\tau$	3 nsec
Min Tracker Bandwidth	$B_T$	1 Hz
Min Pulse Rep. Freq.	$PRF_{min}$	1400 Hz
Max Pulse Rep. freq.	$PRF_{max}$	1800 Hz

## 2.2 Parameter Calculations

The dependencies between the various system parameters and performance requirements presented in the previous section are now examined in detail. In addition to the design equation or rationale used to calculate the parameter values presented in Table 2.1.9, details concerning the specification of the antenna parameters and receiver weighting are also included for completeness.

### 2.2.1 Survey of oceanographic and geodetic signals of interest

A survey was made of those oceanographically and geodetically induced variations in satellite altitude which the altimeter should be designed to track. The survey determined for each such variation, the characteristic amplitude, rise time, and maximum rate of change of altitude. The results of the survey are shown in Table 2.2.1. The briefest rise time (1.3 - 6.5 sec) would be caused by such phenomena as boundary currents and eddies (e.g., the Gulf Stream) and higher frequency undulations of the geoid, while the maximum rate of change of altitude that could be expected would be due to the eccentricity of the orbit itself ( $\approx \pm 50$  m/sec).

### 2.2.2 Tracker bandwidth

The tracker bandwidth should be sufficiently wide such that several uncorrelated tracker outputs are obtained during the shortest rise time in Table 2.2.1. A bandwidth of 1 Hz would meet the criterion at all but the worst case Gulf Stream (10 km width stream, perpendicular intersection of stream and orbit). A bandwidth of 3 Hz, while satisfying the worst case Gulf Stream, would result in an excessive PRF (4.2 kHz) for the  $\frac{1}{2}$  power split-gate tracker. Consequently a tracker bandwidth of

$$B_L = 1 \text{ Hz}$$

is chosen.

TABLE 2.2.1 Survey of Geodetic and Oceanographic Signals of Interest

Phenomenon	Spatial Extent (km)	Amplitude (meters)	Max Range Rate* (m/sec)	Rise Time* (sec)
<b>Western Boundary Currents</b>				
Typical Gulf Stream	100	1.0	.08	13
Worst Case Gulf Stream	10-50	1.0	.15-.8	1.3-6.5
<b>Boundary Current Eddies</b>				
	100 (near stream)	.35	.03	13
	200 (far away)	.05	.002	25
Open Ocean Currents	500-1000	.10	.0008-.0015	65-130
Coastal Sea Level Slope	2200	.60	.002	300
Difference in Sea Level (East/West)	---	.60	---	---
Tsunamis	50 (open seas)	.30-.50	.05-.08	6.5
Geoid Undulations (such as Puerto Rican and Venezuelan Trenches)	100-150	10-20	.5-1.5	13-20
Waves (sea and swell)	7.6 km grid spacing at 1 sample/sec	1-10 <sup>2</sup> (peak to trough)	---	---
Orbit Eccentricity	one revolution	$\pm \epsilon (r_e + h)$ $= \pm 44.4$	48.9	2800 (orbital half-period)

\* at h = 300 n.mi.,  $v_h = 7.63$  km/sec

### 2.2.3 Compressed pulse width

The compressed pulse width (after any tapering effects) is chosen such that the minimum significant wave height to be measured (1.0 meter peak-to-trough) is at least twice the compressed pulse length; i.e., 2 samples in the rise time of the sea echo leading edge. While 3 samples might seem more desirable, the resulting bandwidth (~500 MHz) is considered excessive. Thus, a compressed pulse length of

$$\tau = 3 \text{ nsec (after tapering)}$$

is selected.

### 2.2.4 Pulse return decorrelation time

In order to determine the maximum PRF such that pulse-to-pulse fluctuations in the sea echo are uncorrelated, the decorrelation time of these fluctuations must be found. This decorrelation time will be determined by three effects:

- 1) The Doppler spreading of the spectrum of the compressed return pulse envelope due to the horizontal velocity of the satellite;
- 2) The Doppler spreading due to the random velocities of the scatterers (wave spray);
- 3) The degree of overlap of the footprints associated with successive pulses.

For the orbital parameters of interest, and for a compressed pulse width of 3 nanoseconds, the first effect, Doppler spreading due to horizontal satellite velocity, is the dominant effect.

The doppler spreading is a function of the effective footprint size, which in turn is a result of antenna shaping, surface shaping, and pulse shaping functions. For a satellite altitude of 300 nautical miles, antenna beamwidths of a few degrees, and pulse lengths of a few nanoseconds, the footprint is pulse-limited, as shown in Figure 2.2.1, and hence the decorrelation time is a function of the compressed pulse length.

Assuming uniform return from the pulse-limited footprint, the doppler spectrum is well approximated by a uniform power spectrum between  $\pm f_o$  as shown in Figure 2.2.2. Then the correlation function of the square-law envelope detected output is given by

$$R_1(T) = \frac{\sin^2 (2\pi f_o T)}{(2\pi f_o T)^2}$$

with the first zero occurring at

$$T_1 = \frac{1}{2 f_o} = \frac{\lambda}{4 v_h \sin \theta_{\frac{1}{2}}}$$

where

$$\begin{aligned} \theta_{\frac{1}{2}} &= \text{half the pulse-limited beamwidth} \\ &= \cos^{-1} \left( \frac{h}{h + \frac{cT}{2}} \right) \end{aligned}$$

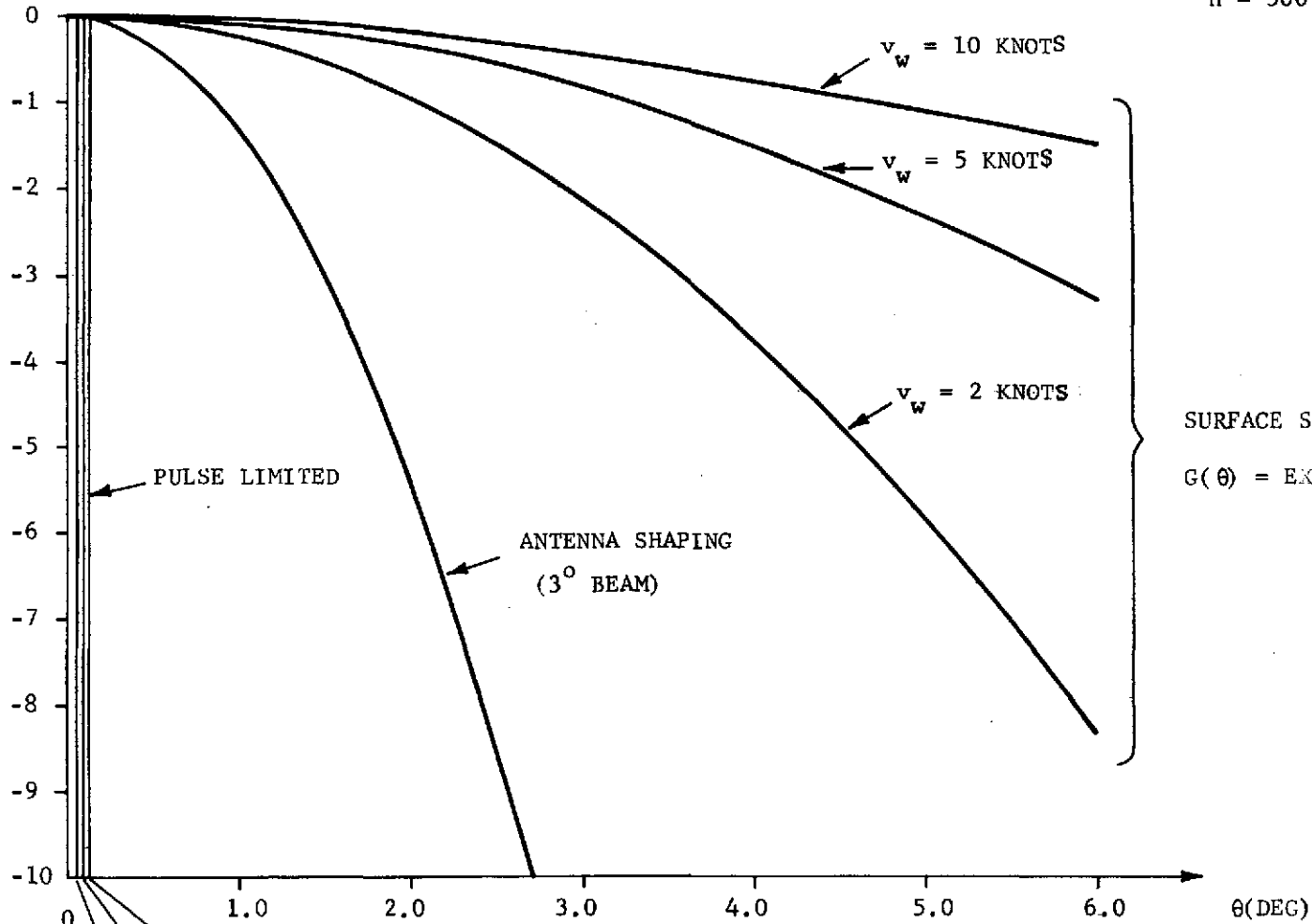
Assuming uniform vertical wave-motion Doppler from  $\pm 3$  m/sec, the square law detector output correlation due to vertical wave-motion is simply

Figure 2.2.1 . ALTIMETER BEAM-SHAPING FUNCTIONS

$\lambda = .02157 \text{ m}$   
 $h = 300 \text{ n.mi.}$

-24-

GAIN (DB)

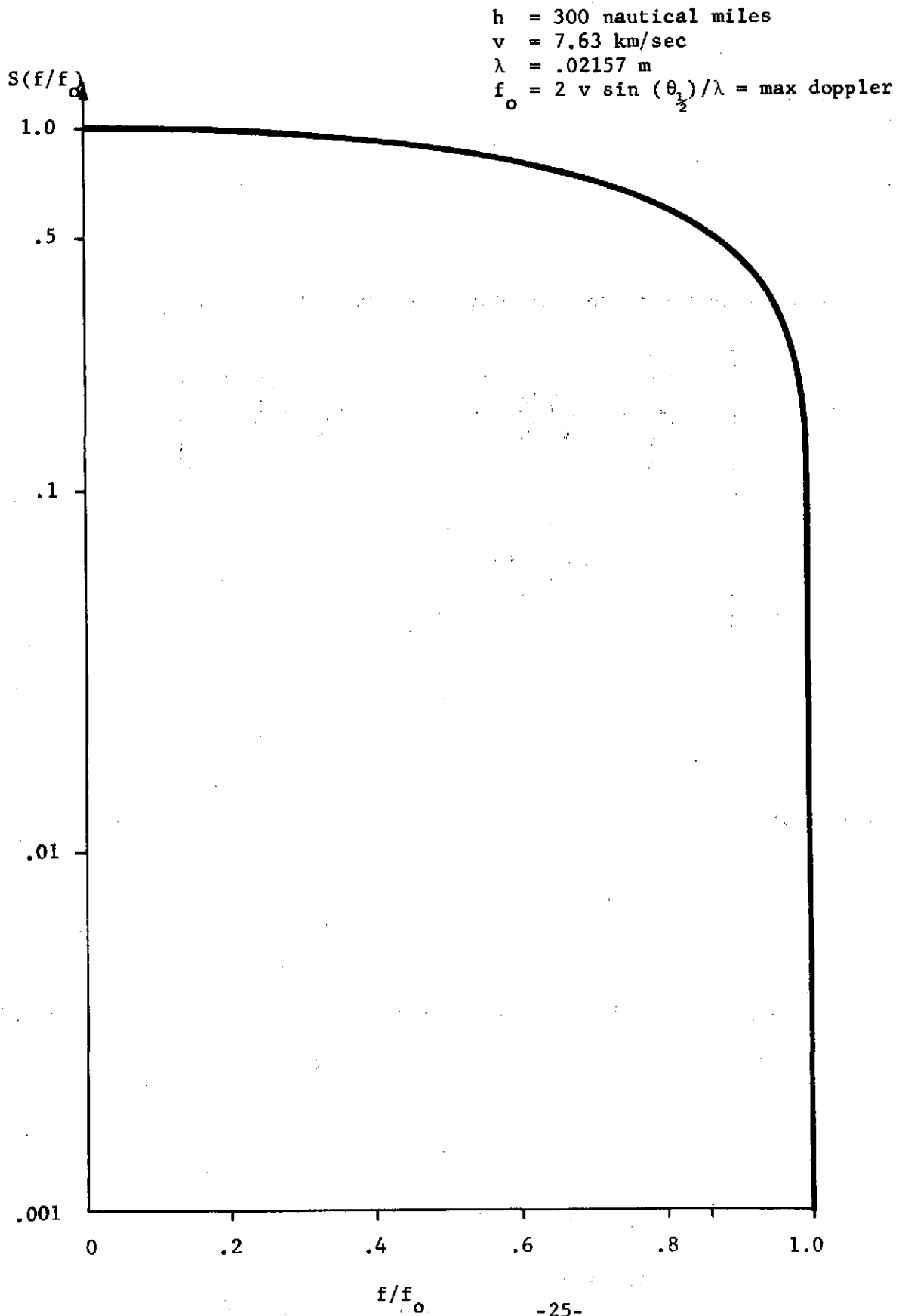


$\theta_{\frac{1}{2}} = .133^\circ @ \tau = 10 \text{ nsec}$   
 $\theta_{\frac{1}{2}} = .094^\circ @ \tau = 5 \text{ nsec}$   
 $\theta_{\frac{1}{2}} = .059^\circ @ \tau = 2 \text{ nsec}$

$$\theta_{\frac{1}{2}} = \cos^{-1} \left( \frac{h}{h + \frac{c\tau}{2}} \right)$$

SURFACE SHAPING  
 $G(\theta) = \text{EXP} \left\{ -\frac{345.96}{v_w} \tan^2 \theta \right\}$

Fig. 2.2.2 DOPPLER SPECTRUM OF RETURN PULSE ENVELOPE DUE TO  
HORIZONTAL VELOCITY OF SATELLITE





$$R_2(T) = \frac{\sin^2(4\pi T v/\lambda)}{(4\pi T v/\lambda)^2}$$

$$v = 3 \text{ m/sec}$$

with 1<sup>st</sup> zero at

$$T_2 = \frac{\lambda}{4v}$$

The correlation proportional to percentage overlap of the footprint is

$$R(\tau) = \begin{cases} \left( \frac{2}{\pi} \right)^2 \left\{ \arctan \sqrt{\left( \frac{2r}{v_h \tau} \right)^2 - 1} - \frac{v_h |\tau|}{2r} \sqrt{1 - \left( \frac{v_h \tau}{2r} \right)^2} \right\}^2, & |\tau| < \frac{2r}{v_h} \\ 0, & \text{otherwise} \end{cases}$$

where

$$r = \sqrt{c\tau h}$$

$R_3(T)$  is zero at

$$T_3 = \frac{2\sqrt{c\tau h}}{v_h}$$

For a 3 nanosecond pulse, mean satellite altitude of  $h = 300$  nautical miles, and  $v_h = 7.63$  km/sec, these decorrelation times are

$$T_1 = .55 \text{ msec}$$

$$T_2 = 1.8 \text{ msec}$$

$$T_3 = 185 \text{ msec}$$

### 2.2.5 Maximum PRF

The maximum PRF to ensure uncorrelated pulse-to-pulse fluctuations is the inverse of the decorrelation time determined in the previous section. Ignoring effects of wave spray and pulse overlap, the maximum PRF is given by

$$\begin{aligned} \text{PRF}_{\text{max}} &= \frac{1}{T_1} \\ &= 1.8 \text{ kHz} \end{aligned}$$

### 2.2.6 S/N and N

The relationship between the number of pulses required, N, and the single-pulse signal-to-noise ratio, S/N, at the output of the pulse compressor is determined by the maximum allowable random error in the tracker  $\sigma_t$ , the maximum significant wave height  $WH_{\text{max}}$  (peak-to-trough) at which this accuracy must be achieved, and the configuration of the tracker. The general form of this relationship is

$$\frac{\sigma_t \sqrt{N}}{T} = f(S/N)$$

where  $f(\cdot)$  is some non-linear function determined by the tracker configuration, and T is the rise time (expressed in meters) of a linear fit to the leading edge of the sea echo. T is given by

$$T = \frac{(3.1) WH_{\text{max}}}{4}$$

Figure 2.2.3 shows a plot of  $f(S/N)$  for a quarter-power split-gate tracker, with an early gate width matched to the compressed pulse length and a late-to-early-gate width ratio of 16. For a S/N of 10 dB,  $f(10 \text{ dB}) = .34$ . For  $WH_{\text{max}} = 10$  meters, and  $\sigma_t = 10/\sqrt{2}$  cm, the number of pulses, N, is

$$\begin{aligned}
 N &= \left[ \frac{T}{\sigma_t} f(S/N) \right]^2 \\
 &= \left[ \frac{(3.1)(10)}{(4)(.1)/\sqrt{2}} (.34) \right]^2 \\
 &= 1400
 \end{aligned}$$

### 2.2.7 Required compression ratio

The compression ratio, CR, is chosen to provide the desired pulse compressor output signal-to-noise ratio. It can be computed by the radar range equation, in which the sea surface backscatter is accounted for by a point target with cross-section equal to the pulse limited footprint area times the backscatter coefficient,  $\sigma^0$ .

For this model, the pulse-compressor output signal-to-noise ratio is given by

$$(S/N)_{\text{IF}} = \frac{P_t (G_t L_G)^2 \lambda^2 \sigma L_s L_t}{(4\pi)^3 h^4 kT_o B_{\text{IF}} F_n}$$

where

$P_t$  = peak transmitter power

$G_t$  = boresight antenna gain

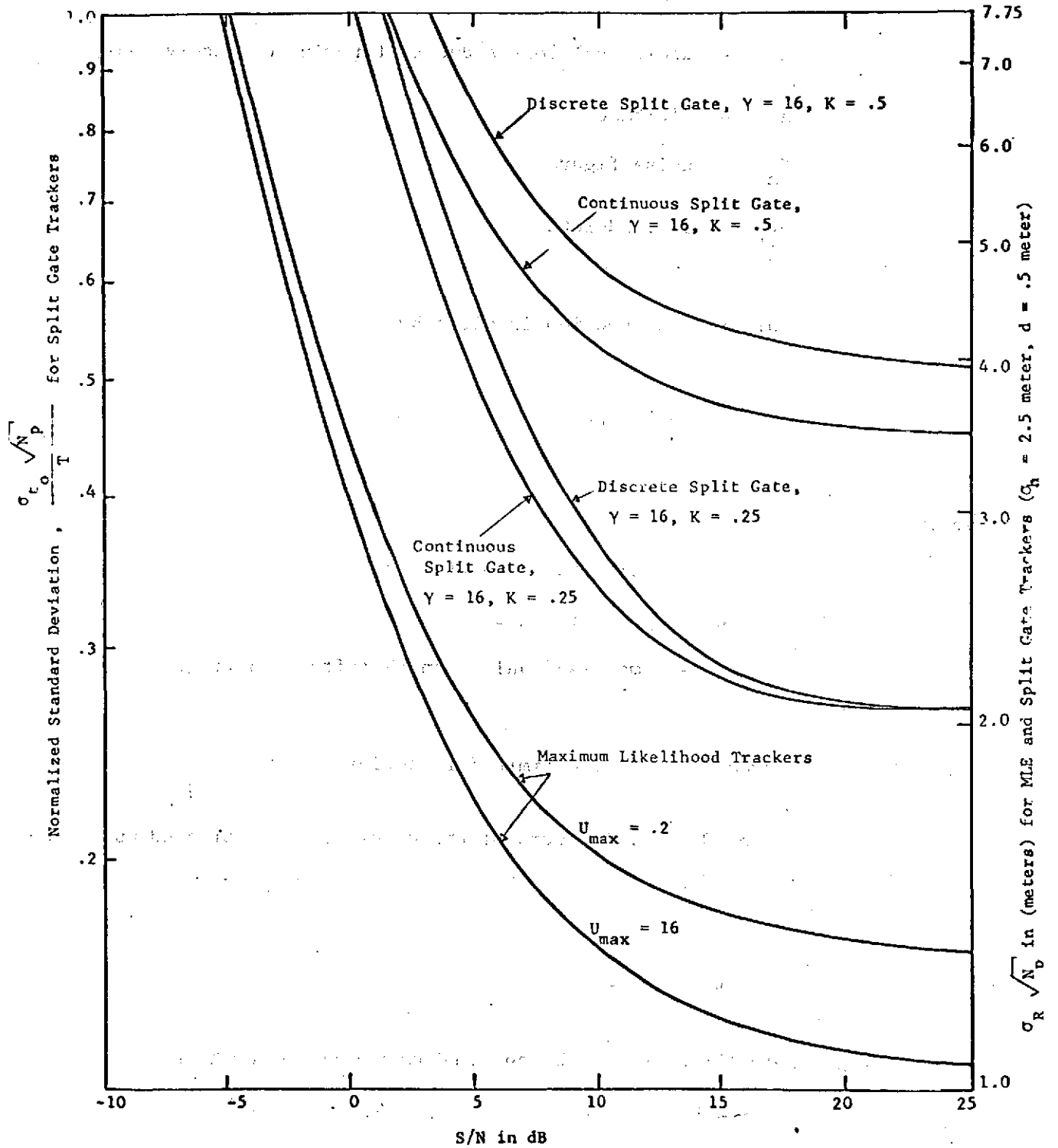


Figure 2.2.3. Comparison of Tracker Accuracies

- $L_G$  = gain loss associated with pointing errors
- $\lambda$  = wavelength
- $\sigma$  = target cross-section
- $L_s$  = system losses
- $L_t$  = additional losses due to tapering on receive only
- $h$  = altitude
- $F_n$  = noise figure
- $B_{IF}$  = IF bandwidth

The target cross-section is given by

$$\sigma = \sigma^0 \pi c h \tau$$

where

$\sigma^0$  = backscatter coefficient

$c$  = speed of light

$\tau$  = compressed pulse length (after tapering)

and  $\pi c h \tau$  is the area of the pulse-limited footprint.

The IF bandwidth, in terms of the after-taper compressed pulse length  $\tau$ , is

$$B_{IF} = \frac{1 + \alpha}{\tau} ,$$

where  $\alpha$  represents the main-lobe broadening over uniform weighting.

Solving for CR,

$$CR = \frac{4(4\pi)^2 h^3 kT_o (1+\alpha) F_n}{P_t (G_t L_G)^2 \lambda^2 \sigma^o C L_s L_t \tau^2} (S/N)_{out}$$

$$= C (S/N)_{out}$$

C is evaluated as follows:

$$4(4\pi)^2 = 28.0 \text{ dB}$$

$$h^2 = (556 \times 10^3)^3 = 172.4 \text{ dB m}^3$$

$$kT_o = 4 \times 10^{-21} \text{ watt-sec} = -204 \text{ dB watt-sec}$$

$$F_n = + 5.5 \text{ dB}$$

$$1+\alpha = 1.23 = .9 \text{ dB}$$

$$P_t = 2\text{kw} = 33 \text{ dBw}$$

$$G_t^2 = 2 (34.9) \text{ dB} = 69.8 \text{ dB}$$

$$L_G = 2 (-.65) \text{ dB} = -1.3$$

$$\lambda^2 = (.02157 \text{ m})^2 = -33.3 \text{ dB m}^2$$

$$\sigma^o = + 6 \text{ dB}$$

$$C = 84.8 \text{ dB m/sec}$$

$$L_s = - 5 \text{ dB}$$

$$L_t = -.55 \text{ dB}$$

$$\tau^2 = (3 \text{ nsec})^2 = -170.5 \text{ dB sec}^2$$

Thus,

$$C = 19.9 \text{ dB},$$

and the required CR for a 10 dB  $(S/N)_{out}$  is 960.

### 2.2.8 Required PRF

The PRF required to average N pulses is determined by the tracker bandwidth,  $B_L$ :

$$\text{PRF}_{\text{req'd}} = N \cdot B_L$$

For  $B_L = 1 \text{ Hz}$ ,  $N = 1400$ ,

$$\text{PRF}_{\text{req'd}} = 1.4 \text{ kHz}$$

Note:  $B_L = 3 \text{ Hz}$  corresponds to  $\text{PRF}_{\text{req'd}} = 4.2 \text{ kHz}$  which exceeds the maximum PRF for uncorrelated returns.

### 2.2.9 Receiver weighting

The effect of range sidelobes on altimetry bias and wave height measurement has been examined in [4]. These results, extended to more general cases and corrected for a computational error, are summarized in Fig. 2.2.4. There, both waveform and tracker bias versus RMS wave height data (normalized to the compressed pulse width,  $\tau_c$ ) are presented for uniform and 25 dB modified Taylor receiver weighting. The tracker used for these computations was a standard  $\frac{1}{2}$  power split-gate with early and late gate widths both matched to the compressed pulse width. For direct comparison, the data for the mean power response biases with and without receiver weighting are also presented in Tables 2.2.2 and 2.2.3, respectively. As shown, there is no appreciable change in bias with or without receiver weighting and the bias that does arise from these range sidelobes is quite small. While computations have not been made for the "modified Split-Gate", quarter power tracker recommended in Section 2.1, it is felt that these biases (while somewhat larger) would remain less than 1cm at  $\sigma_h = 2.5$  meters.

Figure 2.2.4

Normalized bias vs waveheight due to range sidelobes only.

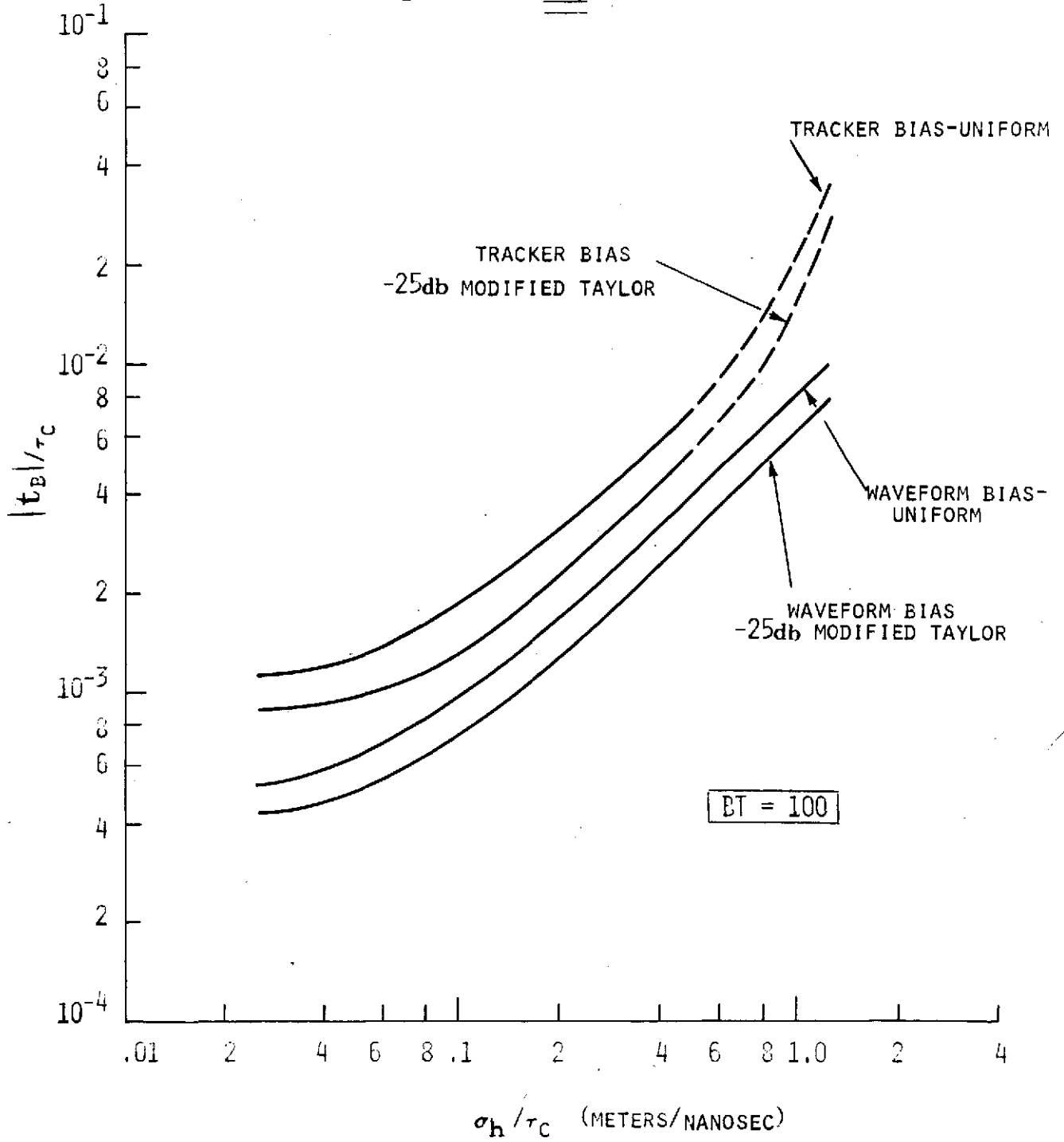




TABLE 2.2.2 Mean Power Response Bias -25 dB Modified Taylor Weighting

$\sigma_h$ (m) \ $\tau_c$ (nsec)	10	5	4	2	
.25	.065	.036	.033*	.025*	bias  in centimeters
.5	.073	.061	.051*	.046*	
1.0	.105	.093	.093*	.089	
2.5	.233*	.225	.228*	.227	

TABLE 2.2.3 Mean Power Response Bias - Uniform Weighting

$\sigma_h$ (m) \ $\tau_c$ (nsec)	10	5	4	2	
.25	.079	.049	.043*	.035*	bias  in centimeters
.5	.093	.069	.069*	.060*	
1.0	.142	.122	.120*	.110	
2.5	.300*	.292	.300*	.292	

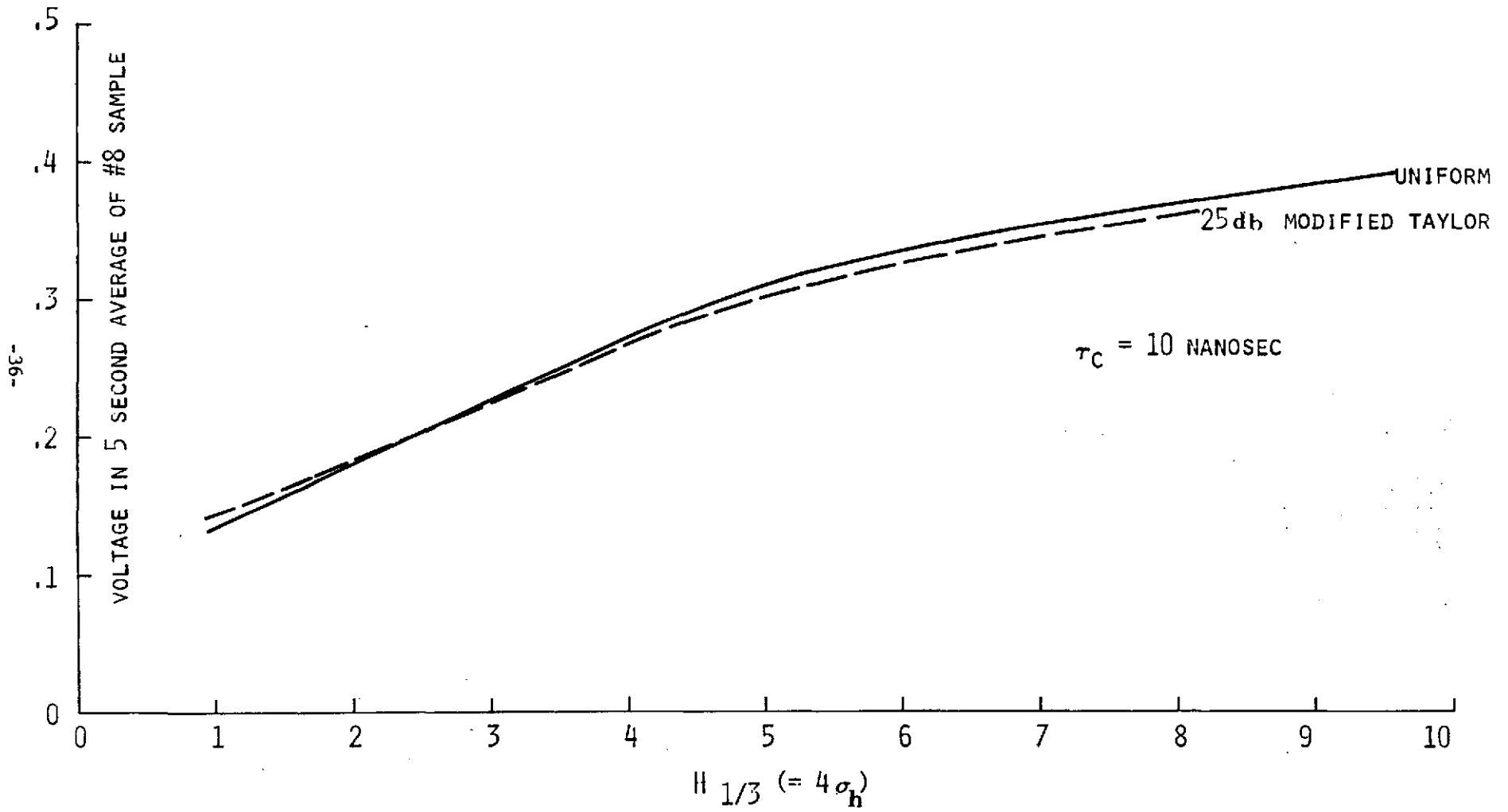
\* Graphical Interpolation

A word of caution- the biases described above are only those due to range sidelobes causing the mean power return to differ from the ideal impulse response; i.e., differ from an asymmetrical function at the half power point. In fact, as shown in Part II, Section 2, tracker bias is, in general, a function of wave height and signal-to-noise ratio for an ideal impulse response.

If, as in GEOS, the average voltage on the No. 8 waveform sampler were used as a measure of wave height, the response sensitivity to wave height shown in Fig. 2.2.5 results. Here, for a compressed pulse width of 10 nsec, the slope of the weighted and unweighted response are essentially the same. For a 3 nsec compressed pulse width the difference would be even less. Thus the only degradation in performance, caused by receiver weighting, would be due to the usual reduction in S/N ratio (about 20% for the 25 dB Modified Taylor).

In summary then, it would seem that the 13 dB sidelobes associated with no receiver weighting cause no problems as far as bias or wave height measurement are concerned. On the other hand, a limited amount of receiver weighting (say 20 or 25 dB sidelobes) provides a slight reduction in bias at the expense of a slight decrease in S/N. Smaller sidelobes have not been considered since phase errors and other tolerance problems associated with the physical realization of a pulse compression technique can (and often do) cause the far out sidelobes to be much larger than the designed value when more than 25 dB reduction is attempted. This being the case, there just doesn't seem to be any good reason for either recommending or rejecting receiver weighting. As such, a 25 dB Modified Taylor receiver weighting has been included in the design, but should be considered optional.

Figure 2.2.5  
AVERAGE SAMPLE VOLTAGE ON NO. 8  
WAVEFORM SAMPLER VERSUS WAVEHEIGHT



## 2.2.10 Antenna parameters

The antenna gain specified in Table 2.1.2 cannot be obtained with an 18" dish at 65% efficiency. Although this is about the highest efficiency which can practically be achieved with a parabolic dish, a higher gain at a given beamwidth can be achieved by using a larger dish (smaller f/D) with effectively a heavy illumination taper to give the desired beamwidth. The efficiency of the larger dish will be even lower (e.g., 55%), but the gain will approach that of a uniformly illuminated dish of the same beamwidth. Using this approach, it is possible to realize an 87% "efficiency" relative to the area of a uniformly illuminated dish of equal beamwidth, with off-the-shelf antenna. Thus, a realizable antenna gain at a  $3^\circ$  beamwidth would be 34.9 dB.

However, the gain must also be corrected for losses due to beam pointing errors. These losses can be accounted for by replacing  $G_t^2$  with  $\overline{G^2}$ , the average value of two-way gain. This average value can be computed by assuming a gaussian beamshape and gaussian distributed pointing errors. Specifically,

$$\overline{G^2} = \int G_t^2 G^2(\theta, \phi) p(\theta, \phi) d\theta d\phi$$

where

$G_t$  = boresight gain (one-way)

$G(\theta, \phi)$  = normalized antenna pattern (one-way)

$$= e^{-\pi(\theta^2 + \phi^2)/B^2}$$

$B$  = equivalent beamwidth

$p(\theta, \phi)$  = probability density of pointing errors

$$= \frac{1}{2\pi\sigma^2} e^{-(\theta^2 + \phi^2)/2\sigma^2}$$

Substituting into the expression for  $\overline{G^2}$  yields

$$\begin{aligned} \overline{G^2} &= G_t^2 \int e^{-2\pi(\theta^2 + \phi^2)/B^2} e^{-(\theta^2 + \phi^2)/2\sigma^2} d\theta d\phi \\ &= G_t^2 \left\{ \int e^{-2\pi\theta^2/B^2} \frac{e^{-\theta^2/2\sigma^2}}{\sqrt{2\pi\sigma^2}} d\theta \right\}^2 \\ &= G_t^2 \left( 1 + \frac{4\pi\sigma^2}{B^2} \right)^{-1} \\ &= (G_t L_G)^2 \end{aligned}$$

Thus the loss due to pointing errors is

$$L_G = \left( 1 + \frac{4\pi\sigma^2}{B^2} \right)^{-\frac{1}{2}}$$

For  $2\sigma = 1^\circ$ , this loss is  $-.65$  dB at  $B = 3^\circ$ .

## References

- [1] D. V. Steward, "Organizing the Design of Systems by Partitioning and Tearing", Nuclear Energy Division, General Electric Co., San Jose, California
- [2] Statement of Work for Study of Radar Pulse Compression for High Resolution Satellite Altimetry, Exhibit A, NASA Statement of Work No. P-2551, June 12, 1972.
- [3] W. Townsend, Statement made at 4<sup>th</sup> monthly contract meeting at NASA, Wallops Station on March 26, 1973, to the effect that a suitable transmitter would be available from Watkins Johnson.
- [4] Dooley, R. P., "The Effect of Range Sidelobes on Radar Altimeters", TSC-W3-1972.

### 3.0

#### SELECTION OF PULSE COMPRESSION TECHNIQUE

In this section the types of pulse compression that were considered for the satellite altimetry experiment are examined in detail. Utilizing the set of nominal system parameters from the previous section, each type of pulse compression is considered on the basis of feasibility, complexity, efficiency and stability. Bandwidth considerations led to the selection of - a full deramp STRETCH (similar to ALCOR) followed by an analog filter bank to separate range returns - as the recommended technique.

### 3.1

#### Summary of Candidates

The following pulse compression techniques have been considered for the satellite altimeter:

- 1) Binary Phase Coding
- 2) Linear Frequency Modulation
- 3) Hybrid (analog/digital)
- 4) STRETCH-ALCOR

The binary (or polyphase) coding techniques are described in Section 3.2. There it is shown that while the digital techniques have the desirable property of being able to change waveform (compression ratio), wave height data cannot be obtained with a simple 1 bit I, 1 bit Q system but requires a "multi-bit" decoder. For the required bandwidth, the complexity of even a 2 bit I, 2 bit Q (plus sign) system is considered to be pushing the state-of-the-art beyond 1973 technology and thus, the phase coded technique is not recommended at this time.

Section 3.3 considers the linear FM technique which is certainly the simplest and most widely used form of pulse compression. The problem with this method is found to be not so much pulse compression per se but the digital read-out of the resulting 300-360 MHz signal. Even with sample-and-hold circuits, digitizing a 300 MHz signal with 6-8 bits per word is not considered practical and the linear FM (full compression) technique is not recommended. Section 3.3 also contains considerable material on the state-of-the-art for the various methods of generating a linear FM signal since these signals are an essential part of the more general STRETCH-ALCOR configuration.

Several hybrid analog/digital techniques are examined in Section 3.4. The hybrid of Barker code and linear FM is used to illustrate the fact that such techniques, while useful for increasing achievable compression ratio, in general require processing at the full signal bandwidth and hence are not recommended. The use of a binary phase coded waveform in a tracking mode, "cross-correlator", is shown to be capable of performing the altimetry but provides little or no information from which wave height can be accurately determined.

The STRETCH-ALCOR techniques are examined in Section 3.5. The general technique is shown to be capable of reducing the bandwidth of the compressed signal and hence the A/D conversion requirement. Bandwidth and delay requirements for the STRETCH dispersive line and sampling frequency for the A/D convertor are given as a function of STRETCH ratio (SR). The full deramp ( $SR = \infty$ ) followed by an analog filter bank to separate range returns is recommended over partial deramp ( $SR > 1$ ) since this technique requires the least sampling frequency ( $< 1$  MHz) for the A/D convertor and a single dispersive line for the generation of both the transmit and receive linear FM waveform. Digital filtering is not recommended since the A/D conversion would require a 21.4 MHz sampling frequency as compared with  $< 1$  MHz for the analog filter bank.



### 3.2 Binary Phase Coding

The applicability of binary (or polyphase) coding to satellite altimeters depends upon three factors:

1. The elimination of range-doppler ambiguities inherent in a linear FM or Chirp waveform.
2. The availability of digital microelectronic signal processing techniques to directly give digital information on altitude and "sea state".
3. Flexibility to change waveform with digital implementation.

These factors can be discussed separately. The binary waveform is often chosen when the velocity of the vehicle or target is so uncertain that an absolute determination of time delay is impossible without an absolute determination of relative radial velocity. The error in time delay ( $\Delta t_d$ ) measurement is proportional to the ratio of the doppler uncertainty ( $\Delta f_d$ ) to the FM dispersion of the waveform ( $\Delta F$ ).

$$\Delta t_d \approx \frac{\Delta f_d}{\Delta F} T$$

where T is the time dispersion.

The source of doppler error is the result of the uncertainty in the eccentricity of the orbit. Since the maximum  $f_d$  is specified at 5 KHz, the uncertainty should be of the order of  $0.5 \times 10^3$  Hz. If we assume  $\Delta F \approx 300$  MHz and  $T \approx 3 \times 10^{-6}$  sec, then  $\Delta t_d \approx .6 \times 10^{-11}$  sec. Thus the ambiguities in the linear FM waveform do not seem to cause a problem and the choice of waveform depends on ease of implementation.

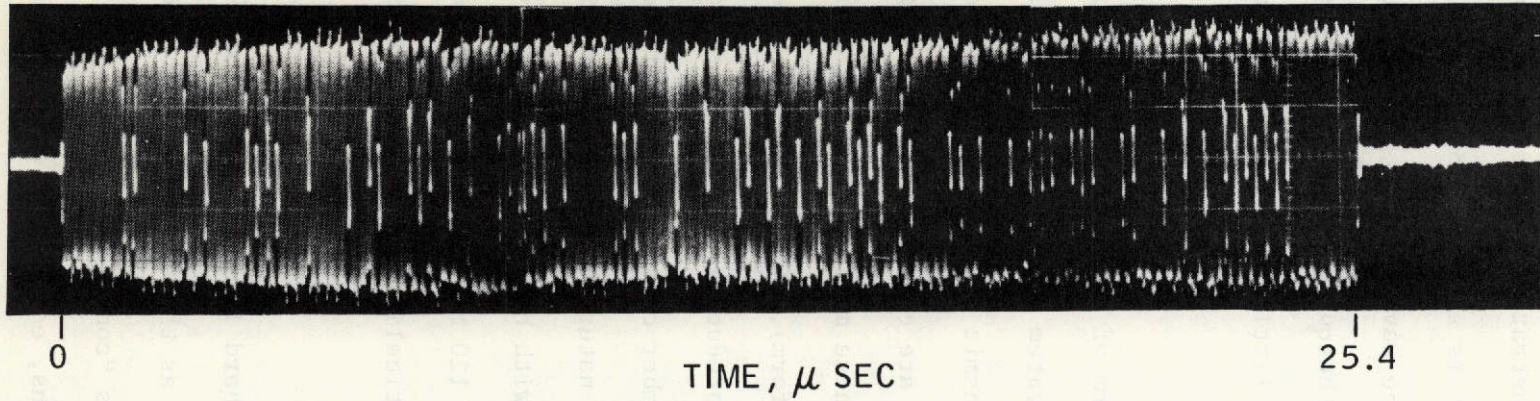
The binary waveform can be implemented either in analog or digital form. With the parameters of interest, an analog implementation would probably also use surface wave techniques. This is illustrated in Figs. 3.2-1 and 3.2-2. However, for a given time-bandwidth product, it is somewhat more difficult to implement the binary phase waveform with surface wave devices [2], [3] and [4]. Since the potential advantage of the binary technique is that the output could be directly in digital form, there seems to be little value in further discussion of analog techniques.

The simplest and most convenient form of decoding for a binary phase-coded waveform is the "one-bit I, one-bit Q" system shown on Fig. 3.2-3. (From [1]) the received signal is mixed with the transmit carrier and only the polarity of the bipolar in-phase and quadrature signals are entered into high speed shift registers, digital comparators and adders. (These must all work at a clock rate equal to the bandwidth of the transmitter waveform). Using digital adders, the maximum output is equal to the time-bandwidth product in each channel for a single point target. This assumes that the number of stages is equal to the time bandwidth product. Many decoders of this nature have been built with 5-20 MHz bandwidths, and a few experimental models with higher bandwidths have been constructed. It seems possible to get to over 120 MHz bandwidth with MECL circuits, but there is question as to the practicality at 300 MHz. This is explored further in ref. [5].

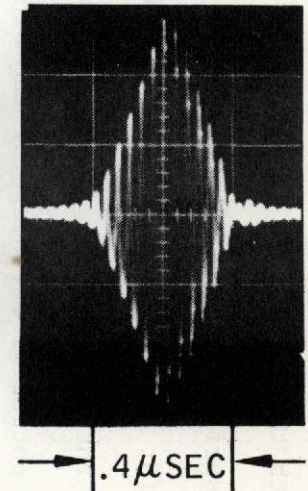
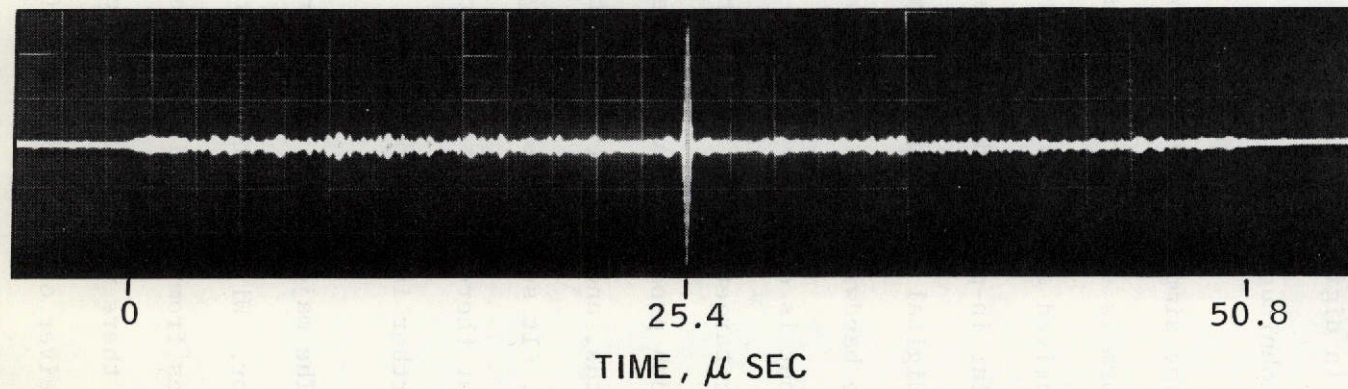
The major cause of concern is the "hard limiter" effect of the one bit processor. With a distributed target such as the sea surface, the dispersed echoes from the various concentric rings "compete" for the quantized signal. If there were only 2 reflecting regions, each would only have an average receiver output amplitude of  $\frac{1}{2}$  TB (down 6 dB). If there are 4 significant reflecting rings each would only be  $\frac{1}{4}$  TB in amplitude (down 12 dB). Thus

PHASE CODED TAPPED DELAY LINES ON LITHIUM NIOBATE  
FILLED DOUBLE ELECTRODE 127 - TAP ARRAY

EXPANDED WAVEFORM



RECOMPRESSED PULSE



-44-

25306-8

From

**HUGHES**  
HUGHES AIRCRAFT COMPANY  
GROUND SYSTEMS GROUP

[2]

Figure 3.2-1

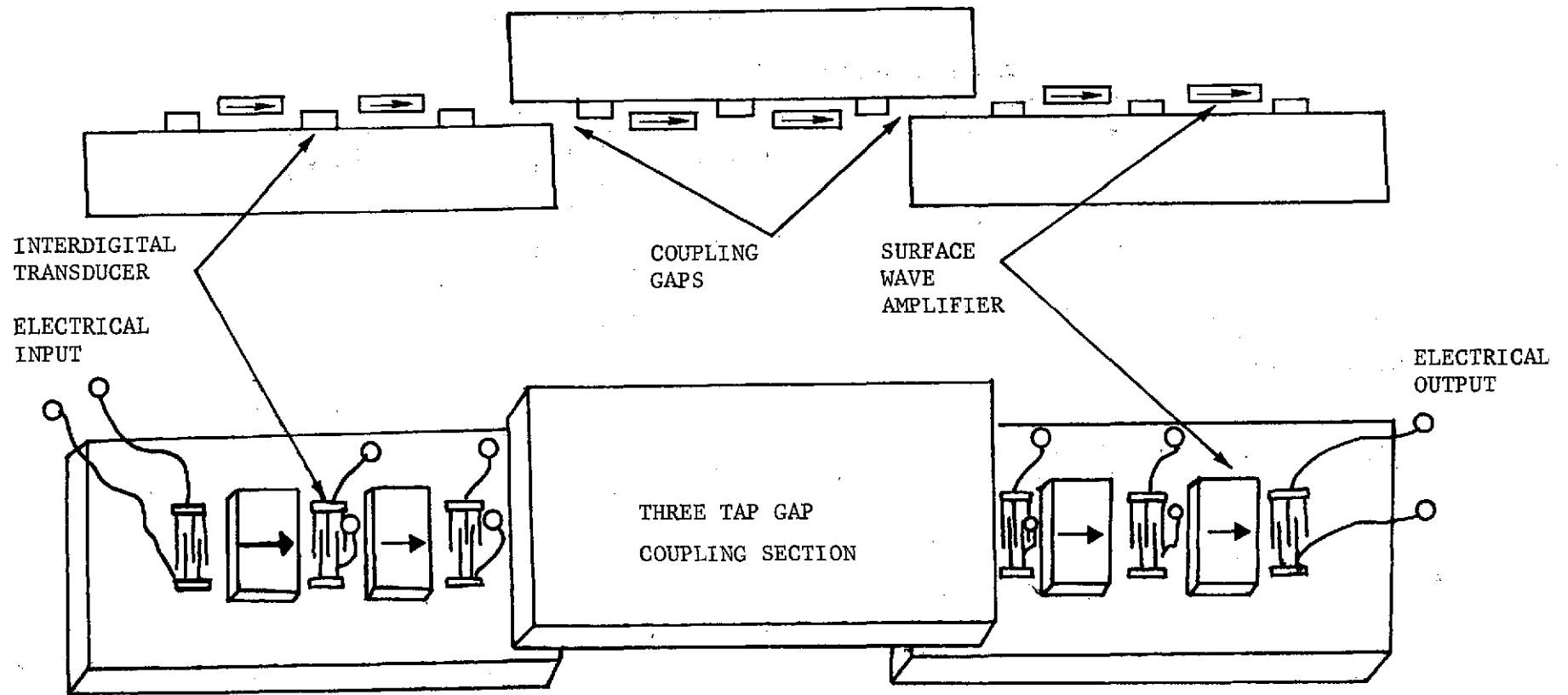
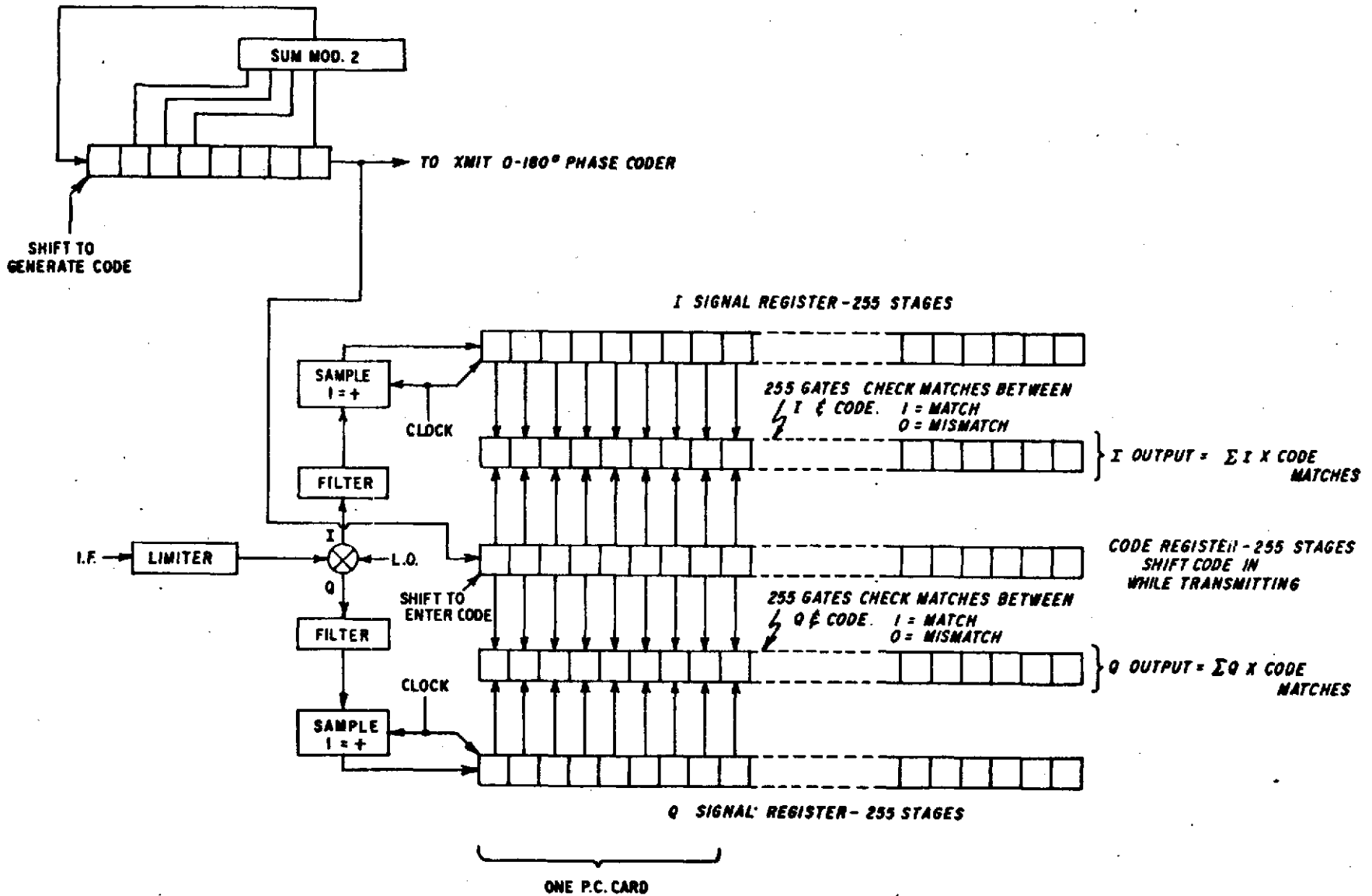


Fig. 3.2-2 Acoustic Surface Wave Tapped Delay Line (From [2])



-46-

FIG. 3.2-3 DIGITAL PULSE COMPRESSOR USING 0-180° BINARY PHASE-CODE MODULATION.

AFTER TAYLOR AND MACARTHUR

the desirable property of the 1 bit processor, i.e. that it suppresses clutter in an air defense radar, will produce a severe distortion of the impulse response.

Thus it appears that a "multi-bit" decoder is required. This would force a much more complex processor. A study of how many bits are required to reproduce the impulse response is given in Part II. While it seems possible to get away with a 2-bit I, 2-bit Q system if thresholds are set properly, the complexity due to pushing the state-of-the-art beyond 1973 technology is disturbing. The phase coded system is not recommended at this time.

### 3.3 Linear FM Techniques

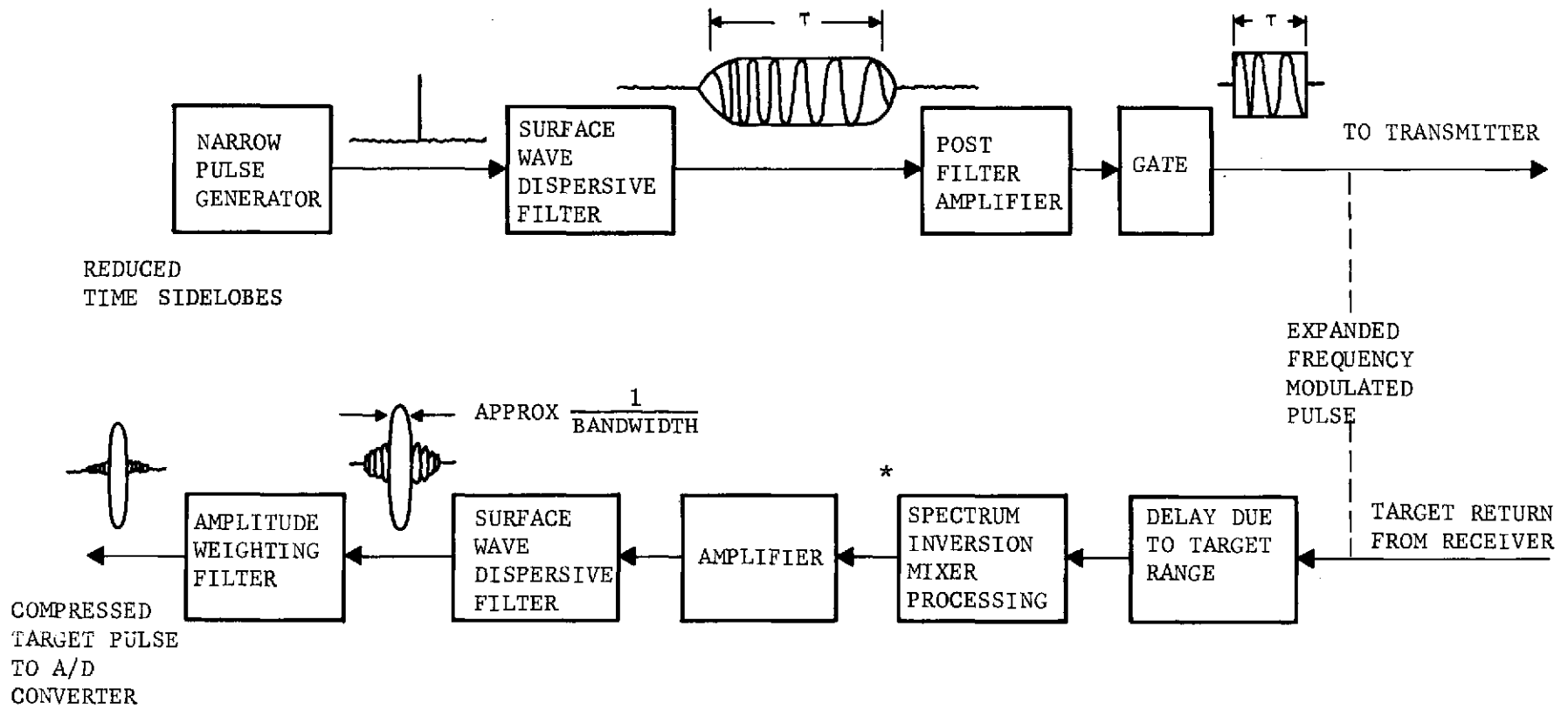
The Linear FM or Chirp System is the simplest and by far the most widely used form of pulse compression. The primary disadvantage of the ambiguity of range and doppler, wherein true range can only be determined when radial velocity is known, is not a problem for satellite altimetry.

The problems of implementation are twofold

1. Achieving the required bandwidth and dispersion with current technology.
2. Performing integration and digital readout of a 300-360 MHz signal.

It is shown in this section that the first problem is not serious except that to obtain the desired bandwidth, the only supplier in 1973 is MIT Lincoln Laboratory. By the time of actual satellite design, there will be many vendors.

The problem of digitizing a 300 MHz signal with 6-8 bits per word is the more severe problem and is the reason for rejecting the relatively simple active Chirp configuration shown on Fig. 3.3.-1. Even if the integration were



\* SPECTRUM INVERSION UTILIZED WHEN DISPERSIVE FILTER IS THE SAME OR IDENTICAL TO THE FILTER USED FOR EXPANSION. NOT USED WHEN COMPRESSION FILTER IS CONJUGATED TO EXPANSION FILTER.

Figure 3.3-1 Expansion/compression portion of a pulse compression radar system.

performed with sample-and-hold circuits and an analog integrator, it is not believed to be practical.

Fortunately there are several variations of Linear FM called STRETCH or ALCOR that reduce the output bandwidth. These are discussed in Section 3.5. There is considerable material in this section on surface wave lines which are an essential part of a STRETCH or ALCOR configuration.

### 3.3.1 Passive generation of Linear FM signals

A linear FM waveform may be generated by a passive or an active technique. In passive generation, a dispersive delay line is excited with an impulse. If the delay line has a bandwidth of 360 MHz, the line output can be translated directly by mixing with a transmitter oscillator to the required transmitter output frequency. If the delay line bandwidth is less than 360 MHz, its output frequency may be multiplied to provide the required sweep bandwidth, and then translated to the correct carrier frequency.

The feasibility of a desired delay line is a strong function of its dispersion bandwidth product. The state-of-the-art of pulse expansion/compression devices is shown in Fig. 3.3-2. For the 360 MHz, 2.8  $\mu$ sec requirement (compression ratio = 1000), it can be seen that the reflective array compressor (RAC) technique described below is the technique (see point A, Fig.

3.3-2. However, since this is a new invention, procurement would be required from MIT Lincoln Lab. Because there are presently no established vendors of the RAC line, this approach would involve some development risk if obtained from industry. Therefore, an equipment configuration using a lower bandwidth delay line followed by frequency multiplication is indicated for the "baseline design".\* A brief description of RAC and other type lines is contained in the following paragraphs.

---

\* See section 4.1 for details.



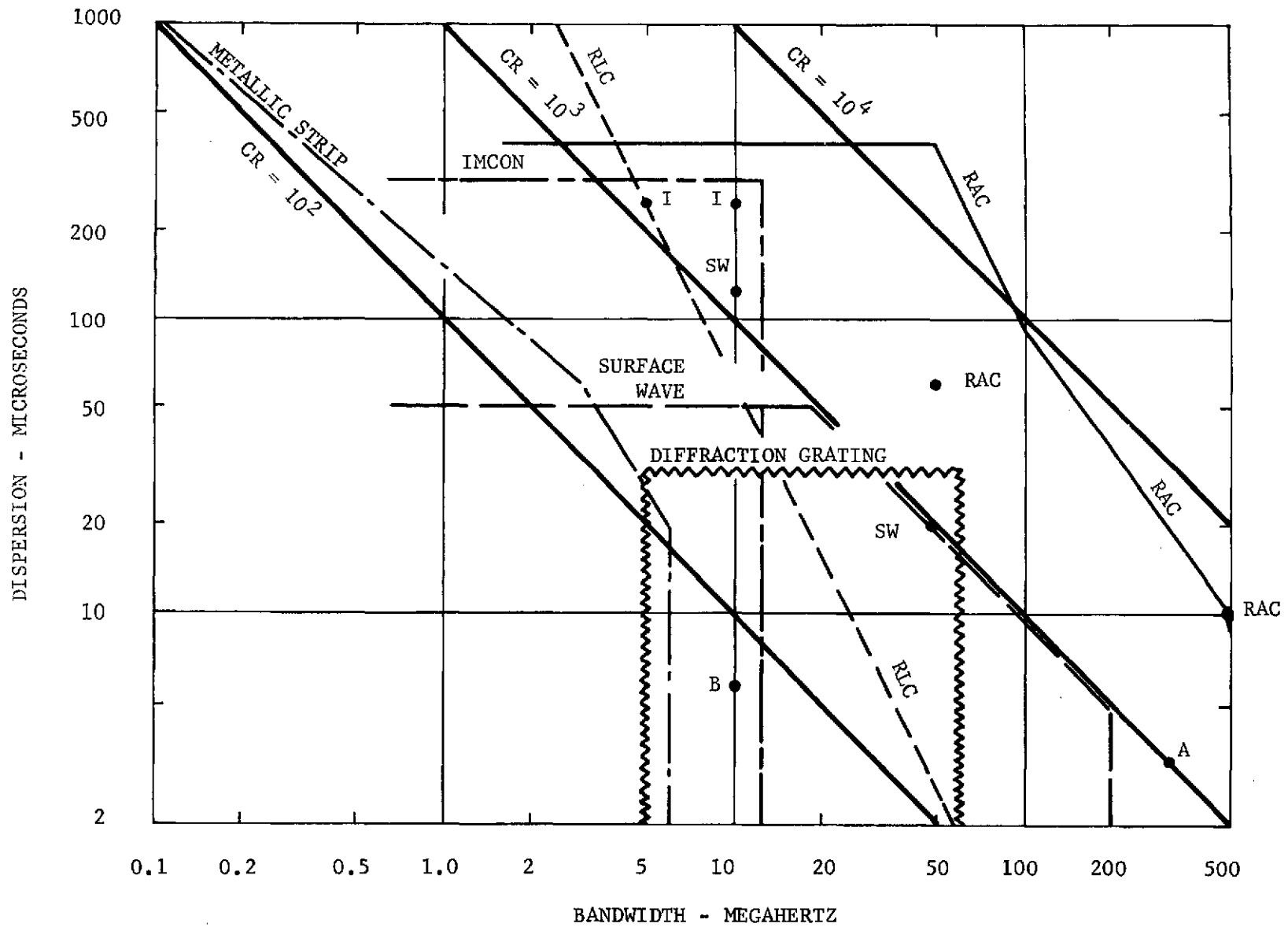


Figure 3.3-2 Operation regions of pulse compression techniques.

### 3.3.2 Reflective array compressor

The reflective array compressor (RAC) is a dispersive delay line which can be used to provide very high pulse compression ratios at large signal bandwidths. This device was originally developed at MIT's Lincoln Laboratory. The potential capability of this device is shown in Fig. 3.3-2. The present MIT line has a bandwidth of 50 MHz and a dispersion of 60  $\mu$ s, giving it a compression ratio of 3000:1. Newer developments are being conducted at MIT and elsewhere on shorter lines having up to 500 MHz bandwidth. (Section 3.3.2.1)

The technique used in the RAC is an extension of the IMCON dispersive delay technique developed at Andersen Laboratories. The basic difference is that the RAC uses surface waves instead of bulk waves in the acoustic medium. The difference relieves the RAC from the bandwidth limitation of the IMCON which is dictated by the thickness of the material, since the desired acoustic waves propagate on the surface.

The RAC represents a significant breakthrough in surface wave dispersive delay lines. The reason for this lies in the fact that the electroacoustic transducers are extremely simple, and are not involved in the dispersive properties of the device. The dispersive characteristics are provided by a "herringbone" grating etched into the surface of the medium. Previous surface wave dispersive lines have transducers which are very large (acoustically) and which determine the dispersive characteristics. For this reason, the amount of dispersion achievable in a single line has been less than 50  $\mu$ s, and more typically  $\approx$  10  $\mu$ s. (A 240  $\mu$ s line is presently under development). As can be seen from Fig. 3.3-2 the RAC is predicted to be capable of dispersions up to 300  $\mu$ s.

The RAC geometry is compared with the present IMCON bulk wave technique and the conventional surface wave technique in Fig. 3.3-3. Note the similarity of the RAC to IMCON, and also the simplicity of the RAC transducers compared to the conventional surface wave line. The RAC also requires a shorter length of material for the same dispersive delay than the conventional design.

Industry engineers are following the RAC development closely and some already have suggested improvements on the MIT design to overcome some of the potential limitations. For lines having the dispersion characteristics required by modern radars, these limitations are mainly: (1) acoustic loss, (2) temperature sensitivity, (3) spurious responses, and (4) dimensional tolerances. For this radar, the last item is the limiting factor because the wide bandwidth forces the line to operate at very short acoustic wavelengths.

### 3.3.2.1 Status of reflective array compressor RAC PC lines

MIT Lincoln Lab has recently completed 10 RAC surface wave lines with the following results:

Dispersion:	10 microseconds
Bandwidth:	512 MHz max
Weighting:	Hamming function
Output Pulse:	3.5 nsec/ $\frac{1}{2}$ power
Sidelobes* :	2 at -25 dB others below 30 dB
Insertion Loss:	55 dB without matching 45-50 dB with matching
Temperature:	45° C oven
Weight:	Line + matching and shielding (without circulators) = 0.91 kg

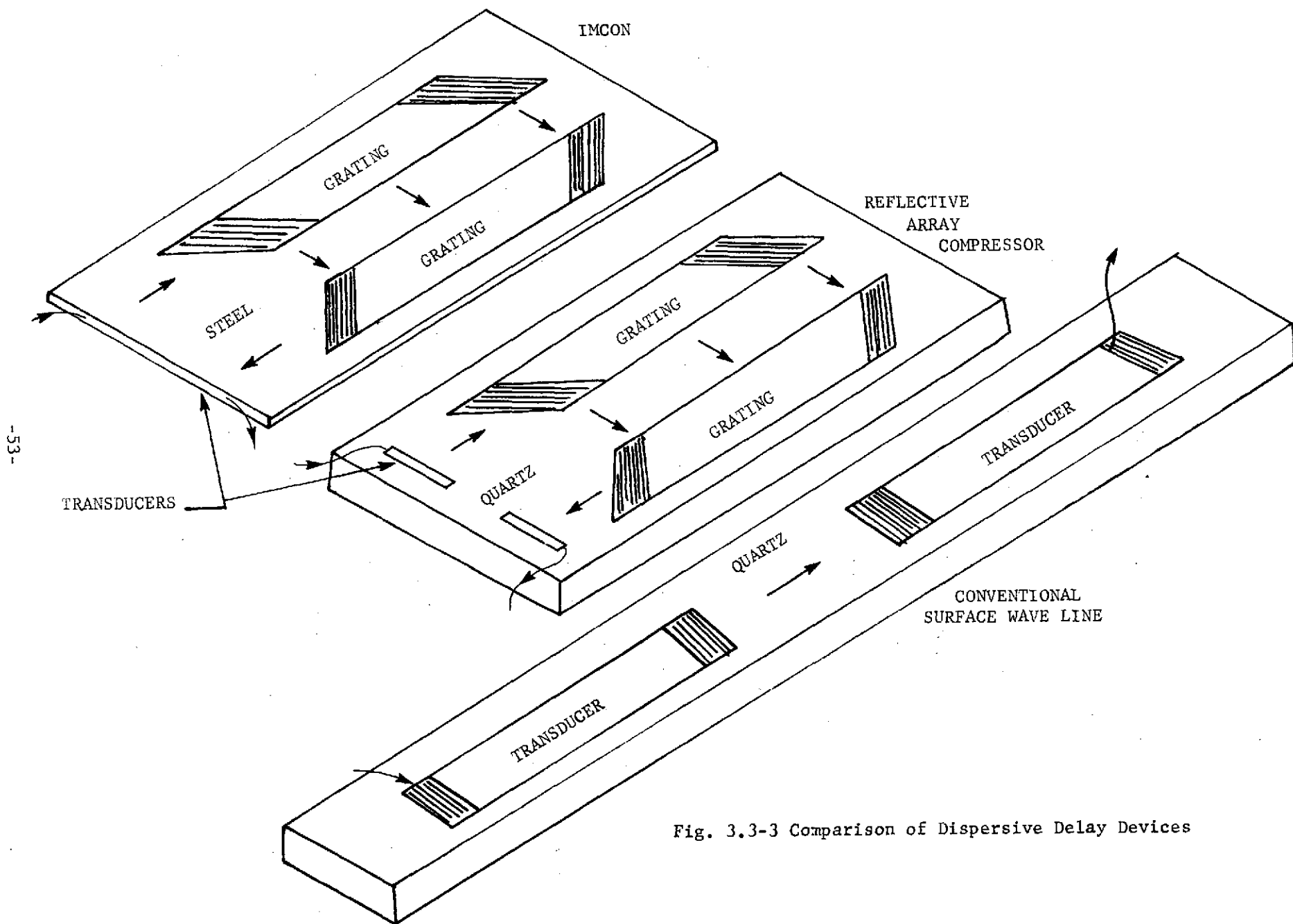


Fig. 3.3-3 Comparison of Dispersive Delay Devices

Temperature:  $\pm 1^{\circ}$  C for good operation  
Stability:  $\pm .01^{\circ}$  C for exact ranging

While these lines do not exactly meet the requirements of a satellite altimeter, they are close enough, and have the advantage of small weight and size as compared to the "multiplier configuration". MIT is willing to supply these lines to NASA with appropriate financial support.

It is felt that this type of configuration would be most suitable for a 1976-1980 satellite where weight and power would be a premium. Industrial companies (Hughes, etc.) should be able to supply sample lines within 18 months. These lines are appropriate for either full analog pulse compression or STRETCH techniques discussed in Section 3.5.

### 3.3.3 Alternate passive FM generators

Several alternate approaches to passive FM generation may be considered if the bandwidth is reduced. These include, in addition to the RAC: IMCON dispersive delay lines, perpendicular diffraction gratings, conventional surface wave lines. Each of these is discussed below.

#### 3.3.3.1 IMCON dispersive delay lines

Andersen Laboratories, a major dispersive delay line manufacturer has delivered "IMCON" delay lines having up to 10 MHz bandwidth, centered around a 20 MHz carrier frequency with dispersions of up to 250 microseconds. This line utilizes bulk wave propagation in steel. Construction of a line of 2.8 microseconds length (see point B, Fig. 3.3-2) should present no design problems. The "IMCON" type line has a linearity of about .01 percent of total

phase change. Its cost would be about \$10,000 each, with some reduction for several units. Thermal control is required for this line to prevent delay changes with temperature from affecting system performance. Heater power could be held to a few watts by close attention to design of an oven containing the line, as well as by controlling spacecraft thermal environment. The line could be packaged in about 10 by 10 by 5 cm including heater and oven. Driven with an impulse of 1 watt peak, the line would produce an expanded output of -30 dBm.

The bandwidth limitation of IMCON devices arises from two sources. First, the acoustic signal loss in steel increases strongly with carrier frequency. Second, spurious propagation modes can occur, if the line thickness is greater than one-half of an acoustic wavelength. Since the speed of sound in steel is approximately .318 cm per microsecond, a half-wavelength at 20 MHz is .0079 cm. This thickness of steel is about the minimum which can be obtained. The input/output transducers mounted on the edge of the line must be bonded very carefully for reliable operation.

For this radar application, an IMCON line with 10 MHz bandwidth would have a time-bandwidth product of only 28. Gating and limiting of this waveform would produce considerable distortion of the spectrum which may affect measurement accuracy. While TSC has not examined the effect of this distortion in detail, it is advisable to avoid it by selecting a line with a larger bandwidth.

#### 3.3.3.2 Perpendicular diffraction gratings (PPDL)

A line utilizing this technique is sketched in Fig. 3.3-4. Linear dispersion is attained by correct spacing of the transducer fingers. Several lines of this type have been in production. Their bandwidth and dispersion limits are shown in Fig. 3.3.-2.

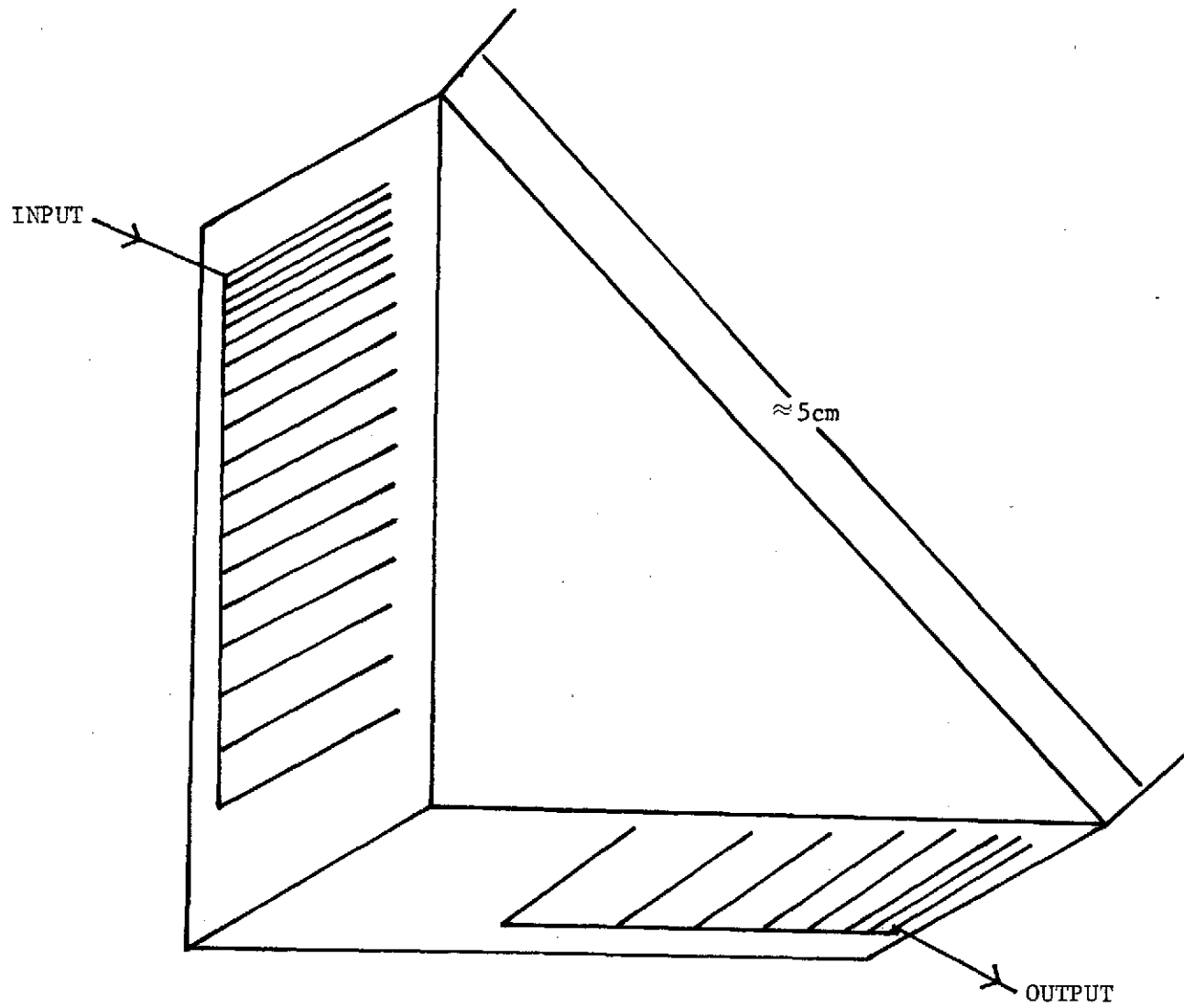


Fig. 3.3-4 Perpendicular diffraction grating delay line (linear FM).

A line having 3 microseconds delay and 60 MHz bandwidths has been built at a center frequency of 120 MHz, and this design could be readily modified to the 2.8 microseconds required by this radar. The time-bandwidth product of approximately 180 is high enough to eliminate the distortion problems of the IMCON, and the bandwidth is low enough to be feasible in practice. The perpendicular diffraction grating technique is a recommended candidate. The line would be fabricated using fused quartz, and would have dimensions approximately 2.5 x 3.8 x 1.3 cm. An oven would be required for temperature stabilization.

### 3.3.3.3 Surface wave lines

Several types of surface wave lines (including the RAC technique) are also feasible for signal bandwidths of 60 MHz and dispersions of 2.8 microseconds (see Fig. 3.3.-2). While the RAC type is preferred in terms of performance, the conventional designs may be more readily available. However, difficulties may be encountered in meeting linearity requirements with the conventional designs.

### 3.3.4 Status of other surface wave lines

A status report on surface wave lines for wide bandwidth pulse compression systems is given as a result of a visit to Hughes Aircraft, Fullerton, California\*. The primary system that Hughes has built is illustrated on Fig. 3.3-5 and has the following characteristics: [4]

100 MHz bandwidth	}	TB = 1000
10 microsecond dispersion		
300 MHz center frequency		
30-40 dB insertion loss		
60 dB dynamic range		

---

\* Dr. Tom Bristol, Ben Harrington, Hank Gerard (714-871-3232, X4756)



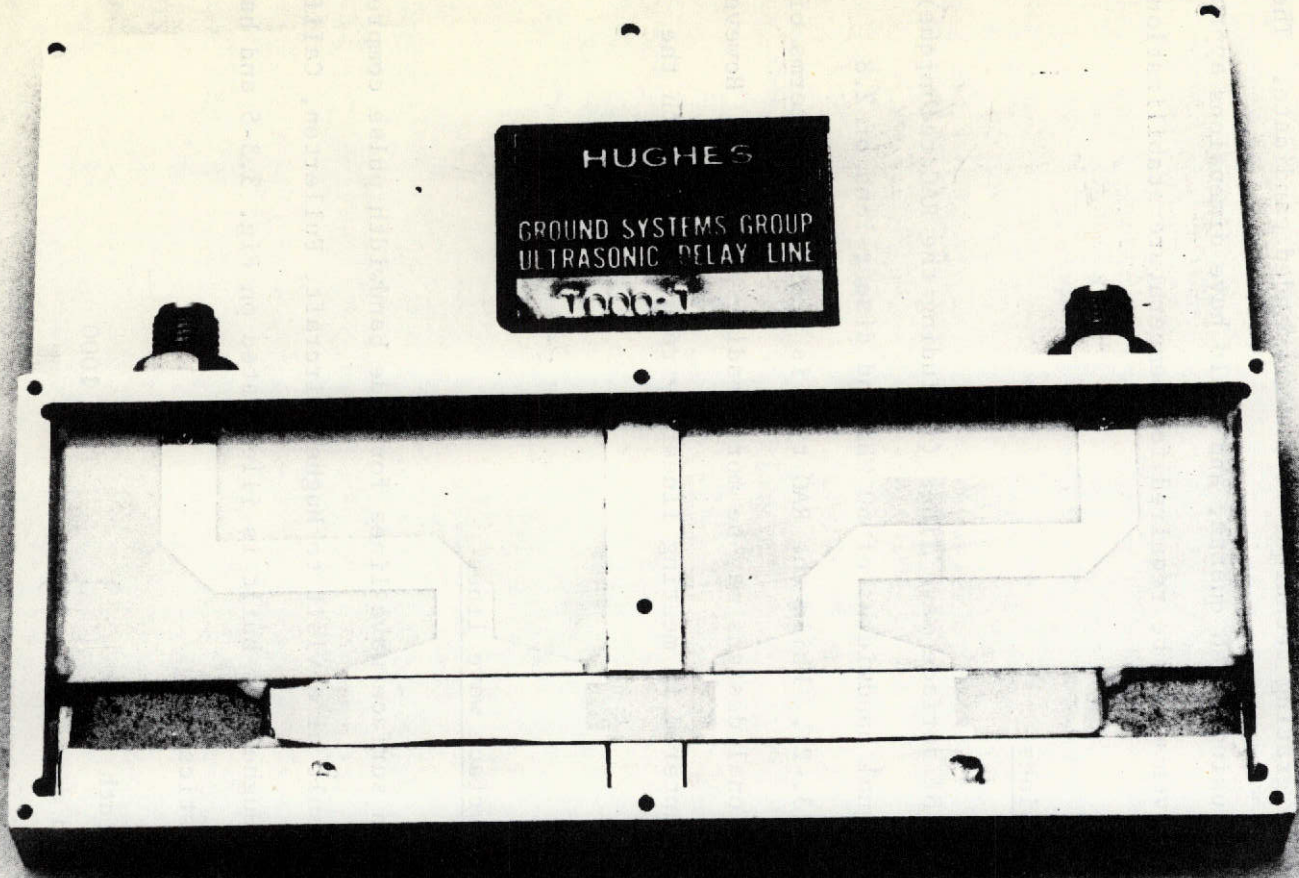
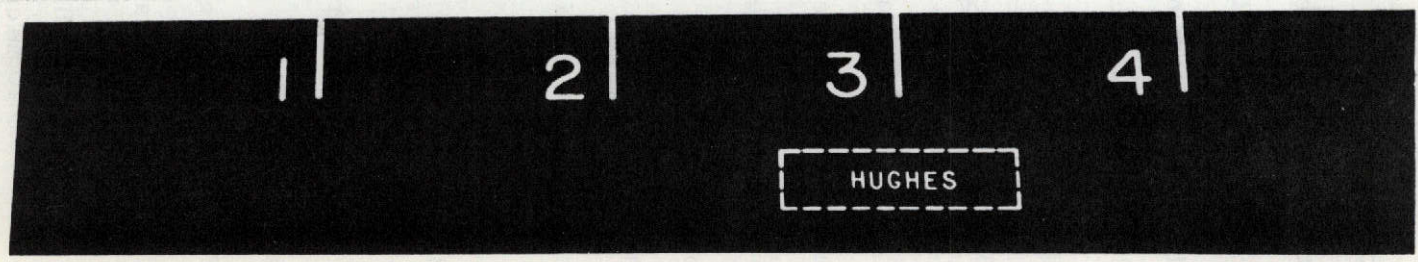


Figure 3.3-5



3600 0.1 MIL electrodes  
28 dB sidelobes (single line)  
22 dB sidelobes (double line)  
VSWR 1.3 to 1.5  
Size 7.6 cm by 10.2 cm

The primary tradeoff in these lines is between the lower losses of lithium niobate and the better velocity variation control and lower sidelobes of quartz lines. The quartz lines have about 26 dB more insertion loss. Lithium Niobate is used in the new RAC lines constructed at MIT.

With the newer photographic techniques and mesh fabrications, the following parameters would be available from Hughes Aircraft Company in the late 1973 period.

200-300 MHz bandwidth  
2-3 microsecond dispersion  
500 MHz center frequency  
40 dB losses (Li. niobate)  
60-70 dB loss (quartz)  
Plus or minus  $2\frac{1}{2}^{\circ}$  C yields 1.04 times Hamming  
pulse width, and 0.5 dB loss in S/N

It can be seen that 1000 to 1 compression ratios are relatively easily obtained. However, several companies will have capability for much better performance within the next six months to a year.

There is a procurement out of ECOM, Ft. Monmouth, to build a 250 MHz bandwidth line with 40 microsecond dispersion, 30 dB sidelobes, and 50 dB insertion loss. This is a compression ratio of 10,000 to 1 which is in excess of the likely altimeter requirements. Hughes has won this procurement and will likely be the first U.S. contractor capable of producing lines with the desired characteristics. This, of course, is in addition to the RAC work at MIT. It

is likely that Hughes Aircraft will have this capability within one year to 18 months. Discussions with Raytheon and Autonetics did not yield any additional capability.

These lines are, of course, essential to any Chirp system that might be proposed. They would also be used in a STRETCH type system.

### 3.4 Hybrid Pulse Compression Techniques

There are several hybrid pulse compression techniques that could be considered for altimetry. One possibility is to combine a linear FM ramp with a Barker Phase Code. For example, if a bandwidth of 330 MHz was required with a 3.3 microsecond dispersion, this could be accomplished with eleven phase coded segments of 600 nanoseconds duration. Each segment would then contain a 300 nsec to 3.0 nanosecond Chirp ( $TB = 100$ ). The transmit waveform would look like Figure 3.4-1-a and the decoded received waveform line Fig. 3.4.-1b for a point target. The time sidelobes would not be a problem if the Barker Code (length 7, 9, 11, 13) is used.

The receiver block diagram is shown on Fig. 3.4.-1-c. The signals are mixed to a convenient IF and successively pass through a dispersive line with a  $TB = 100$ , a weighting network to reduce close-in sidelobes, and a tapped delay line phase coder matched to the Barker Code.

The advantage of this technique is that the relatively simple pulse compression line ( $TB = 100$ ) is easily made with surface wave techniques. While the tapped delay line can also be constructed with surface wave devices at about 1 GHz center frequency, the tolerances are quite tight. At this point, it is felt that the technology will advance within the next two years to make this

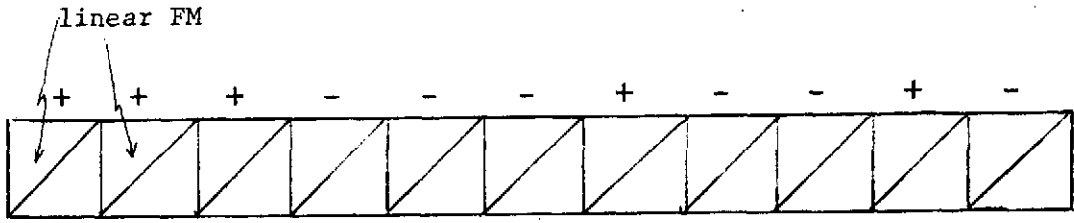


Figure. 3.4-1a Hybrid of Barker Code and Linear FM

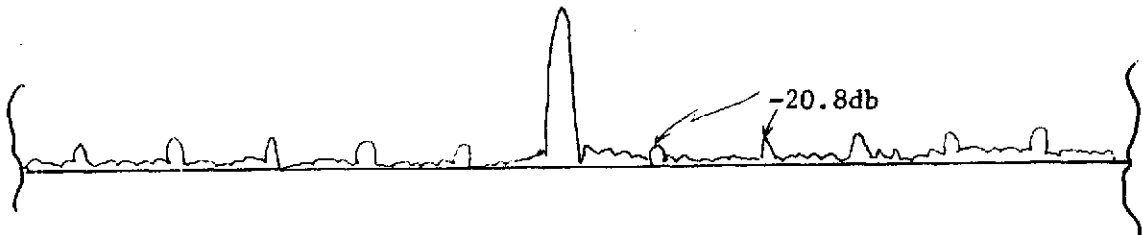


Figure 3.4-1b Detected Output Waveform for Point Target

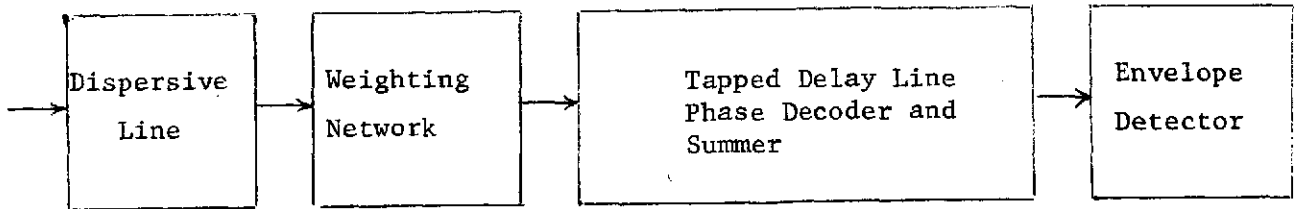


Figure 3.4-1c Receiver Block Diagram

Figures 3.4-1 A Hybrid pulse compression technique.

approach slightly more difficult than the "all chirp" system and it would only be recommended if surface wave lines of 360 MHz bandwidth with adequate TB were not available.

There are also several hybrids of digital and analog techniques that are practical in some circumstances but these generally require processing at the full bandwidth of the signal and hence with about 360 MHz bandwidth they are not generally attractive. The primary technique that might be applicable is a combination of STRETCH and digital pulse compression. If, for example, a 36:1 stretch were used with a 3.6 microsecond pulse, the received signal for about 100 nsec of echo would be available over a 3.6 microsecond period and the bandwidth would be 10 MHz. A digital pulse compression system could be implemented using FFT or similar techniques. There is some advantage in that flexibility is achieved but at too high a price in hardware complexity.

#### 3.4.1 Cross correlator

There is another possible use of the binary phased coded waveform in a tracking mode. It comes under the names of "cross-correlator", "delay lock discriminator" and others. A binary phase coded waveform with a known code and starting point is transmitted. The transmit code is stored and the code generator is started just before the expected target echoes (an "early gate"). The code is applied to the receiver local oscillator. The mixer output is then a decoded pulse if the target echo and the delayed code are in coincidence. A second delayed code (one bit additional delay) is applied to a second local oscillator and mixer for a "late gate". The difference in the "DC component" between the "early" and late gates is the time delay error signal and is used as a vernier on the "expected" time delay (altitude) the error signal looks like Fig. 3.4-2.

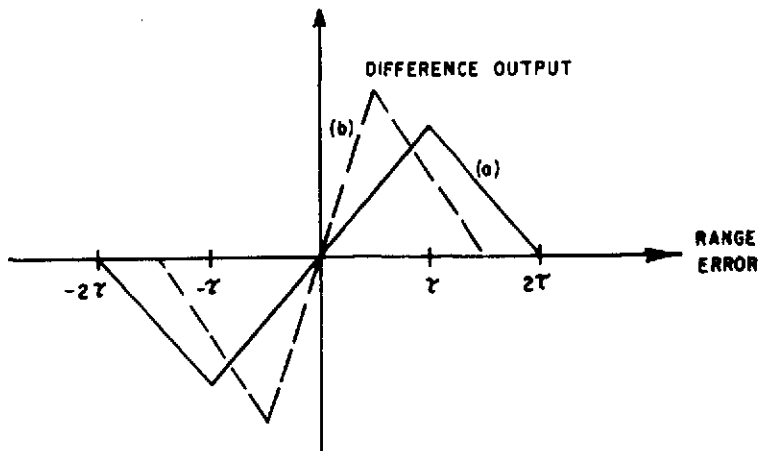


Fig. 3.4-2 EARLY-LATE INTEGRATOR DIFFERENCE OUTPUT Vs RANGE ERROR  
(UNFILTERED)

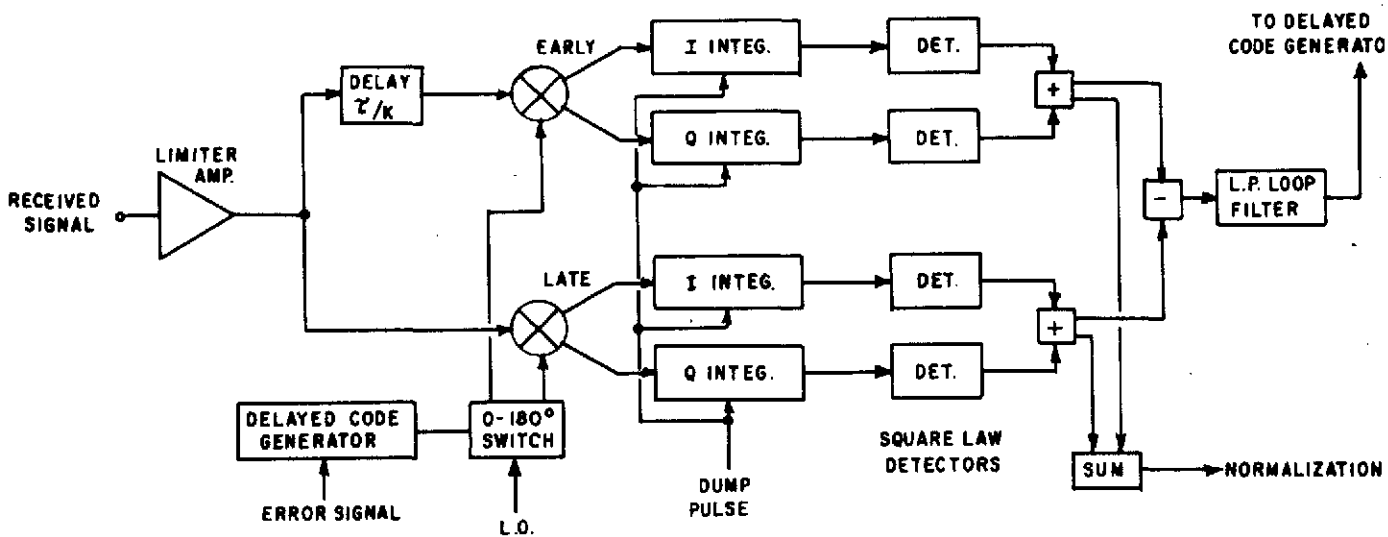


Fig. 3.4-3 SWITCHED L.O. LINEAR DECODER AND RANGE TRACKER, RANGE DETERMINED FROM CONTENTS OF DELAYED CODE GENERATOR.

The processing may be performed at IF or with bipolar video with the latter configuration shown on Fig. 3.4.-3. An accurate measure of time delay is available on a point target and compensation could be devised for the sea echo. The advantages are in the flexibility to change the code and hence the resolution and the absence of any dispersive line requirement.

This technique might be recommended if altimetry were the only goal. However, we do not get the full impulse response, and do not see an accurate method of wave-height estimation. It will not be considered further.

### 3.5 STRETCH-ALCOR Techniques

A strong candidate for the pulse compression system is the use of the STRETCH or ALCOR technique in order to reduce the A/D conversion requirement. In this approach the received signals are partially de-ramped by a linear FM de-ramp function which can be generated either by active or passive means. The difference frequency signals are now LFM signals with a reduced bandwidth. To compress these signals a dispersive delay line is required with a bandwidth and delay given by

$$BW = \frac{B}{SR} \left[ 1 + \frac{N_{RB}}{TB} (1 - SR) \right]$$

$$TD = T \left[ 1 + \frac{N_{RB}}{BT} (1 - SR) \right]$$

In these equations,

B = transmitted chirp bandwidth

SR = desired STRETCH ratio

$N_{RB}$  = number of range bins to be stretched

T = transmitted chirp pulse duration

The results of the STRETCH operation are compressed pulses whose compressed pulse lengths have been increased from  $\frac{1}{B}$  to  $\frac{SR}{B}$ . After the STRETCH process, envelope detected outputs may now be sampled by an A/D converter operating on the reduced bandwidth pulses. This represents one technique for avoiding the use of high speed converters operating at the full bandwidth B.

### 3.5.1 Methods of implementation

There are several ways in which STRETCH or ALCOR can be implemented. A general block diagram is shown on Fig. 3.5-1, and the variations include

- 1) Passive Generation (dispersive line) with passive generation of a ramp at another slope
- 2) Passive Generation with the same slope on receive with a filter bank for the "range gates"
- 3) Active Generation (swept oscillators) on transmit with a passive dispersive line for compression
- 4) Active Generation with an active swept oscillator on receive

All of these methods have been tried and the choice depends on the flexibility desired and the complexity allowed. For example, the use of passive dispersive lines on receive, 2), does not allow a variable slope to examine a variable range window. In the active generation technique, more complexity is required if the transmit and receive slopes are different.

One example, that demonstrates the feasibility of building a system with the parameters of interest, is the MIT ALCOR system shown on Fig. 3.5-2. A transmit waveform of almost 500 MHz bandwidth and 10 microsecond dispersion is achieved by multiplying the output of a dispersive line by a factor of 42 from approximately an 11.8 MHz ramp to a 493 MHz ramp. This ramp is mixed with



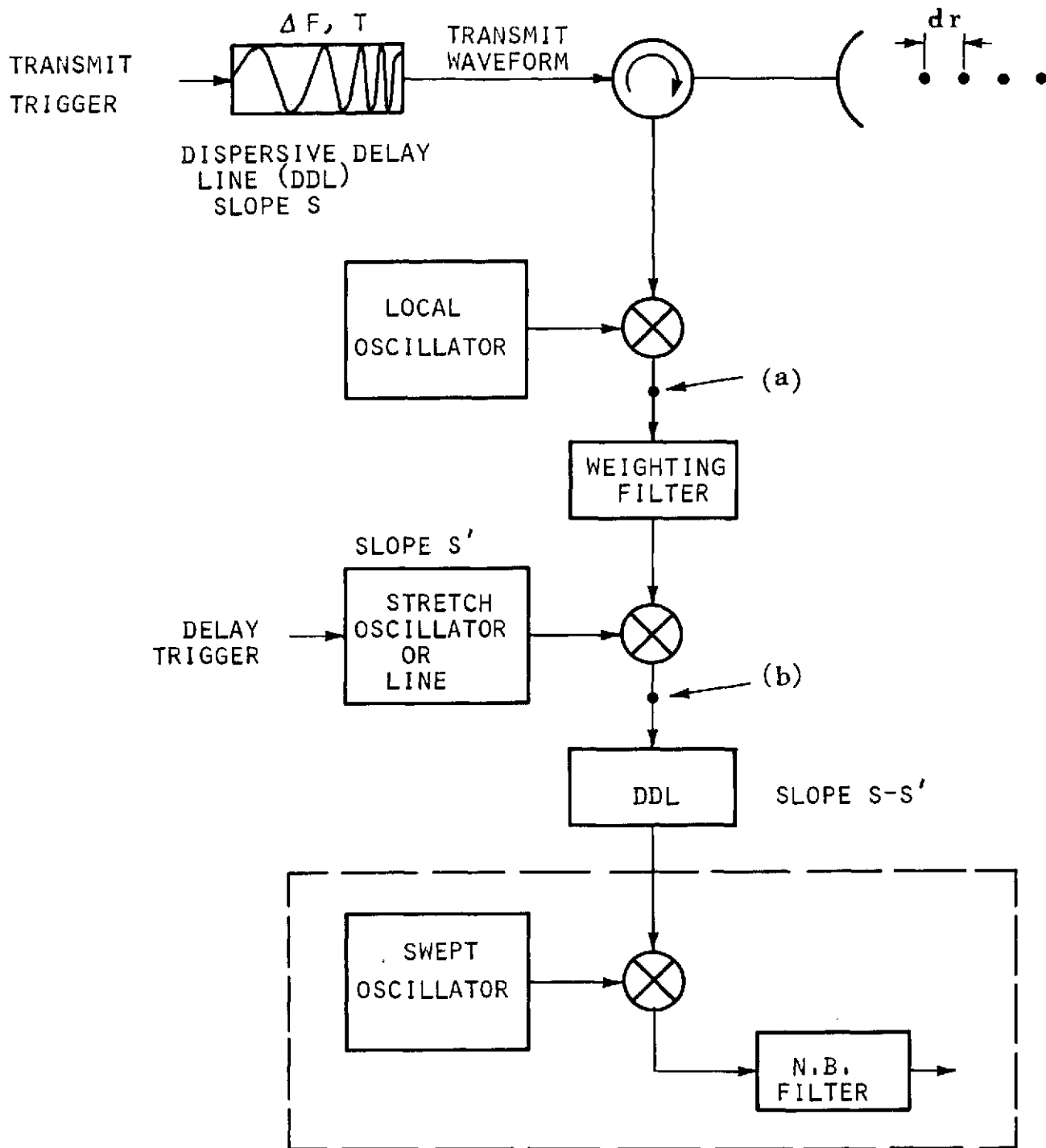
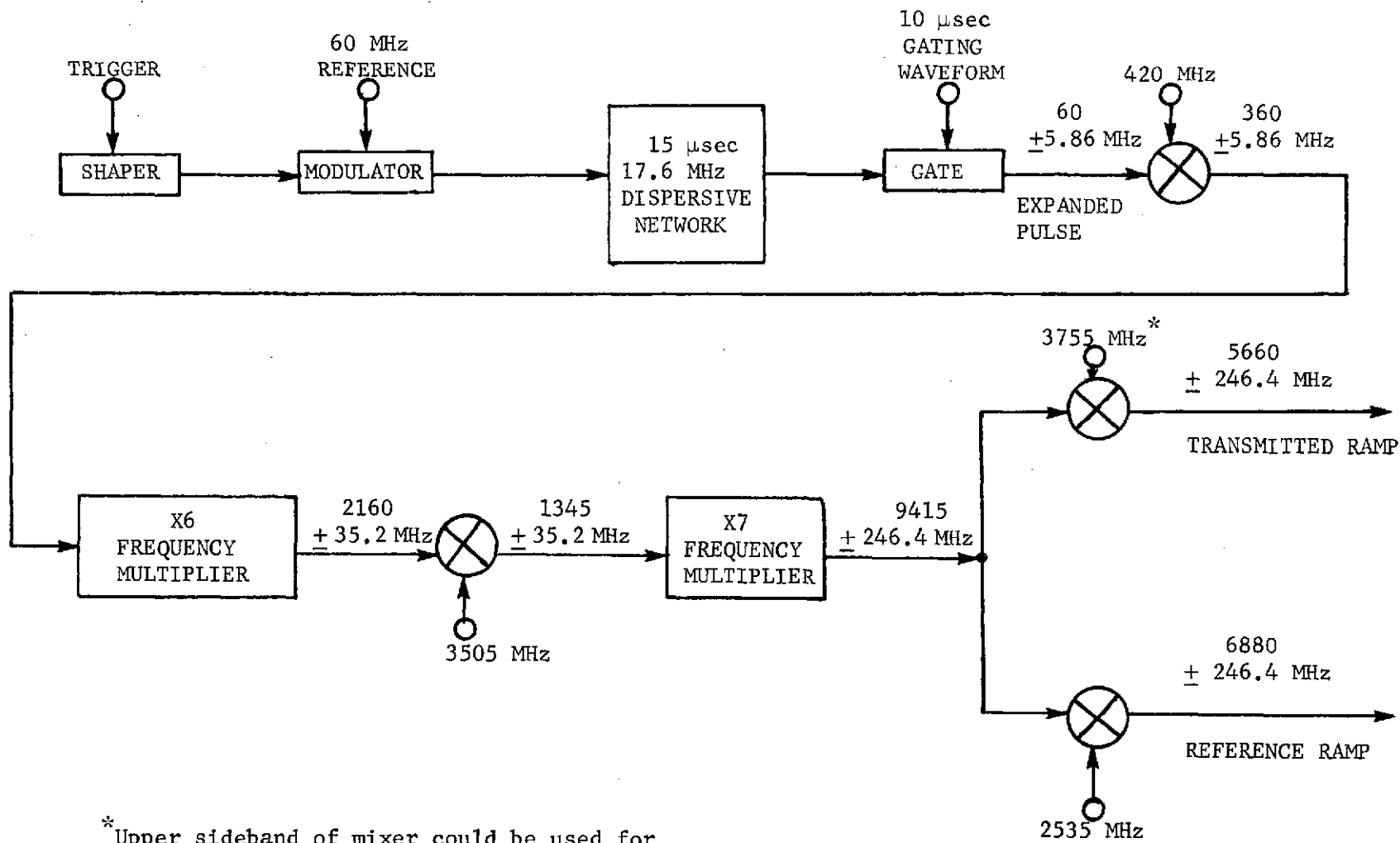


Figure 3.5-1

BASIC STRETCH BLOCK DIAGRAM



\*Upper sideband of mixer could be used for Transmission at 13,270 MHz.

Figure 3.5-2 Elements of the wideband ramp generator implemented for ALCOR. Project Report RDT-13, Lincoln Lab MIT, 20 July 1967.

a local oscillator for transmission and another local oscillator for a "reference ramp". A resolution of 0.5 meters was achieved and sidelobes were expected to be in the 30 to 35 dB range.

### 3.5.2 Dispersive line and A/D requirements for STRETCH

The design equations for STRETCH were used to compute the required dispersive line bandwidth (BW) and time delay (TD) required as functions of the STRETCH ratio (SR). Results were obtained for a range window corresponding to 60 contiguous range cells. For  $B = 360$  MHz and  $T = 2.8$   $\mu$ sec, the curves of Fig. 3.5-3 were obtained. Also, the required A/D conversion rate  $f_s$  vs STRETCH ratio was obtained, and is shown in Fig. 3.5-4. The parameter  $K$  represents the oversampling ratio of the compressed and stretched output pulses.  $K = 1$  represents taking one sample per output pulse width. Since the compressed pulse width before STRETCH is  $\frac{1}{B}$ , the pulse width after STRETCH is  $\frac{SR}{B}$ . For  $K$  samples per output pulse, we get

$$f_s = \frac{KB}{SR}$$

If it is desired to keep  $f_s$  below 1 MHz (to simplify A/D requirements), then one should use a STRETCH ratio of about 400-1000.

One might assume that for  $SR = \infty$ , the samples could be taken as slowly as desired. Note, however, that in this case of complete deramping, it is required that range cells be separated by filters of bandwidth  $1/T$ . If these filters are to be formed digitally, the deramped spectrum must first be A/D converted. Since for the baseline parameters this spectrum has a total bandwidth of 11.5 MHz (30 range cells, separated in frequency by .385 MHz for  $T = 2.8$   $\mu$ sec), a sampling rate of  $f_s = 11.5$  MHz for the A/D would be required

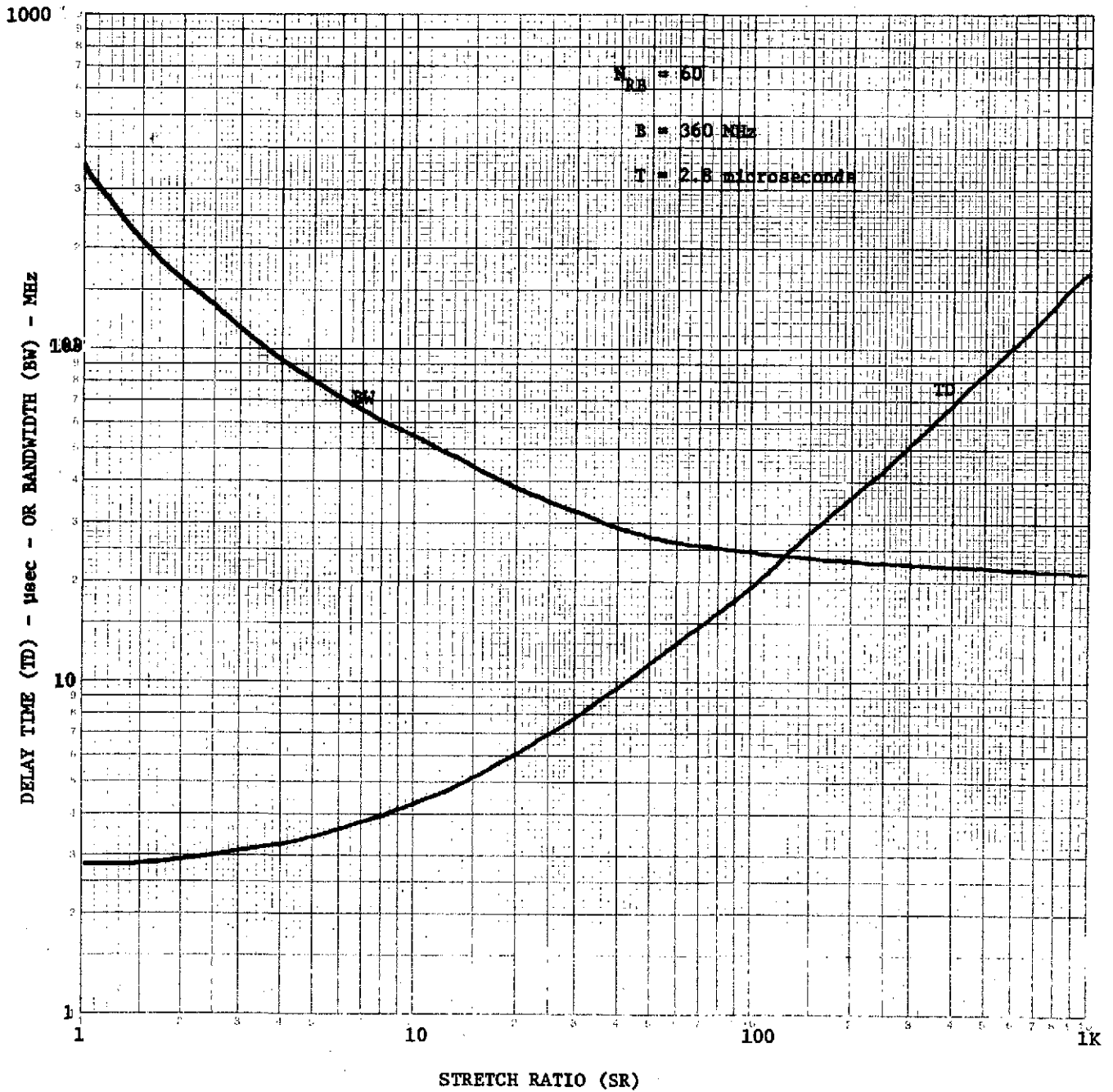


Fig. 3.5-3 Bandwidth and Delay Requirements for STRETCH Dispersive Line

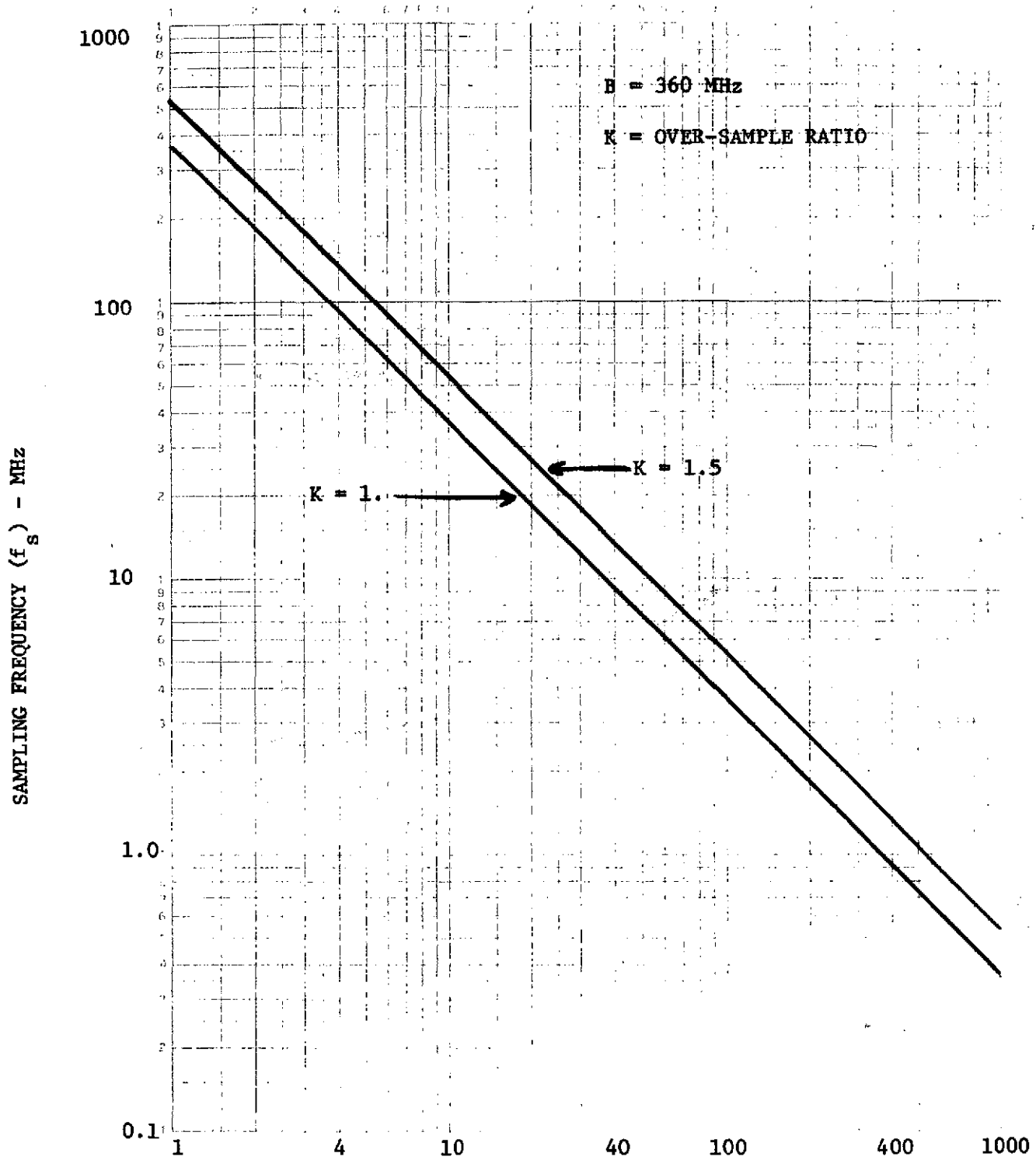


Fig. 3.5-4 STRETCH RATIO (SR)

Sampling Rate vs STRETCH Ratio

for this case. If analog filters are used, the A/D conversion takes place after filtering and (with multiplexing) the sampling rate can be less than 1 MHz.

### 3.5.3 Recommended techniques

An examination has been made of the following cases:

1. Dispersive line pulse compression with  $SR = 1$  (Both passive and active pulse generation).
2. STRETCH pulse compression for  $SR > 1$ , followed by A/D conversion. (Both active and passive generation of the transmit and the receive deramp signals).
3. Full deramp followed by a filter bank to separate range returns. (Both analog and digital filtering are being considered).

The first case is just linear FM without STRETCH and has been described in Section 3.3. This method was rejected because of the A/D requirements in digitizing a 300 MHz signal. The choice between the second and third case is made on the basis of simplicity. STRETCH pulse compression for  $SR > 1$  requires the generation of 3 different linear FM waveforms (one for transmit and two for receive deramp signals, see Fig. 3.5-1) whereas full deramp can be achieved with a single dispersive network. The accuracy and tolerance problems associated with matching three linear FM waveforms are an added incentive for rejecting STRETCH pulse compression for  $SR > 1$  (Case 2). For the full deramp case the analog filter bank is preferable to digital filtering, because of the reduction in bandwidth requirements on the A/D converter as described in Section 3.5.2.

In summary then, the recommended pulse compression technique is a full deramp method followed by an analog filter bank to separate range returns. Considerations concerning the implementation of such a scheme are presented in the next section.

### References

- [1] Nathanson, F. E., Radar Design Principles, McGraw Hill, 1969, Chap. 12.
- [2] Bristol, T. W., et. al, "Further Applications of Double Electrodes in Acoustic Surface Wave Devices", IEEE-GMTT International Microwave Symposium.
- [3] Ebersol, E. T., "Acoustic Devices Get Exciting", Microwaves, Nov. 1972, pp. 12-13.
- [4] Gerard, H. M., et. al, "The Design and Applications of Highly Dispersive Acoustic Surface Wave Filters", Hughes Aircraft, Fullerton FR72-14-1025, 12 September, 1972.
- [5] Zinger, W. H., "Characteristics of MECL II Logic Elements for an 80 Mc, 2-Bit Signal, 2-Bit Code Digital Correlator", APL/JHU, MRT-6-008, 12 September, 1968.

In this section recommendations are made concerning the implementation of the selected pulse compression technique. Included are the method of FM generation and range processing. An analysis showing the accuracy with which the ramp and deramp functions must be generated is also given.

The state-of-the-art of pulse expansion/compression devices was described in Section 3.3. For the 360 MHz, 2.8  $\mu$ sec requirement (compression ratio = 1000), it was shown that the reflective array compressor (RAC) technique is the preferred method (see point A, Fig. 3.3-2.) However, since this is a new invention, procurement would be required from MIT Lincoln Lab. Because there are presently no established vendors of the RAC line, this approach would involve some development risk if obtained from industry. Therefore, an equipment configuration using a lower bandwidth delay line followed by frequency multiplication is indicated for the "baseline design".

The approach recommended for FM generation is to use a passive dispersive line with a bandwidth of 60 MHz. The vendor of the line would be free to use any of the techniques discussed, depending upon his experience and design capability. While TSC would prefer to see the implementation using RAC, PPDL, and conventional surface waves in that order, all approaches should be capable of meeting the specifications.

The delay line output is translated to a higher frequency by mixing with a 2.33 GHz carrier and selecting the upper sideband output. This operation reduces the fractional bandwidth of the FM signal and prevents spectral overlap



in the ensuing X6 multiplication process. Standard multiplier designs as well as several commercially produced multiplier assemblies are available. The output of this multiplier chain will be a maximum for a 2.8 microsecond long linear FM ramp of 360 MHz bandwidth centered at 14.7 GHz. An RF switch directs the ramp to either the transmitter or receiver chain in response to a control signal from the central timing unit. The dimensions of the line would be approximately 2.5 x 3.8 x 1.3 cm plus an oven.

#### 4.2 Range Processing

In the full-deramp system, a contiguous comb filter set is required for processing of the gated and shaped return signal. Total signal bandwidth of the comb set is 11.5 MHz and at least 30 range bins are required within this band; maximum bandwidth per filter, therefore, is 385 kHz. Center frequency is open and may be chosen to give optimum filter performance.

Four possible filtering methods are available:

1. Passive LC filters
2. Active filters
3. Discrete crystal filters
4. Monolithic crystal filters

Features of each of these approaches are listed in Table 4.2-1.

The requirements placed upon the filter set are rather minimal. The quality factor, or Q, which is the primary determinator in filter feasibility, is only 50. Input signal level can be made sufficiently high that ultra-low filter losses are unnecessary. Furthermore, since only 30 range bins are required, size is not a major factor.

TABLE I. Features of Filter Approaches

	<u>PASSIVE LC FILTERS</u>	<u>ACTIVE FILTERS</u>	<u>DISCRETE CRYSTAL FILTERS</u>	<u>MONOLITHIC CRYSTAL FILTERS</u>
Power Consumption including Input Amplifier	LOW	HIGH	LOW	LOW
Size	Large	Larger	Medium	Small
Reliability	Good Many passive components	Fair Many active and passive components	Good Few components Proven crystal reliability	Probably Good Few components Monolithic Construction but unproven
Calibration Effort	Large Many Adjustments	Large Many Adjustments	None No Adjustments	Small Only Frequency Shift requires Adjustment
Parts Cost	Low	Medium	Medium	Highest* Possible Modifications of Monolithic Masks
Design Risk	Low	Medium	Low	High*

\*Both risk and cost of monolithic filter may be smaller in 1980 time-frame

To work at the rather wide bandwidths (about 2%) required in this system, crystal filters, both monolithic and discrete, would require paralleling. Since crystal filters at the required I.F. are limited to approximately 100 kHz bandwidth, four filters would be paralleled for each range bin. This would be possible, but the advantages of crystal filters -- size, weight, and reliability -- would not be realized.

Both active and passive filtration would be feasible at these frequencies. Indeed, to a first approximation, active and passive filters have the same A-C characteristics. Active filters, however, would consume power. If each active filter were to need only 100 milliwatts of D-C power, then the comb filter set would require about 3 watts. While this figure is entirely reasonable for a ground or airborne system, it is not at all desirable in a spacecraft.

The contiguous comb filter set baseline design, therefore, is chosen as passive L-C filtration. A major disadvantage of this scheme is that adjustments would be required. Calibration time for the airborne system would be relatively large, and the spacecraft system would require further effort in either selecting fixed components to replace adjustable ones or in fixing the adjustments immovably. Filter reliability would be excellent, however. Only low-failure-rate passive components would be required, none of which would be electrically stressed to any significant degree.

The contractor would have the option of either building these filters or buying them from an outside company. Many manufacturers make L-C comb sets as a standard product line. Alternately, many aids exist for internal filter design.

Following the filter bank, detectors and a means of sampling the detector outputs will be required. Simple diode detectors may be used on the filter outputs;

analog multiplexers will then follow these detectors. Inaccuracy due to droop on the detector outputs may be circumvented by using FET multiplexers with very large OFF resistance and following the multiplexer output with a fast sample-and-hold amplifier. This scheme allows extended sampling of the filter outputs during as much as the full pulse repetition interval, and therefore permits very light, low-cost analog-to-digital conversion for data transmission. All devices used in the detector are light-weight and low power units. Most are made as integrated circuits. Indeed, many such devices are already NASA-qualified and/or MIL-qualified. In addition to the units already described, some timing and logic will be required for clocking the multiplexers and the A/D conversion chain.

#### 4.3 Ramp/De-Ramp Generation Requirements

This section will present an analysis of the accuracy with which the ramp and de-ramp functions must be generated. It must be kept in mind that since pulse-to-pulse processing is not employed, the accuracy requirement need only be imposed on a single pulse basis. After a ramp is generated (either actively or passively) and transmitted, a de-ramp signal will be required within a time interval less than 1 millisecond which matches the ramp function within some accuracy. The following analysis will determine this required degree of matching of the two functions and the linearity requirement which both must achieve.

Consider the transmit pulse which ideally would be a linear FM signal of duration T seconds and bandwidth B Hz. We will model the actual ramp as a signal whose frequency versus time is given by

$$f_1 = \dot{f}_1 t + \Delta f_1 \sin \omega t$$

where

$$\dot{f}_1 = \text{slope of ramp}$$

$$\Delta f_1 = \text{peak frequency error (deviation from ideal ramp)}$$

$\omega$  = modulating frequency of error

Note that  $\frac{\omega T}{2\pi}$  = number of cycles of sinusoidal frequency error across the transmit pulse.

Next consider the de-ramp signal. This signal will be initiated at the expected time of the first return. Since the last target return of interest will be received a maximum of  $\Delta t$  seconds after the first, ideally the de-ramp signal duration should be  $T + \Delta t$  seconds. However, since  $T = 2.8 \mu\text{sec}$  and  $\Delta t \sim 140 \text{ nsec}$ , the de-ramp signal could also be  $T$  seconds long with little loss of received energy. The de-ramp signal can be written

$$f_2 = \dot{f}_2 (t - \Delta t) + \Delta f (t - \Delta t) + \Delta f_2 \sin \omega(t - \Delta t)$$

In this equation we have allowed the de-ramp to differ from the received signal in four ways:

1. it can have a different slope, to allow for partial de-ramp (STRETCH),
2. it can have a slope error  $\Delta f$ , which could arise if the ramp and de-ramp were generated by separate techniques or separate circuits,
3. it can have a different amplitude of frequency error,  $\Delta f_2$ ,
4. it can have a delay error  $\Delta t$  which will vary from zero to about 140 nanoseconds, for the first and last target returns respectively.

After mixing the received signal with the de-ramp signal and retaining only difference frequency terms, we obtain the following signal

$$f_1 - f_2 = (\dot{f}_1 - \dot{f}_2)t + \dot{f}_2 \Delta t - \Delta f t + \Delta f \Delta t \\ + [\Delta f_1 \sin \omega t - \Delta f_2 \sin \omega(t - \Delta t)]$$

These five terms will be analyzed separately to determine their effects on the range response of the pulse compression system.

### First Term

This term is a residual LFM term which will be required whenever STRETCH is used. The slope  $\dot{f}_1 - \dot{f}_2$  is assumed to be precisely matched to the STRETCH dispersive line. The effect of a mismatch is included in the third term and will be analyzed there.

### Second Term

The  $\dot{f}_2 \Delta t$  term represents the desired frequency shift due to the range difference between the first target return and one displaced from it by a distance corresponding to  $\Delta t$  seconds. In the case of full de-ramp, for example, this term represents the conversion of range displacement to frequency displacement. Adjacent range cells are thus detected separately in the outputs of adjacent filters.

### Third Term

If the slopes of the ramp and de-ramp functions are in error, the signals after de-ramp will contain an error frequency term which is linear with time. This gives rise to quadratic phase effects which degrade range resolution and range sidelobes. Exact computer simulations of the system impulse response show that one can allow about  $\pi/2$  of quadratic phase to build up from center to end of the pulse duration without significant degradation of the range resolution or sidelobe levels.

### Slope Accuracy of Generating $\dot{f}_1$ or $\dot{f}_2$

The accuracy is determined on the basis of allowing  $\pi/2$  quadratic phase to accumulate (center-to-end) due to an error  $\Delta f$ . Consider a signal

$$f = (\dot{f} + \Delta \dot{f})t \quad \left(-\frac{T}{2} < t < \frac{T}{2}\right)$$

Then the quadratic phase error due to  $\dot{\Delta f}$  is given by

$$\begin{aligned}\Delta\phi &= 2\pi \int_0^{T/2} \dot{\Delta f} t dt \\ &= \frac{\pi}{4} \dot{\Delta f} T^2\end{aligned}$$

Setting  $\Delta\phi = \pi/2$ , we find

$$\dot{\Delta f} = \frac{2}{T^2}$$

Note that  $\dot{f} = \frac{B}{T}$

Expressed as a percent error in slope  $\dot{f}$ , we find from the above

$$\frac{\dot{\Delta f}}{\dot{f}} = \frac{2}{BT}$$

For  $B = 360$  MHz,  $T = 2.8$   $\mu$ sec,

$$\frac{\dot{\Delta f}}{\dot{f}} \approx 0.2\%$$

Total excursion  $\Delta f$  is given by

$$\Delta f = \dot{\Delta f} T = \frac{2}{T} = .714 \text{ MHz}$$

Hence, if we wish to sweep from zero to 360 MHz, the end point frequency can be  $360 \pm 0.714$  MHz.

#### Fourth Term

The term  $\dot{\Delta f} \Delta t$  represents a constant frequency shift which will give rise to a range measurement error. In order to make its effects negligible, we can require that the frequency shift correspond to no more than one-tenth of a range resolution cell. Since one range cell translates to a frequency shift of  $\frac{1}{T}$  Hz in the case of complete de-ramp (i.e., adjacent filters are spaced by  $\frac{1}{T}$  Hz), we will impose the constraint

$$\dot{\Delta f} \Delta t \leq \frac{1}{10T}$$

Note, however, that the quadratic phase constraint has already led to the relationship

$$\dot{\Delta f} = \frac{2}{T^2}$$

Hence using this allowable value of  $\dot{\Delta f}$  in the above gives rise to

$\frac{\Delta t}{T} \leq \frac{1}{20}$ . For our baseline design,  $\Delta t = 140$  nanoseconds and  $T = 2.8$   $\mu$ seconds.

Hence, we conclude that if the quadratic phase constraint is met, the frequency shift due to the fourth term will not degrade the achievable range measurement accuracy significantly.

#### Fifth Term

The fifth term, due to an assumed sinusoidal deviation of the ramp or de-ramp function from ideal linear FM waveforms, can be rewritten in the form

$$f = \Delta f \sin(\omega t + \theta)$$



Where

$$\Delta f = \sqrt{(\Delta f_1 - \Delta f_2 \cos \omega \Delta t)^2 + (\Delta f_2 \sin \omega \Delta t)^2}$$

$$\theta = \tan^{-1} \frac{\Delta f_2 \sin \omega \Delta t}{\Delta f_1 - \Delta f_2 \cos \omega \Delta t}$$

Examination of the above will show that if  $\Delta f_1 = \Delta f_2$ , then  $\Delta f$  will range between zero and  $2\Delta f_1$ . With little loss in generality of results, we can ignore the constant phase angle  $\theta$  and consider the worst case example of a frequency error

$$f = \Delta f \sin \omega t$$

#### Sinusoidal Frequency Error

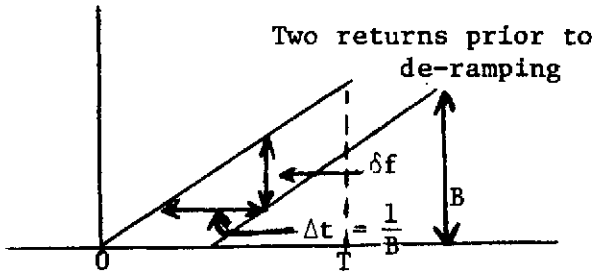
The phase error associated with this frequency error is given by

$$\Delta \phi = 2\pi \int \Delta f \sin \omega t dt = \frac{2\pi \Delta f}{\omega} \cos \omega t$$

The peak value of this phase error is

$$\Delta \phi_p = \frac{2\pi \Delta f}{\omega} = \frac{\Delta f}{f_m} \quad f_m = \text{modulation frequency, i.e. } \frac{\omega}{2\pi}$$

For a system utilizing full de-ramping, we integrate the de-ramped signal for a time T seconds, to form a filter of -4 dB bandwidth  $\frac{1}{T}$ . This filter has a  $\sin x/x$  shape with its first null at  $\frac{1}{T}$ . Adjacent filters are spaced  $\frac{1}{T}$  Hz, in order to compress pulses separated by  $\Delta t = \frac{1}{B}$  (see sketch below):



Note  $f = \frac{B}{T}$

$$\frac{\delta f}{\Delta t} = \frac{B}{T}$$

so  $\delta f = \frac{B\Delta t}{T}$

For  $\Delta t = \frac{1}{B}$ ,

$$\delta f = \frac{1}{T}$$

If after de-ramping we get a CW pulse of length T which has a small residual sinusoidal phase shift of peak value  $\Delta\phi_p$  due to a sinusoidal frequency error in the de-ramping signal, then paired echos in the filter output response will be created of value  $\frac{\Delta\phi_p}{2}$  relative to peak response and displaced from it by  $\pm f_m$  the modulating frequency of the error. For one cycle across the de-ramped pulse,  $f_m = \frac{1}{T}$ . For N cycles,  $f_m = \frac{N}{T}$ . If we wish to keep this sidelobe response (which is equivalent to a range sidelobe) less than 23 dB, for example, we need

$$20 \log_{10} \frac{\Delta\phi_p}{2} = -23$$

so

$$\Delta\phi_p = 0.14$$

Hence

$$\Delta f = 0.14 f_m$$

For  $f_m = \frac{1}{T}$  (probably the lowest, or worst case value),

$$\Delta f = \frac{0.14}{T} = \frac{0.14}{2.8 \times 10^{-6}} = 50 \text{ kHz}$$

Since in the worst case,  $\Delta f = 2\Delta f_1$  we obtain  $\Delta f_1 = 25 \text{ kHz}$ . This is the allowable peak sinusoidal frequency deviation from a straight line for the case of one cycle variation across the pulse. For higher frequency variation, the allowable peak error increases. For 10 cycles across the pulse,  $f_m = \frac{10}{T}$ ,  $\Delta f = 500 \text{ kHz}$ , and  $\Delta f_1 = 250 \text{ kHz}$ .

#### 4.3.1 Summary

The following summarizes the conclusions reached regarding the required accuracy of generating the ramp and de-ramp functions. Those conclusions apply to either active or passive generation techniques.

1. The ramp and de-ramp functions must have slopes which meet the following linearity requirements:

##### a. Full De-Ramp

$$\dot{f}_1 - \dot{f}_2 \leq \Delta \dot{f}$$

##### b. STRETCH

$$(\dot{f}_1 - \dot{f}_2) - \dot{f}_0 \leq \Delta \dot{f}$$

where  $\dot{f}_0$  = design slope for selected dispersive  
STRETCH line

In both cases, the tolerances on  $\Delta \dot{f}$  are given by  $\Delta \dot{f} = \frac{2}{T}$ . For the selected design (full de-ramp) this leads to a percent linearity requirement of

$$\frac{\Delta \dot{f}}{\dot{f}} \leq 0.2\%$$

2. If (1) above is met, then the range measurement error due to the  $\Delta f \Delta t$  term will be negligible for the selected baseline system.
3. To keep slowly varying frequency deviations from degrading sidelobes, the peak allowable frequency deviations are:
  - a.  $\Delta f_1 < 25$  kHz (one cycle of variation across pulse)
  - b.  $\Delta f_1 < 250$  kHz (ten cycles of variation across pulse)

When  $\frac{\omega T}{2\pi} < 1$ , these very slowly varying frequency deviations begin to look like slope errors and are essentially accounted for by the specification on  $\Delta f$  in (1) above.

## PART II

### SUPPORTING STUDIES

#### 1.0 INTRODUCTION AND SUMMARY

In Part I, the design of a high resolution satellite altimeter was discussed. During the design effort, several supporting studies were conducted. The results of those studies are reported here.

Section 2 discusses the investigations of improved altitude tracking algorithms. The form of the maximum likelihood estimator (MLE) for simultaneously estimating epoch, signal-to-noise ratio, and wave height is derived, and its performance is computed. In addition, modifications to the standard split-gate tracker are analyzed, and it is shown that the split-gate tracker performance can be improved by increasing the width of the late gate and lowering the position of the early gate on the leading edge of the return.

Section 3 considers the performance of a digital binary phase code receiver. It is shown that a multi-bit digital processor of at least 2 bits plus sign is required for adequate performance. This result is due to the distributed nature of the target (sea surface). The results show that for a compression ratio of 1000 and an uncompressed signal-to-noise ratio of -20 dB, the compressed output signal-to-noise ratio is only 4.1 dB. This is a 5.9 dB loss relative to a linear system. A system with 2 bits plus sign gives an output signal-to-noise ratio of 7.9 dB (i.e. about 2 dB loss relative to a linear system).

Section 4 makes a comparison of Barrick's model of the sea surface return with several experimentally derived values. It is found that Barrick's model agrees reasonably well with the data trend versus wind velocity. However, it is found that his model predicts values for the cross-section per unit area which are somewhat higher than the measured values, and a reduction of Barrick's model by about 6 dB gives a more conservative model.

Section 5 describes the recommended changes in the system parameters for an aircraft mounted altimeter. It is necessary to modify the selected set of system parameters given in Part I, since that design is based on orbital parameters whereas the breadboard unit will actually be tested using an aircraft.

## 2.0 IMPROVED ALTITUDE TRACKING ALGORITHMS

### 2.1 Introduction and Summary

The general problem in altimetry is that of estimating the time of occurrence, epoch, of the leading edge of radar reflection from an extended noise-like target. (i.e., the sea surface). Here, a variety of techniques for estimating this epoch are developed and compared with the performance of a standard split-gate tracker. Both the optimum, maximum likelihood estimator, and sub-optimum, "modified split-gate" tracker, techniques are shown to provide considerable improvement in performance when compared with the conventional split-gate tracker.

In Section 2.2, the forms of the maximum likelihood estimator (MLE) and of the minimum mean square error estimator (MMSE) are derived. The asymptotic variances of the MLE for simultaneously estimating epoch, wave height and signal-to-noise ratio are computed.

For the special case in which the wave height is assumed known, the MLE and MMSE are shown to be very similar to a split-gate tracker. In both cases, the width of the late gate is much larger than the early gate width. It is also shown that at high signal-to-noise ratio the MLE places the center of the early gate well below the half power point on the leading edge of the return.

These results suggested that a conventional split-gate tracker which has equal early and late gate widths and which centers the early gate on the leading edge of the return signal may not be optimum. By appropriately designing the gates and their position, the performance of a split-gate tracker may be improved.

In Section 2.3 the performance of a split-gate tracker is derived, and the effect of changing the gate widths and the placement of the early gate is examined. For the parameter values considered, it is shown that the standard deviation of the tracking error can be reduced by a factor of 0.74 by increasing the width of the late gate. If, in addition to increasing the width of the late gate, the early gate is centered on the quarter power point of the leading edge of the return, the standard deviation of the tracking error is reduced by a total factor of 0.5.

The performance of an "optimized" split-gate tracker is computed. The optimized tracker shows significant improvement over the conventional tracker. In particular, it does not display the saturation effect at large signal-to-noise ratios. However, the optimized tracker must be adaptive in the sense that it has to vary the position of the early gate as a function of signal-to-noise ratio

Bias errors of a split-gate tracker are computed and shown to be a function of wave height and signal-to-noise ratio. In general, the tracker output must be corrected for these errors. It has not been determined whether these errors are more easily compensated in the tracker itself, or by "off-line" corrections on the ground. It should be noted however, that a tracker which compensates for signal-to-noise ratio and wave height is, in effect, estimating these parameters as well as epoch. Such a tracker may be nearly as complicated as a MLE.

In the initial work on the split-gate tracker, it is assumed that the data is sampled at time intervals far enough apart in range so that the sampled values are independent (discrete case). Since this is an unrealistic assumption for an analog split-gate tracker, the split-gate tracker equations are re-derived



assuming that the sampled values are no longer independent. The continuous case (analog) is then approximated by letting the time samples occur at very closely spaced intervals.

In Section 2.4, the accuracy expressions derived for the continuous split-gate, the discrete split-gate, and the MLE trackers are evaluated and compared.

## 2.2 Optimum Processing

From standard statistical theory, it is known that the Cramer-Rao bound gives a lower bound for the variance of unbiased "regular" estimates, and (if there are a sufficiently large number of samples  $V_i$ ) maximum-likelihood processing approximately achieves this lower bound. As usual, the derivation of a maximum likelihood processor for altimetry begins with an appropriate set of assumptions and definitions.

Here, it is assumed that the received signal is a stochastic process which is Gaussian, has zero ensemble mean, and is nonstationary: specifically, its average power varies with respect to time. It is also assumed that

- (a) The average power of the signal stochastic process can be described by a function  $f(t, \underline{\alpha})$  where  $\underline{\alpha}$  is a multi-dimensional parameter.
- (b) The observed data actually consist of a set of samples of the received power at a discrete set of times  $t_i$ .
- (c) The objective is to estimate some component of  $\underline{\alpha}$ .

Of particular interest is the case where

$$f(t, \underline{\alpha}) = a g(t-t_0, \underline{\beta})$$

where

$g(t_i-t_0, \underline{\beta})$  is the normalized signal shape (mean power) returned at time  $t$  when the epoch is  $t_0$ .

$\underline{\beta}$  is a vector of parameters needed to describe the return signal shape (e.g. wave height, sidelobe level etc.).

and

$t_0$  is the time of arrival (epoch) of the signal.

$a$  is the signal-to-receiver-noise level.

If it be assumed that the received power is measured at a set of time instants  $t_i$  separated by a range resolution cell width of the radar, then the observed data consist of a set of samples  $V_i$  which have the following statistical properties:

- (a)  $V_i$  are statistically independent
- (b)  $V_i$  has probability density functions

$$P_i(V_i) dv = \frac{1}{V_i} \exp[-V_i/\bar{V}_i] dv$$

where

$V_i$  is the returned power (relative to receiver-noise) from the  $i^{\text{th}}$  signal sample.

and

$$\bar{V}_i = E(V_i) = a g(t_i-t_0) + 1$$

Now, as is well known, maximum likelihood processing would consist of maximizing the joint probability density function for a set of N samples.

$$P(V_1, V_2, \dots) = \prod_{i=1}^N (1/\bar{V}_i) \exp(-V_i/\bar{V}_i)$$

The set of N resolution cells,  $i=1, \dots, N$ , is a specific set of cells-- say,  $i=1$  corresponds to the cell at some specified range beyond the "first target".

Maximization of P is the same as minimization of  $-\log_e P$ . Thus, the maximum likelihood estimate of  $t_o$  is obtained by minimizing with respect to  $a$ ,  $t_o$ , and  $\beta$  the quantity

$$Q_{MLE}(t_o, a, \beta) = \sum_{i=1}^N \frac{V_i}{ag(t_i - t_o, \beta) + 1} + \sum_{i=1}^N \log_e [ag(t_i - t_o, \beta) + 1] \quad (2.1)$$

If the minimizing values are given by  $\hat{a}$ ,  $\hat{t}_o$ ,  $\hat{\beta}$ , then the maximum likelihood estimate of  $t_o$  is  $\hat{t}_o$ . Furthermore  $\hat{a}$  and  $\hat{\beta}$  are also maximum likelihood estimates of  $a$  and  $\beta$ , respectively.

It is also well known that the minimum mean square error is obtained by minimizing the function:

$$Q_{\text{MMSE}}(t_o, a, \underline{\beta}) = \sum_{i=1}^N (V_i - a g(t_i - t_o, \underline{\beta}) + 1)^2 \quad (2.2)$$

Thus the form of the MLE or MMSE processor can be obtained by differentiating  $Q_{\text{MLE}}$  or  $Q_{\text{MMSE}}$  with respect to the appropriate variable, and setting the result equal to zero.

### 2.2.1 Form of the MLE and MMSE

As a first step towards obtaining the MLE and MMSE, it will be assumed that the signal-to-noise ratio,  $a$ , the signal epoch,  $t_o$ , and the waveheight,  $\sigma_h$  are unknown. The shape of the function for the returned power will be that of an ideal receiver [1] and the range sidelobes will be neglected. Thus,

$$g(t, \underline{\beta}) = P(\beta t) \quad (2.3)$$

where

$$P(t) = \frac{1}{\sqrt{2\pi}} \int_{-\infty}^t \exp(-U^2/2) dU \quad (2.4)$$

is the normal probability integral and

$$\beta = \frac{c}{2 \sigma_h}$$

$\sigma_h$  = rms waveheight

$c$  = velocity of light.

Now let

$$\bar{V}(t) = ag(t-t_0, \beta) + 1,$$

Then

$$Q_{MLE}(t_0, a, \beta) = \sum_{i=1}^N \left( \frac{v_i}{\bar{V}} + \log_e \bar{V} \right) \quad (2.5)$$

and the MLE for  $t_0, a, \beta$  must satisfy the equations:

$$\frac{\partial Q_{MLE}}{\partial t_0} = \sum_i \left( \frac{v_i - \bar{V}}{\bar{V}^2} \right) \frac{\partial \bar{V}}{\partial t_0} = 0 \quad (2.6)$$

$$\frac{\partial Q_{MLE}}{\partial a} = \sum_i \left( \frac{v_i - \bar{V}}{\bar{V}^2} \right) \frac{\partial \bar{V}}{\partial a} = 0 \quad (2.7)$$

$$\frac{\partial Q_{MLE}}{\partial \beta} = \sum_i \left( \frac{v_i - \bar{V}}{\bar{V}^2} \right) \frac{\partial \bar{V}}{\partial \beta} = 0 \quad (2.8)$$

Now

$$\frac{\partial \bar{V}}{\partial t_0} = -a \frac{\partial g(t_i - t_0)}{\partial t_0} = -\frac{a\beta}{\sqrt{2\pi}} \exp\left(-\frac{\beta^2}{2} (t_i - t_0)^2\right) \quad (2.9)$$

$$\frac{\partial \bar{V}}{\partial a} = g(t_i - t_o) = P(\beta(t_i - t_o)) \quad (2.10)$$

$$\frac{\partial \bar{V}}{\partial \beta} = -a \frac{\partial g}{\partial \beta} = \frac{-a(t_i - t_o)}{\sqrt{2\pi}} \exp\left(-\frac{\beta^2}{2}(t_i - t_o)^2\right) \quad (2.11)$$

And the MLE must satisfy:

$$\sum_i \left[ \frac{v_i - aP(\beta(t_i - t_o)) - 1}{(aP(\beta(t_i - t_o)) + 1)^2} \right] \exp\left(-\frac{1}{2}\beta^2(t_i - t_o)^2\right) = 0 \quad (2.12)$$

$$\sum_i \left[ \frac{v_i - aP(\beta(t_i - t_o)) - 1}{(aP(\beta(t_i - t_o)) + 1)^2} \right] P(\beta(t_i - t_o)) = 0 \quad (2.13)$$

and

$$\sum_i \left[ \frac{v_i - aP(\beta(t_i - t_o)) - 1}{(aP(\beta(t_i - t_o)) + 1)^2} \right] (t_i - t_o) \exp\left(-\frac{1}{2}\beta^2(t_i - t_o)^2\right) = 0 \quad (2.14)$$

The equations in this form do not give much insight into the form of a MLE; however, if a simplifying assumption is made, the nature of the MLE becomes more apparent.

The first assumption, is that the sample rate is high compared to the rise time of the leading edge, (i.e., the Nyquist rate or higher). Then,

$$\sum_i \frac{\exp(-\frac{1}{2}\beta^2(t_i-t_o)^2)}{P(\beta(t_i-t_o))+1/a} = \frac{1}{\beta\Delta t} \sum_i \frac{\exp(-\frac{1}{2}\beta^2(t_i-t_o)^2)\beta\Delta t}{P(\beta(t_i-t_o))+1/a}$$

$$\approx \frac{1}{\beta\Delta t} \int \frac{\exp(-\frac{1}{2}u^2)}{P(u)+1/a} du = \frac{K_{MLE}^1}{\beta\Delta t} \quad (2.15)$$

and similarly,

$$\sum_i \frac{P(\beta(t_i-t_o))}{P(\beta(t_i-t_o))+1/a} \approx \frac{1}{\beta\Delta t} \int \frac{P(u)}{P(u)+1/a} du = \frac{K_{MLE}^2}{\beta\Delta t} \quad (2.16)$$

and

$$\sum_i \frac{(t_i-t_o) \exp(-\frac{1}{2}\beta^2(t_i-t_o)^2)}{P(\beta(t_i-t_o))+1/a} \approx \frac{1}{\beta^2\Delta t} \int \frac{u \exp(-\frac{1}{2}u^2)}{P(u)+1/a} du$$

$$= \frac{1}{\beta^2\Delta t} K_{MLE}^3 \quad (2.17)$$

and equations (2.12 and (2.13 become:

$$\sum V_i h(\beta(t_i-t_o)) - \frac{a}{\beta\Delta t} K_{MLE}^1 = 0 \quad (2.18)$$

$$\sum V_i g(\beta(t_i-t_o)) - \frac{a}{\beta\Delta t} K_{MLE}^2 = 0 \quad (2.19)$$

$$\sum V_i (t_i - t_0) h(\beta(t_i - t_0)) - \frac{a}{\beta^2 \Delta t} K_{MLE}^3 = 0 \quad (2.20)$$

where:

$$h_{MLE}(t) = \frac{\exp(-\frac{1}{2}t^2)}{\{P(t)+1/a\}^2} \quad (2.21)$$

and

$$g_{MLE}(t) = \frac{P(t)}{(P(t)+1/a)^2} \quad (2.22)$$

These functions are plotted for several different signal-to-noise ratios in Figs. 2.1 and 2.2. As might be expected, at higher signal-to-noise ratios, the weighting functions place more emphasis on the leading edge of the pulse. A more surprising feature is the relatively high weight placed on signal values which are equal to or less than the noise level.

Heuristically, the MLE estimators may be considered as being implemented with three filters. The shape of each filter's response is governed by the signal-to-noise ratio and the time scale factor is governed by the wave-height parameter. A brute force approach to obtaining the MLE would then be to repeatedly filter the data, changing the parameters  $a$  and  $\beta$  on each pass until an epoch,  $t_0$  is found for which the equations 2.18 - 2.20 are satisfied.



Figure 2.1

MLE Impulse Response for the  
Filter in eq. (19)

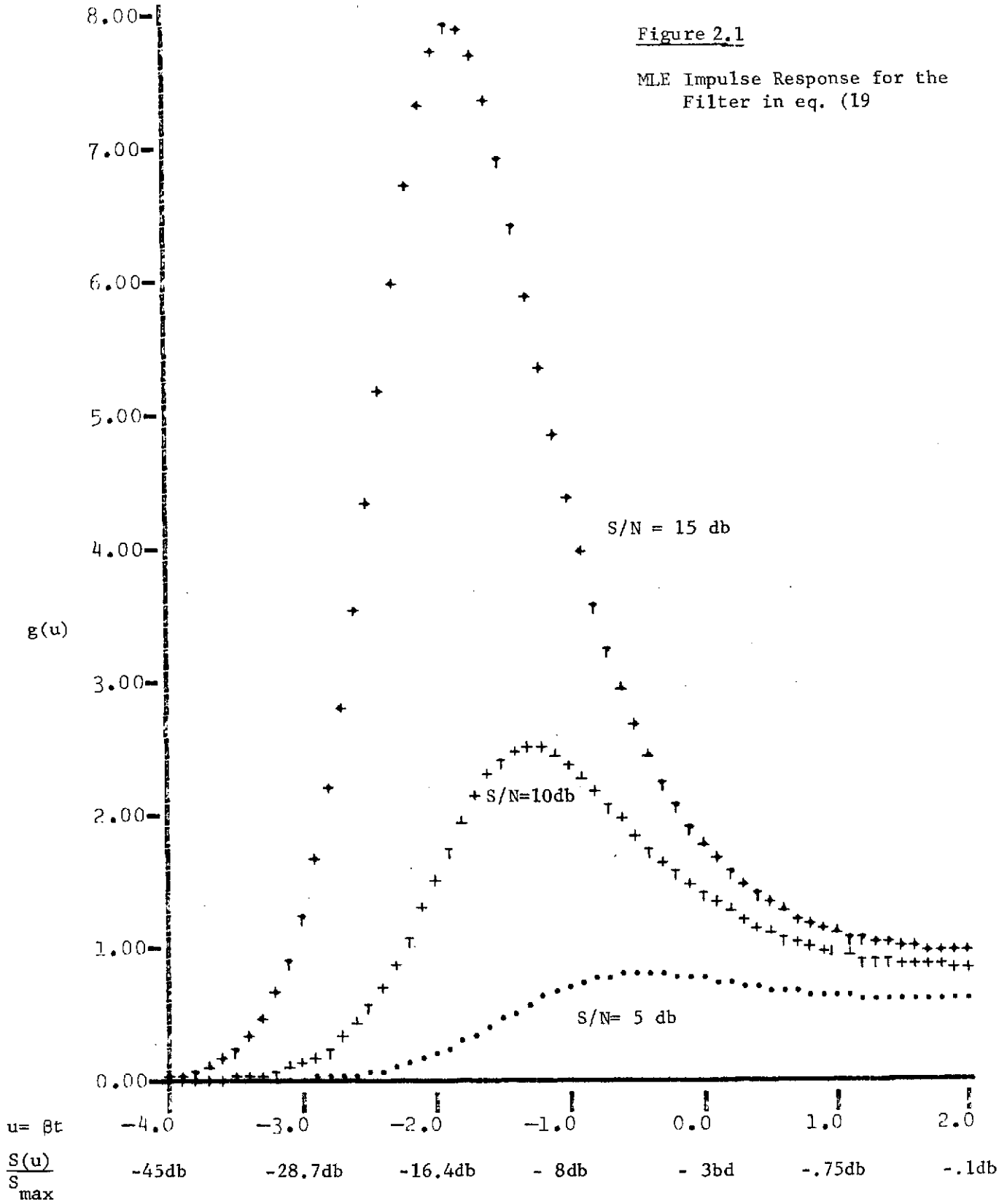
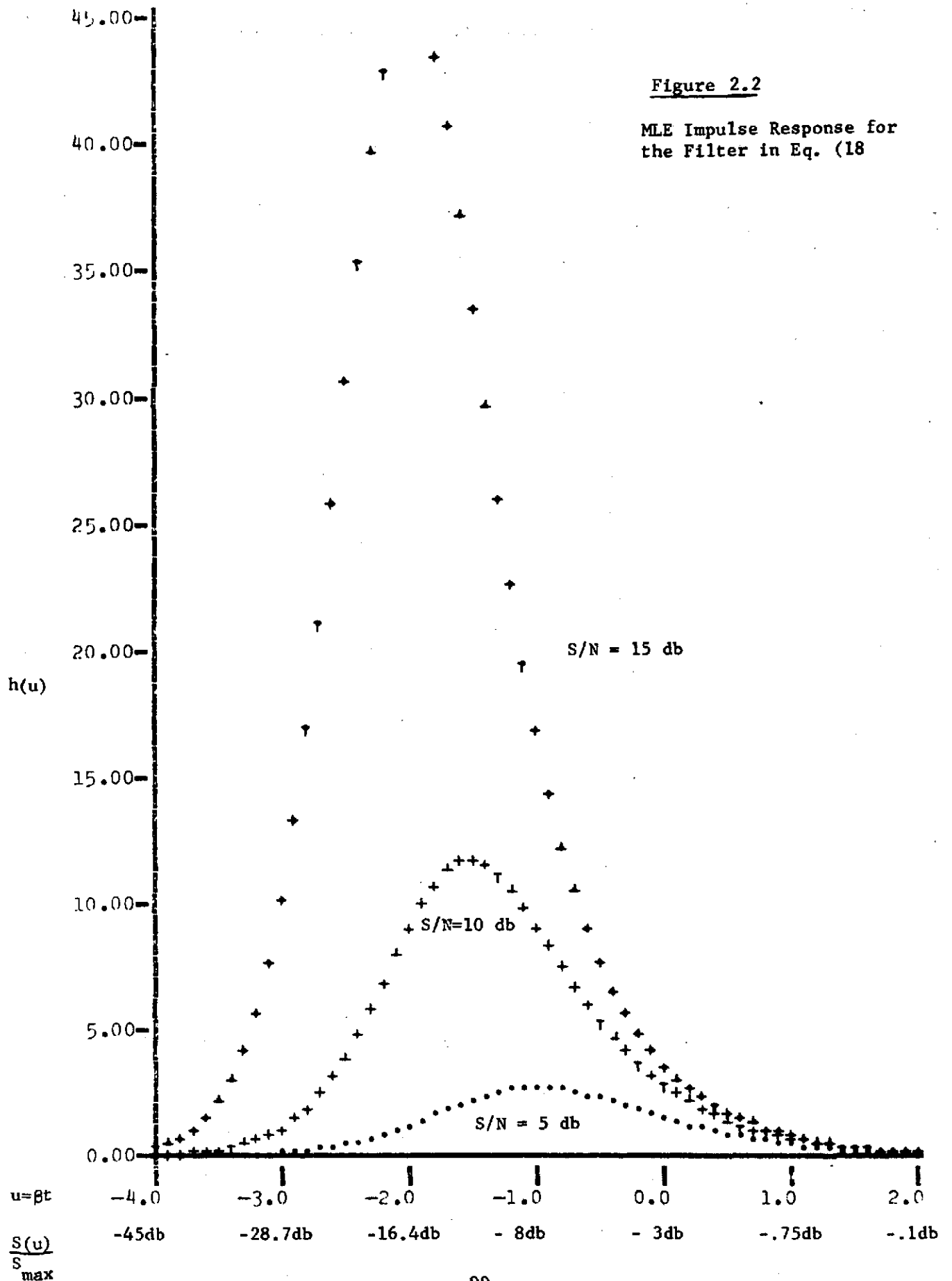


Figure 2.2

MLE Impulse Response for  
the Filter in Eq. (18)



If equation 2.2 is differentiated, the MMSE is obtained. As it turns out, the form of the equations to be solved is identical to that for the MLE. However, the constants and filter impulse responses become:

$$K_{\text{MMSE}}^1 = \int [P(u) + 1/a] \exp(-\frac{1}{2}u^2) du$$

$$K_{\text{MMSE}}^2 = \int (P(u) + 1/a) P(u) du$$

$$K_{\text{MMSE}}^3 = \int u [P(u) + 1/a] \exp(-\frac{1}{2}u^2) du \quad (2.23)$$

$$h_{\text{MMSE}}(u) = \exp(-\frac{1}{2}u^2)$$

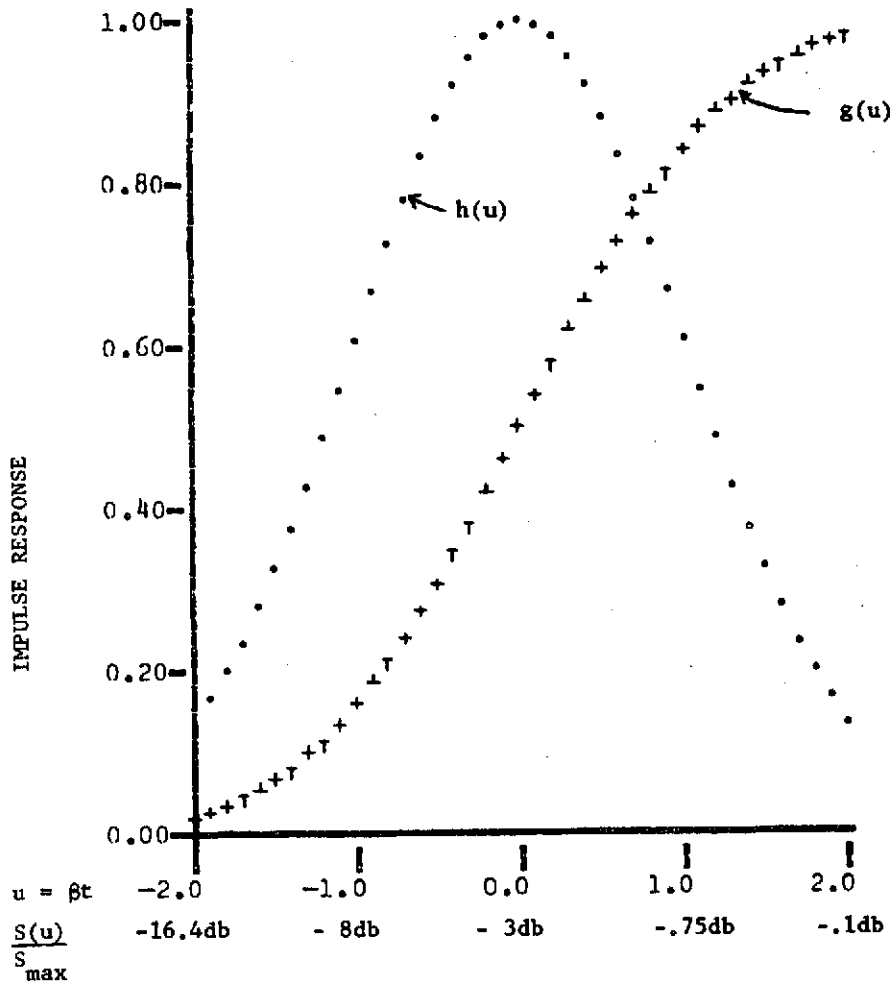
$$g_{\text{MMSE}}(u) = P(u)$$

The MMSE weighting functions are plotted in Figure 2.3.

If the wave height, or equivalently the returned pulse shape is assumed known, then the MMSE for epoch becomes equivalent to a split gate tracker. That is, since  $\beta$  is assumed known, then only eq. 2.18 and 2.19 need to be solved. The signal-to-noise ratio,  $a$ , can be eliminated from these equations to yield:

Figure 2.3

MMSE Filter Impulse Response



$$\sum_i V_i h(\beta(t_i - t_0)) - C \sum_i V_i g(\beta(t_i - t_0)) - B = 0 \quad (2.24)$$

where

$$C = \frac{\int P(u) \exp(-\frac{1}{2}u^2) du}{\int P^2(u) du}$$

$$B = \sqrt{2\pi} + C$$

Thus the estimate for epoch is obtained by passing the data through an early gate with impulse response  $h(\beta t)$ ; subtracting the output of a late gate with impulse response  $Cg(\beta t)$ ; subtracting a bias term  $B$ , and then taking as the epoch, the point at which the resulting output passes through zero.

### 2.2.2 Variance of the MLE

The asymptotic variance (as the number of pulses averaged increases) of the MLE is computed in this section. Since all the trackers require a large number of pulses to be integrated for the design goals to be met, it is felt that the asymptotic analysis is appropriate.

It is known from the theory of maximum likelihood estimators (see Wilks [2]) that the covariance matrix for the MLE is the inverse of the covariance matrix of the score.

The score is defined as follows:

Let.

$$\nabla = \begin{pmatrix} \frac{\partial}{\partial a} \\ \frac{\partial}{\partial t_0} \\ \frac{\partial}{\partial \beta} \end{pmatrix}$$

be the gradient operator. Then the score is defined as:

$$S(V_1, V_2, \dots, V_{NN_p}) = \nabla \log p(V_1, V_2, \dots, V_{NN_p}) \quad (2.25)$$

Thus the covariance matrix for the MLE is given by

$$R_{MLE} = R_S^{-1} = (E SS^T)^{-1} \quad (2.26)$$

Lank [3] shows that for the altimetry problem, the covariance matrix of the score is given by:

$$\begin{aligned} R_S &= \sum_i (\nabla \log \bar{V}_i) (\nabla \log \bar{V}_i)^T \\ &= \sum_i \left( \frac{\nabla \bar{V}_i}{\bar{V}_i} \right) \left( \frac{\nabla \bar{V}_i}{\bar{V}_i} \right)^T \end{aligned} \quad (2.27)$$

Recall that

$$\bar{V}_i = a P (\beta(t_i - t_0) + 1) \quad (2.28)$$

so that

$$\nabla \bar{V}_i = \begin{pmatrix} P (\beta(t_i - t_0) + 1) \\ -a\beta P (\beta(t_i - t_0) + 1) \\ a(t_i - t_0) P (\beta(t_i - t_0) + 1) \end{pmatrix} = \begin{pmatrix} \frac{\partial \bar{V}}{\partial a} \\ \frac{\partial \bar{V}}{\partial t_0} \\ \frac{\partial \bar{V}}{\partial \beta} \end{pmatrix} \quad (2.29)$$

Thus,

$$R_s = \begin{pmatrix} R_{aa} & R_{at_0} & R_{a\beta} \\ R_{at_0} & R_{t_0 t_0} & R_{t_0 \beta} \\ R_{a\beta} & R_{t_0 \beta} & R_{\beta\beta} \end{pmatrix} \quad (2.30)$$

Where:

$$\begin{aligned} R_{aa} &= \sum_i \left( \frac{P_i}{\bar{V}_i} \right)^2 \\ R_{at_0} &= \sum_i -a\beta \frac{P_i \dot{P}_i}{\bar{V}_i} \\ R_{a\beta} &= \sum_i a(t_i - t_0) \frac{P_i \dot{P}_i}{\bar{V}_i} \\ R_{t_0 t_0} &= \sum_i a^2 \beta^2 \left( \frac{\dot{P}_i}{\bar{V}_i} \right)^2 \\ R_{t_0 \beta} &= \sum_i -a^2 \beta (t_i - t_0) \left( \frac{\dot{P}_i}{\bar{V}_i} \right)^2 \\ R_{\beta\beta} &= \sum_i a^2 (t_i - t_0)^2 \left( \frac{\dot{P}_i}{\bar{V}_i} \right)^2 \end{aligned} \quad (2.31)$$

and where

$$P_i = P(\beta(t_i - t_0)) \quad (2.32)$$

The computation of the above matrix can be simplified if it is assumed that the samples are closely spaced in time: Then

$$R_{aa} = \frac{1}{a^2 \beta \Delta t} \sum_i [P_i \sqrt{\bar{v}_i}/a]^2 \beta \Delta t \quad (2.33)$$

or

$$R_{aa} \approx \frac{N_p}{a^2 \beta \Delta t} \int \left[ \frac{P(u)}{\bar{H}(u)} \right]^2 du \quad (2.34)$$

where

$$\bar{H}(u) = P(u) + 1/a \quad (2.35)$$

Applying similar approximations to all the correlation coefficients yields:

$$\begin{aligned} R_{aa} &= \frac{K_{aa}}{a^2 \beta \Delta t} \cdot N_p & ; & \quad K_{aa} = \int \left[ \frac{P(u)}{\bar{H}(u)} \right]^2 du \\ R_{at_0} &= \frac{K_{at_0}}{a \Delta t} \cdot N_p & ; & \quad K_{at_0} = \int \frac{P(u) \dot{P}(u)}{\bar{H}^2(u)} du \\ R_{a\beta} &= \frac{K_{a\beta}}{a\beta^2 \Delta t} \cdot N_p & ; & \quad K_{a\beta} = \int \frac{uP(u) \dot{P}(u)}{\bar{H}^2(u)} du \\ R_{t_0 t_0} &= \frac{\beta}{\Delta t} K_{t_0 t_0} \cdot N_p & ; & \quad K_{t_0 t_0} = \int \left[ \frac{\dot{P}(u)}{\bar{H}(u)} \right]^2 du \\ R_{t_0 \beta} &= \frac{1}{\beta \Delta t} K_{t_0 \beta} \cdot N_p & ; & \quad K_{t_0 \beta} = \int u \left[ \frac{\dot{P}(u)}{\bar{H}(u)} \right]^2 du \\ R_{\beta\beta} &= \frac{1}{\beta^3 \Delta t} K_{\beta\beta} \cdot N_p & ; & \quad K_{\beta\beta} = \int \left[ \frac{u \dot{P}(u)}{\bar{H}(u)} \right]^2 du \end{aligned} \quad (2.36)$$



The coefficients can be evaluated directly using:

$$P(u) = \frac{1}{\sqrt{2\pi}} \int_{-\infty}^u \exp(-t^2/2) dt \quad (2.37)$$

However to do so, numerical integration techniques must be used. To simplify the calculations,  $P(u)$  is approximated by

$$\begin{aligned} P(u) &= \alpha u + 1/2 & u \in (-1/2\alpha, 1/2\alpha) \\ &= 1 & u \in (1/2\alpha, \infty) \\ &= 0 & u \in (-\infty, -1/2\alpha) \end{aligned} \quad (2.37)$$

The constant,  $\alpha$ , is chosen so that the ramp defined above approximates the normal integral in a minimum mean square sense. Thus:

$$\alpha \approx .3227 \quad (2.39)$$

Using this approximation yields

$$K_{aa} = \frac{1}{\alpha} \left[ 1 - \frac{2}{a} \log(1+a) + \left( \frac{1}{1+a} \right) + \frac{(\beta \alpha T_{\max} - 1/2) a^2}{(1+a)^2} \right]$$

$$K_{at_0} = - \left[ \log(1+a) - \frac{a}{1+a} \right]$$

$$K_{a\beta} = \frac{1}{\alpha} \left[ 1 - \left( \frac{a+4}{2a} \right) \log(1+a) + \frac{(a+2)}{2(1+a)} \right]$$

$$K_{t_0 t_0} = \frac{\alpha a^2}{1+a}$$

$$K_{t_o\beta} = - \left[ \log(1+a) - \left(\frac{a}{2}\right) \frac{(a+2)}{(a+1)} \right]$$

$$K_{\beta\beta} = \frac{1}{\alpha} \left[ 1 - \left(\frac{a+2}{a}\right) \log(1+a) + \frac{(2+a)^2}{4(1+a)} \right] \quad (2.40)$$

Then letting

$$K = \begin{pmatrix} K_{aa} & K_{at_o} & K_{a\beta} \\ K_{at_o} & K_{t_o t_o} & K_{t_o\beta} \\ K_{a\beta} & K_{t_o\beta} & K_{\beta\beta} \end{pmatrix} \quad (2.41)$$

and

$$D = \begin{pmatrix} 1/a & 0 & 0 \\ 0 & \beta & 0 \\ 0 & 0 & 1/\beta \end{pmatrix} \quad (2.42)$$

yields

$$R_s = \begin{pmatrix} N \\ P \\ \beta\Delta t \end{pmatrix} D K D \quad (2.43)$$

So that

$$R_{MLE} = R_s^{-1} = \frac{\beta\Delta t}{N P} D^{-1} K^{-1} D^{-1} \quad (2.44)$$

In particular,

$$\sigma_a = a \sqrt{\frac{\beta\Delta t}{N P}} \left[ K^{-1} \right]_{aa}^{1/2} \quad (2.45)$$

$$\sigma_{t_o} = \frac{1}{\beta} \sqrt{\frac{\beta\Delta t}{N P}} \left[ K^{-1} \right]_{t_o t_o}^{1/2} \quad (2.46)$$

and

$$\sigma_\beta = \beta \sqrt{\frac{\beta\Delta t}{N P}} \left[ K^{-1} \right]_{\beta\beta}^{1/2} \quad (2.47)$$

Note that matrix K depends only on the parameters

$$U_{\max} = \alpha \beta T_{\max} \quad (2.48)$$

and  $\alpha$ . Here  $T_{\max}$  is the time measured from the half power point to the end of the observation interval.

The quantities  $[K^{-1}]_{aa}^{1/2}$ ,  $[K^{-1}]_{t_o t_o}^{1/2}$ , and  $[K^{-1}]_{\beta\beta}^{1/2}$  are plotted in Figure

2.4, 2.5 and 2.6.

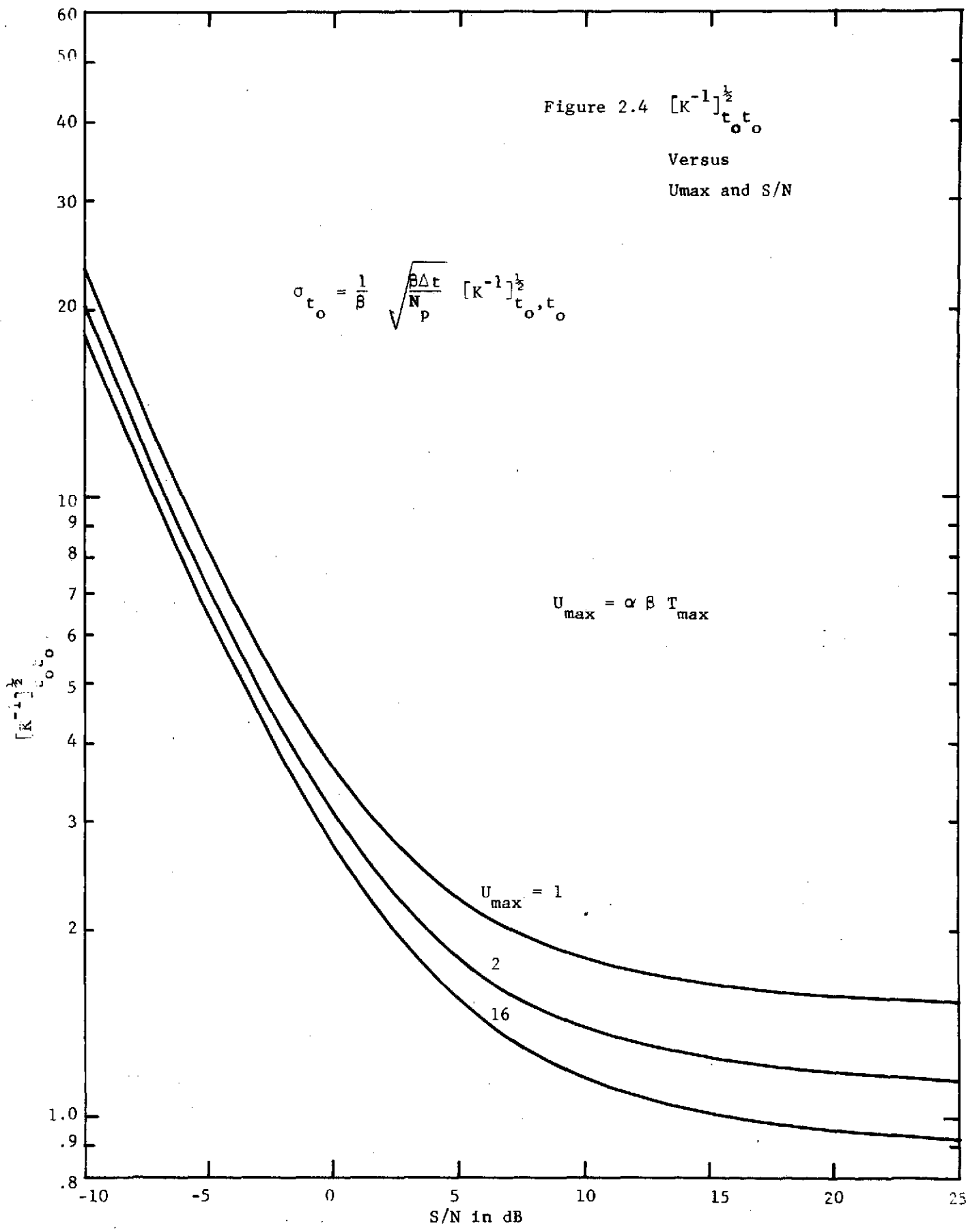
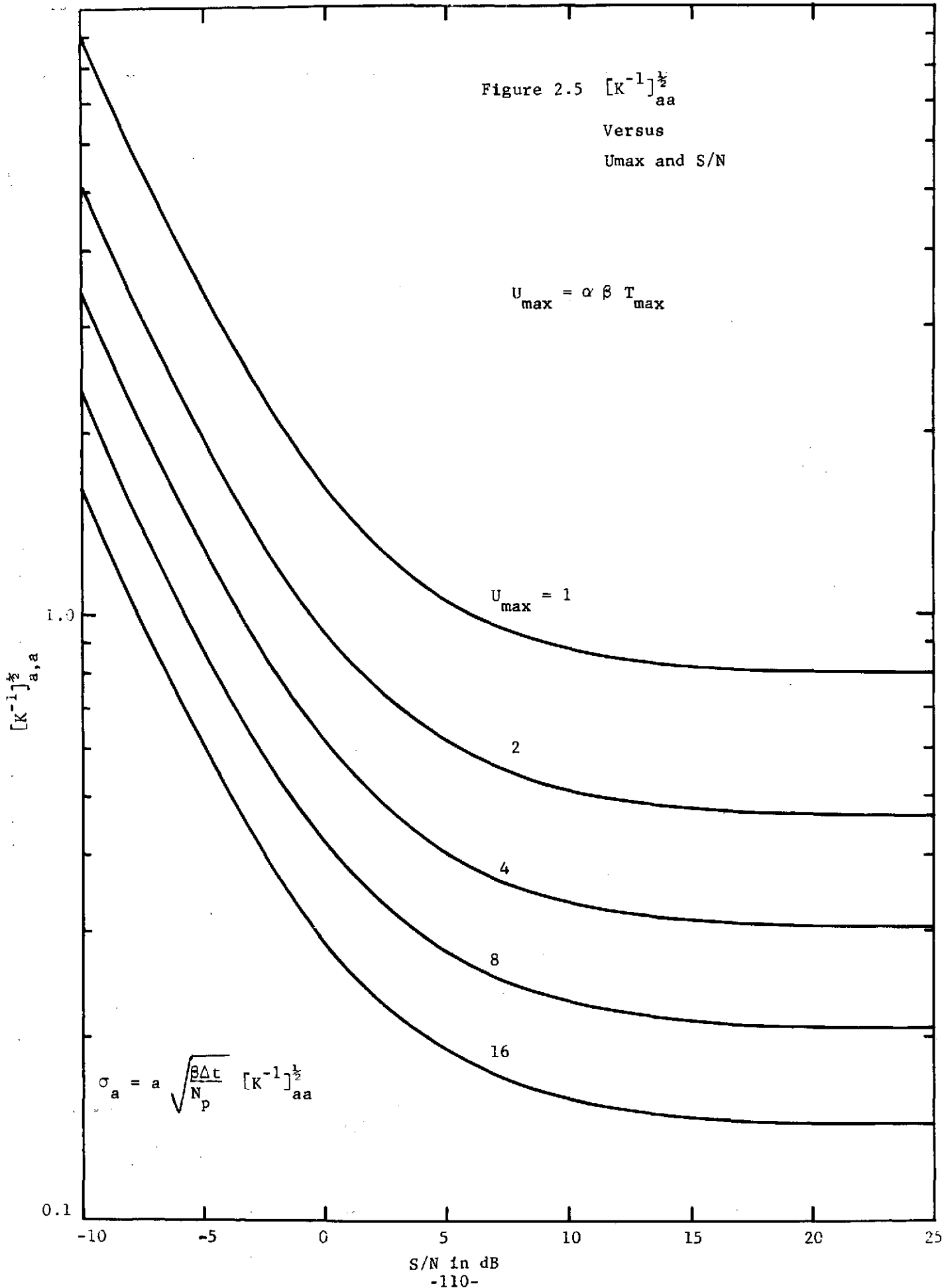
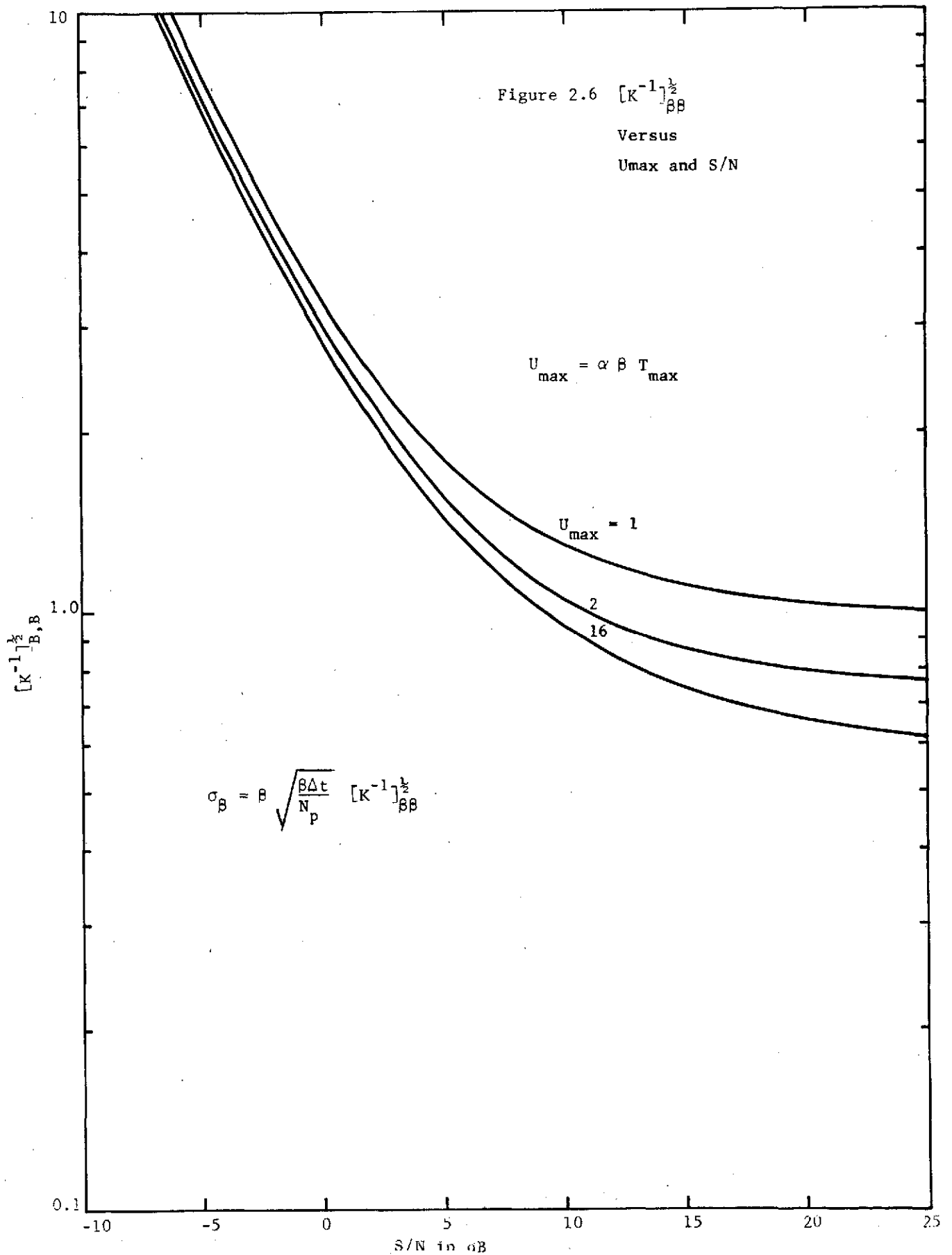


Figure 2.5  $[K^{-1}]_{aa}^{\frac{1}{2}}$   
 Versus  
 $U_{\max}$  and S/N

$$U_{\max} = \alpha \beta T_{\max}$$





## 2.3 Split-Gate Trackers

In this section the performance of a split-gate tracker is derived, and the effect of changing the gate widths and the placement of the early gate is examined. Bias errors are computed and shown to be a function of wave height and signal-to-noise ratio. Finally, the model is extended to include correlated samples to approximate an analog (continuous) tracker.

### 2.3.1 Discrete Case

#### 2.3.1.1 Variance of a split-gate tracker

To keep the derivations relatively simple, a sampled system will be assumed. A split-gate tracker estimates the epoch of a signal by balancing the output of an early gate with that of a late gate. Specifically, let:

$t_i$  ,  $i = 0, \pm 1, \pm 2, \dots$  be the times at which the signal is sampled,

$V(t_i)$  be the square law detected output of the receiver  
at time  $t_i$ ,

$\sum_i \delta(t_i - t) h_i$  be the impulse response of the early gate,

$C \sum_i \delta(t_i - t) g_i$  be the impulse response of the late gate,

and  $C$  be a constant (to be determined later) which makes  
the tracker unbiased.

Note that the Kronecker delta functions arise from the assumption of a sampled system.

For any time delay,  $\tau_0$ , between the tracker estimated epoch and the true epoch, the error voltage of the split-gate tracker is given by:

$$\mathcal{E}(\tau_0) = \sum_i V(t_i - \tau_0) (h_i - C g_i) \quad (2.49)$$

The tracker feedback loops function so that the error voltage is held at zero. Thus the tracker estimated epoch is given by the solution of:

$$\mathcal{E}(\tau_0) = 0 \quad (2.50)$$

If the loop time constants are long, and the tracking error is unbiased, then  $\tau_0$  will be nearly zero. Expanding  $\mathcal{E}(\tau_0)$  in a Taylor series about  $\tau_0 = 0$  and substituting into (2.50) yields:

$$\tau_0 \approx \frac{\mathcal{E}(0)}{\left. \frac{\partial \mathcal{E}(\tau)}{\partial \tau} \right|_{\tau=0}} \quad (2.51)$$



Let  $k = E \left. \frac{\partial \mathcal{E}(\tau)}{\partial \tau} \right|_{\tau=0}$  be

the mean tracking error slope. Using (2.51), one has:

$$\text{Var } \tau_0 = \frac{\text{Var } \mathcal{E}(0)}{k^2} \quad (2.52)$$

The quantities  $k$  and  $\text{Var } \mathcal{E}(0)$  depend on the shape of the early and late gates, and on the characteristics of the mean power return,  $\bar{V}(t)$ . The special case sketched in Fig. 2.7 is now considered. As in Section 2.2.2, it is assumed that the ramp is chosen to approximate the normal integral in a mean square sense.

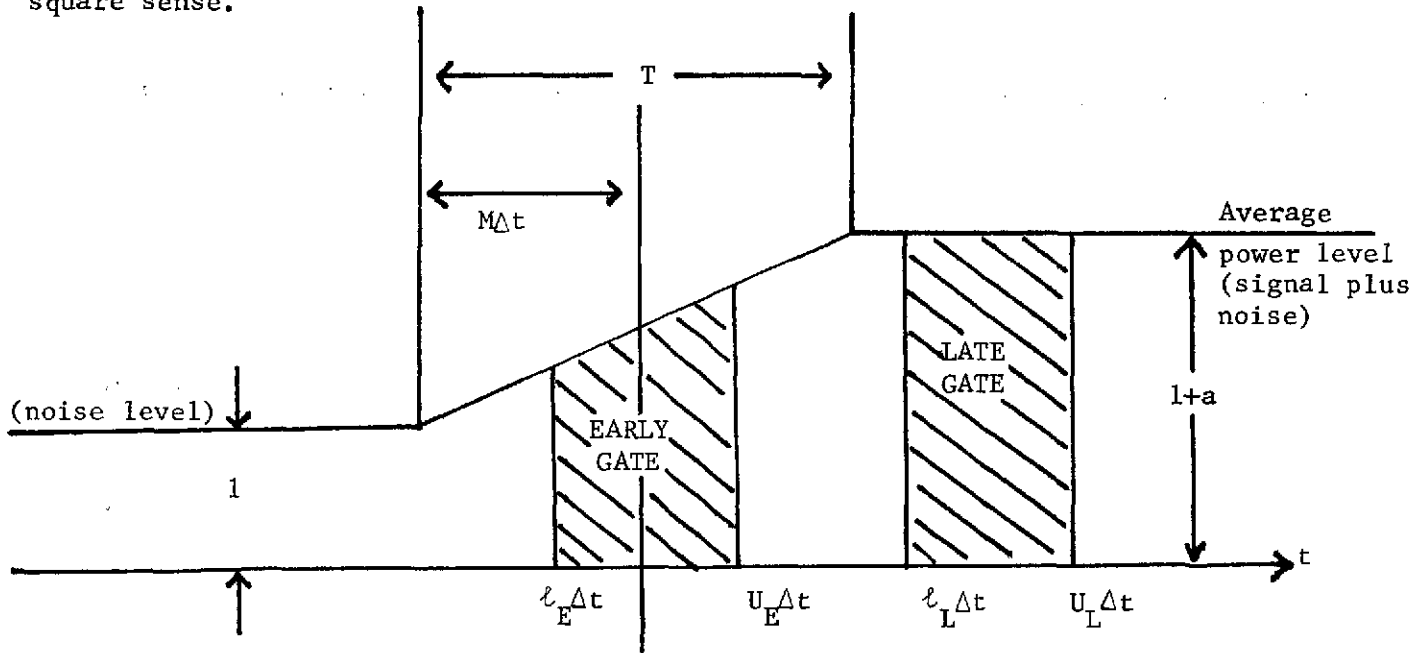


Fig. 2.7 Sketch of the average returned power level, and the gate positioning.

That is, the following simplifications are made:

- i) Square - non-overlapping gates are assumed.
- ii) The late gate is positioned on the plateau.
- iii) The early gate is positioned on the leading edge.
- iv) The signal return power is modeled as a linear ramp rising to a flat plateau.
- v) The receiver noise level is unity.

If the following definitions are made:

$\Delta t$  = time between samples

$a$  = signal-to-noise ratio

$T$  = rise time of the leading edge

$M = T/2\Delta t$ ;  $(2M+1)$  = total number of samples available on the leading edge

$N_E$  = number of samples in the early gate

$N_L$  = number of samples in the late gate

$\bar{V}_{l_E}$  = average power return at the first sample in the early gate

$N_p$  = number of pulses averaged

It is shown in section 2.3.1.4 that the tracking variance is

given by:

$$\text{Var } \tau_0 = \frac{(\Delta t)^2}{N_p} \left\{ \frac{1}{N_E} \left[ \left( \frac{\bar{V}_{l_E}}{a/2M} \right)^2 + \left( \frac{\bar{V}_{l_E}}{a/2M} \right) (N_E - 1) + \frac{(N_E - 1)(2N_E - 1)}{6} \right] + \frac{1}{N_L} \left[ \frac{\bar{V}_{l_E}}{a/2M} + \frac{N_E - 1}{2} \right]^2 \right\} \quad (2.53)$$

Note that for a fixed early gate width,  $N_E$ , the variance of the tracking error, is minimized by making  $N_L$  as large as possible and by making  $\bar{V}_{\ell_E}$  as small as possible. This is consistent with previous results which showed that the MLE used as large a late gate width as possible, and tended to push the early gate position as far down the leading edge as possible.

In general, the optimum width for the early gate depends on the ratio  $\bar{V}_{\ell_E} / (a/2M)$ ; however, it can be shown that for high signal-to-noise ratio,  $a$ , the optimum early gate width is  $N_E=1$ . In this case, the tracker variance becomes

$$\text{Var } \tau_0 = \frac{(2M\Delta t)^2}{N_p} \left( \frac{\bar{V}_{\ell_E}}{a} \right)^2 = \frac{T^2}{N_p} \left( \frac{\bar{V}_{\ell_E}}{a} \right)^2 \quad (2.54)$$

Thus for the "optimized" split-gate tracker, the standard deviation of the tracking error is inversely proportional to signal-to-noise ratio. A consequence of optimizing the tracker gates is that the tracker saturation effect no longer occurs. This improved performance does, however, require increased complexity in the tracker. Note that in order to achieve optimum performance,  $\bar{V}_{\ell_E}$ , the average power output from the early gate, must be held constant independent of the signal-to-noise ratio. It can be shown that this can be done only if the normalizing constant is changed as a function of signal-to-noise ratio. Thus an "optimized" split-gate tracker would have to be adaptive in that it must estimate signal-to-noise ratio, and then adjust the early gate position accordingly.

2.3.1.2 Conventional Split-Gate Tracker

In most cases, it is more convenient to design a tracker which tracks a power level that is a constant ratio of the plateau level, e.g., the half power point or the quarter power point. In this case, the normalizing constant does not have to be adaptive at high signal-to-noise ratio. To compare such a tracker to the "optimized" split-gate tracker, consider the case:

(1)  
 $N_E = 2$ ,  $M = 1$ , and  $\bar{V}_E = 1+k/a$  (i.e. the tracker is adjusted to track the  $k$  power point ( $0 \leq k \leq 1$ )). For this case, the tracker variance is given by

$$\text{Var } \tau_0 = \frac{T^2}{N_P} (1/32 + \frac{1}{2}k^2(1+1/\gamma) + k/a(1+1/\gamma) + (\frac{1}{2}a^{-2})(1+1/\gamma)) \quad (2.56)$$

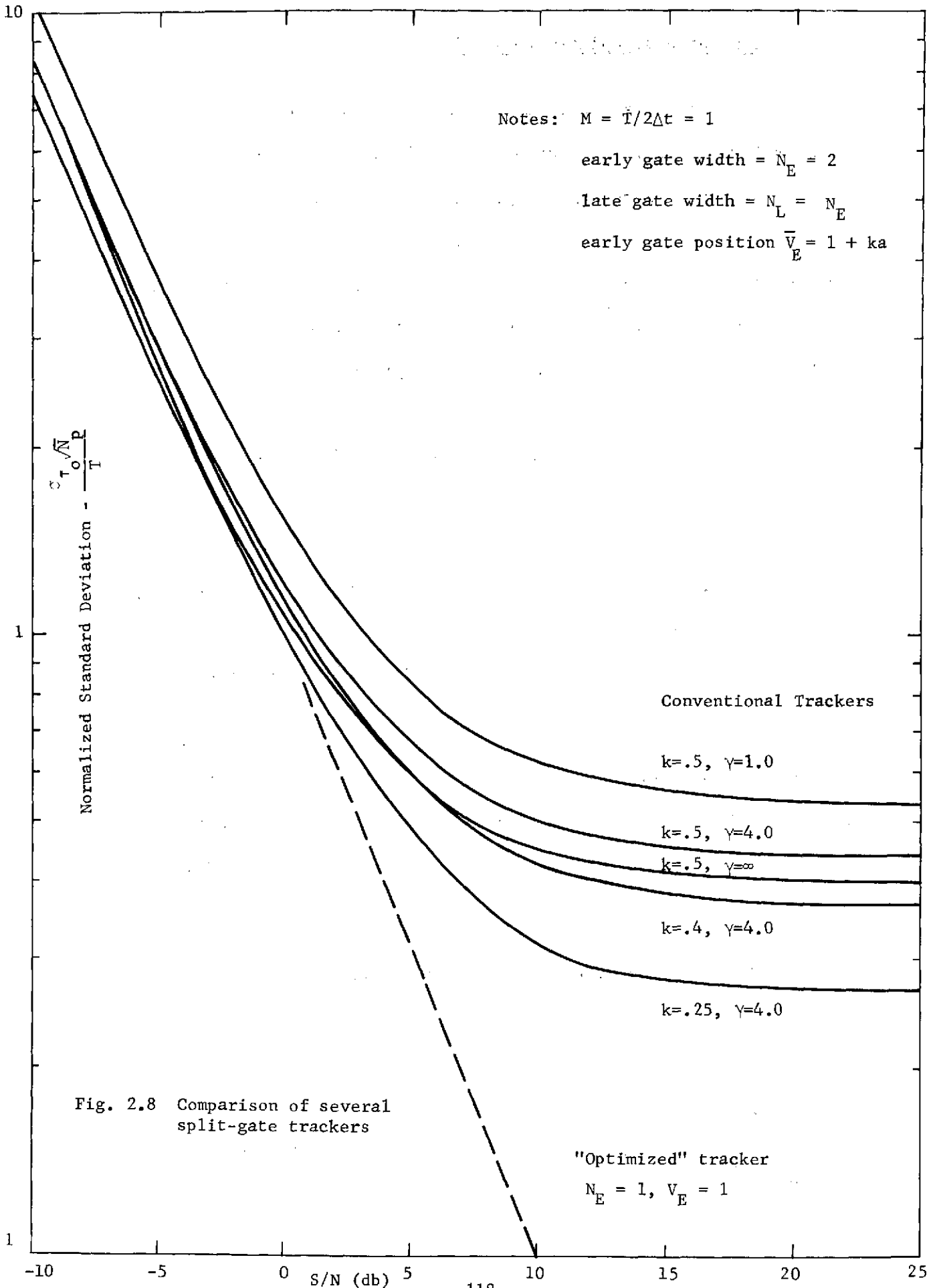
In the above expression,  $\gamma$  is the ratio of the late gate width to the early gate width (i.e.  $\gamma = N_L/N_E$ ). The effect of increasing the late gate width (increasing  $\gamma$ ) and of changing the tracking point,  $k$ , is shown in Fig. 2.8.

The case  $k = \frac{1}{2}$ ,  $\gamma = 1$ , corresponds to the conventional split-gate tracker. Relative to this case, increasing the late gate width, and lowering the position of the early gate both improve tracking performance. As can be seen, the greatest effect seems to be due to lowering  $k$  (the early gate position).

For comparison the "optimized" split-gate tracker performance is also shown. As can be seen, considerable performance improvement is possible.

---

(1) Note that  $\bar{V}_E$  is the average power at the midpoint of the early gate. In general  $\bar{V}_E \neq \bar{V}_{t_E}$ .



2.3.1.3 Split-Gate Tracker Bias

A common practice for reducing tracker bias error entails subtracting an estimate of the noise,  $\eta_0$  from the return waveform. i.e. clamping the return waveform to  $\eta_0$ . In this case, the normalizing constant (Section 2.3.1.4) is given by:

$$C_a = \frac{N_E}{N_L} \frac{\bar{V}_E}{1-\eta_0 + a}$$

where  $\bar{V}_E$  is the average power at the midpoint of the early gate. If the tracker is adjusted to track the k power point, then

$$\bar{V}_E = 1-\eta_0 + ka$$

and

$$C_a = \frac{N_E}{N_L} \frac{1-\eta_0 + ka}{1-\eta_0 + a} \tag{2.57}$$

If the constant is set for the wrong signal-to-noise ratio, say  $a_0$ , then there exists a bias  $\tau_0$  such that the mean error signal is zero at  $\tau_0$ . Thus,

$$E(\mathcal{E}(\tau_0)) = 0 = N_E(1-\eta_0 + a(k + \frac{\tau_0}{T})) - C_{a_0} N_L(1-\eta_0 + a) \tag{2.58}$$

and the bias normalized to waveheight is given by:

$$\frac{\tau_o}{T} = \frac{1-\eta_b}{a} (1-\rho) + (k-\rho) \quad (2.59)$$

where

$$\rho = \frac{1-\eta_o + ka_o}{1-\eta_b + a_o} \quad (2.60)$$

Note that while the bias is a function of waveheight and signal-to-noise ratio for any  $k \neq 1$ , it can be made arbitrarily small by accurately estimating the noise level. That is, as  $\eta_o \rightarrow 1$  the bias approaches zero since  $\rho \rightarrow k$ .

#### 2.3.1.4 Derivations

The tracker error signal is given by:

$$\mathcal{E}(\tau_o) = \Sigma \left[ v(t_i - \tau_o) (h_i - C g_i) \right] \quad (2.61)$$

The tracker will be unbiased if

$$E \mathcal{E}(0) = 0$$

Thus the normalizing constant is given by:

$$C = \frac{\Sigma \bar{V}(t_i) h_i}{\Sigma \bar{V}(t_i) g_i} \quad (2.62)$$

where  $\bar{V}(t_i) = E V(t_i)$  is the mean receiver power output at time  $t_i$ .

The mean error slope is given by

$$k = \left. \frac{\partial E\mathcal{E}(\tau)}{\partial \tau} \right|_{\tau=0} = \sum \dot{\bar{V}}(t_i) (h_i - C g_i) \quad (2.63)$$

And the variance of the tracking error signal is given by:

$$\text{Var } \mathcal{E}(0) = \sum \text{Var} [V(t_i)] (h_i - C g_i)^2 \quad (2.64)$$

where the samples are assumed to be uncorrelated. (i.e.  $E(V_i - \bar{V}_i)(V_j - \bar{V}_j) = 0, i \neq j$ )

For Gaussian processes (exponentially distributed power),

$$\text{Var} [V(t_i)] = (E V(t_i))^2 = \bar{V}^2(t_i) \quad (2.65)$$

Thus the tracking error variance is given by combining (2.63, (2.64, (2.65 and (2.52 to yield:

$$\text{Var } \tau_0 = \frac{\text{Var } \mathcal{E}(0)}{k^2} = \frac{\sum \bar{V}^2(t_i) (h_i - C g_i)^2}{\left[ \sum \dot{\bar{V}}(t_i) (h_i - C g_i) \right]^2} \quad (2.66)$$



For the model assumed in Fig. 2.7,

$$\begin{aligned}
 \bar{V}(t) &= 1 & t \leq -T/2 = -M\Delta t \\
 &= 1+a & t \geq T/2 = M\Delta t \\
 &= 1 + \frac{a}{2} + \frac{at}{T} & -T/2 \leq t \leq T/2
 \end{aligned} \tag{2.67}$$

For the square-non-overlapping gates assumed, let  $(\Delta t)\ell_E$ ,  $(\Delta t)U_E$  be the position of the lower and upper edge of the early gate, and let  $\ell_L$ ,  $U_L$  refer to the late gate.

Then

$$\begin{aligned}
 \sum \bar{V}(t_i) h_i &= N_p N_E \left( 1 + a/2 + a/2 (\ell_E + U_E)/2M \right) \\
 &= N_p N_E \left( \bar{V}_{\ell_E} + \frac{a}{2M} \left( \frac{N_E - 1}{2} \right) \right)
 \end{aligned} \tag{2.68}$$

and

$$\sum \bar{V}(t_i) g_i = N_p N_L (1 + a) \tag{2.69}$$

where  $N_E = U_E - \ell_E + 1$  is the width of the early gate,  $N_L$  is the width of the late gate,  $N_p$  is the number of pulses integrated, and  $\bar{V}_{\ell_E}$  is the mean power at the lower end of the early gate.

The derivative of  $\bar{V}(t)$  is given by:

$$\begin{aligned}
 \dot{\bar{V}}(t) &= 0 & t < -T/2, \quad t > T/2 \\
 &= \frac{a}{T} & |t| \leq T/2
 \end{aligned} \tag{2.70}$$

Thus

$$\begin{aligned}
 k &= \sum_i \dot{\bar{V}}(t_i) (h_i - C g_i) = N_p \sum_{\ell_E}^{U_E} a/T = N_p \frac{N_E a}{T} \\
 &= N_p \frac{N_E a}{2M\Delta t} \tag{2.71}
 \end{aligned}$$

Finally, (for non-overlapping gates)

$$\text{Var } \mathcal{E}(0) = \sum_{\ell_E}^{U_E} \bar{V}^2(t_i) + C^2 \sum_{\ell_L}^{U_L} \bar{V}^2(t_i) \tag{2.72}$$

But,  $\bar{V}(t_i) = 1 + a$ ,  $\ell_L \leq i \leq U_L$ , since the late gate is on the plateau.

Similarly,  $\bar{V}(t_i) = 1 + a/2 + (ia/2M)$ ,  $\ell_E \leq i \leq U_E$ , since the early gate is on the leading edge.

Thus,

$$\begin{aligned}
 \text{Var } \mathcal{E}(0) &= N_p \sum_{\ell_E}^{U_E} \left(1 + \frac{a}{2} + \frac{a}{2M} i\right)^2 + C^2 N_L N_p (1 + a)^2 \\
 &= N_p N_E \left( \bar{V}_{\ell_E}^2 + \frac{a}{2M} \bar{V}_{\ell_E} (N_E - 1) + \left(\frac{a}{2M}\right)^2 \frac{(N_E - 1)(2N_E - 1)}{6} \right) \\
 &\quad + C^2 N_L N_p (1 + a)^2 \tag{2.73}
 \end{aligned}$$

Substituting (2.62), (2.68 and (2.69 for C yields

$$\text{Var } \mathcal{E}(0) = N_E N_P \left\{ \bar{V}_{\ell_E}^2 + \frac{a}{2M} \bar{V}_{\ell_E} (N_E - 1) + \left(\frac{a}{2M}\right)^2 \frac{(N_E - 1)(2N_E - 1)}{6} \right\} \\ + \frac{N_E^2}{N_L} N_P \left( \bar{V}_{\ell_E} + \frac{a}{2M} \frac{(N_E - 1)}{2} \right)^2 \quad (2.74)$$

Substituting (2.74 and (2.71 into (2.52 yields the equation for the tracking error given as equation (2.53 in Section 2.3.1.1.

### 2.3.2 Continuous Case

In the previous section on the split-gate tracker, it was assumed that the data was sampled at time intervals far enough apart in range so that the sampled values were independent. In this section, the split-gate tracker equations are re-derived assuming that the sampled values are no longer independent. The continuous case (analog) is then approximated by letting the time samples occur at very closely spaced intervals.

The derivation follows very closely the one given in the previous sections, thus only the modifications of that derivation will be given.

In Section 2.3.1 it was shown that the variance of the tracking error for a single pulse is given by eq. (2.66).

$$\text{Var } t_o = \frac{\text{Var } \epsilon(0)}{k^2} \quad (2.75)$$

where

$$k = \left. \frac{\partial E \epsilon(t)}{\partial t} \right|_{t=0} \quad (2.76)$$

is the mean error slope, and

$$\epsilon(t_o) = \sum V(t_i - t_o) (h_i - Cg_i) \quad (2.77)$$

is the tracker error signal;

Further,

$V(t_i)$  is the value of the square law detected envelope at time  $t_i$

$h_i$  is the early gate response of the tracker

$g_i$  is the late gate response

and  $C$  is a normalizing constant.

It was shown that  $k$  is given by:

$$k = \frac{N_E a}{T} \quad (2.78)$$

where  $T$  is the width of the leading edge of the return. This result is not affected by correlation between the samples.

The variance of  $\epsilon(0)$ , however, must be recomputed.

Now,

$$\text{Var } \epsilon(0) = \sum_{ij} (h_i - Cg_i)(h_j - Cg_j) \text{Covar } [V(t_i)V(t_j)] \quad (2.79)$$

It can be shown, that for jointly Gaussian random variables, the covariance of the square law detected output is given by

$$\text{Covar } V(t_i)V(t_j) = \bar{V}_i \bar{V}_j \rho_{ij}^2 \quad (2.80)$$

where  $\bar{V}_i = E V(t_i)$ , and  $\rho_{ij}$  is the correlation between the Gaussian variables.

If the early and late gates are separated enough to be independent, then the variance of  $\epsilon(0)$  becomes:

$$\text{Var } \epsilon(0) = \sum_{\text{e.g.}} \bar{V}_i \bar{V}_j \rho_{ij}^2 + C^2(1+a)^2 \sum_{\text{e.g.}} \rho_{ij}^2 \quad (2.81)$$

where for simplicity, the gates are assumed to be square. The quantity,  $a$ , is the signal-to-noise ratio. The first and second sums above are over the early and late gates respectively.

On the early gate,

$$\bar{V}_i = \bar{V}_E + \frac{a}{T} t_i \quad (2.82)$$

Let  $U_i = \frac{t_i}{T}$ ,  $\delta = \frac{\bar{V}_E}{a}$ , then

$$\frac{\bar{V}_i}{k} = \frac{T}{N_E} (\delta + U_i) \quad (2.83)$$

also

$$\frac{C(1+a)}{k} = \frac{\delta T}{N_L} \quad (2.84)$$

Thus, the tracking error becomes.

$$\begin{aligned} \text{Var } t_o &= \frac{\text{Var } \epsilon(0)}{k^2} \\ &= T^2 \sum_{\text{e.g.}} (\delta + U_i)(\delta + U_j) \frac{\rho_{ij}^2}{N_E} + T^2 \delta^2 \sum_{\text{e.g.}} \frac{\rho_{ij}^2}{N_L} \\ &= \delta^2 T^2 \left\{ \frac{\sum_{\text{e.g.}} \rho_{ij}^2}{N_E} + \frac{\sum_{\text{e.g.}} \rho_{ij}^2}{N_L} \right\} \\ &\quad + 2\delta T^2 \sum_{\text{e.g.}} \frac{U_i \rho_{ij}^2}{N_E} + T^2 \sum_{\text{e.g.}} \frac{U_i U_j \rho_{ij}^2}{N_L} \end{aligned} \quad (2.85)$$

If one assumes, stationarity,

$$\rho_{ij} = \rho_{i-j}, \quad (2.86)$$

then it can be shown by symmetry arguments that:

$$\sum U_i \rho_{ij}^2 = 0 \quad (2.87)$$

Finally letting  $Z_i = t_i / \Delta_E$  where  $\Delta_E$  is the width of the early gate, one has:

$$\begin{aligned} \frac{\text{Var } t_o}{T^2} &= \delta^2 \left\{ \frac{1}{N_E^2} \sum_{\text{e.g.}} \rho_{ij}^2 + \frac{1}{N_L^2} \sum_{\text{e.g.}} \rho_{ij}^2 \right\} \\ &\quad + \frac{\Delta_E^2}{T^2} \frac{1}{N_E} \sum_{\text{e.g.}} Z_i Z_j \rho_{ij}^2 \end{aligned} \quad (2.88)$$

This expression can be shown to be equivalent to that in Section 3.1 for independent samples.

The summations in equation 2.88 have been evaluated for a Gaussian shape correlation function. These results are shown in Figure 2.9 and 2.10. The results are given versus  $N$  the number of samples in the gate, and  $\rho_{1/2}$  the correlation between a sample in the middle of the gate, and one at the edge of the gate. The results for  $N = 10$ , approximate fairly closely the continuous case.

In the next section, the tracking error for the sampled split-gate, continuous split-gate, and MLE trackers are compared.

$$\frac{1}{N^2} \sum \rho_{ij}^2 \text{ Versus } N \text{ and } \rho_{1/2}$$

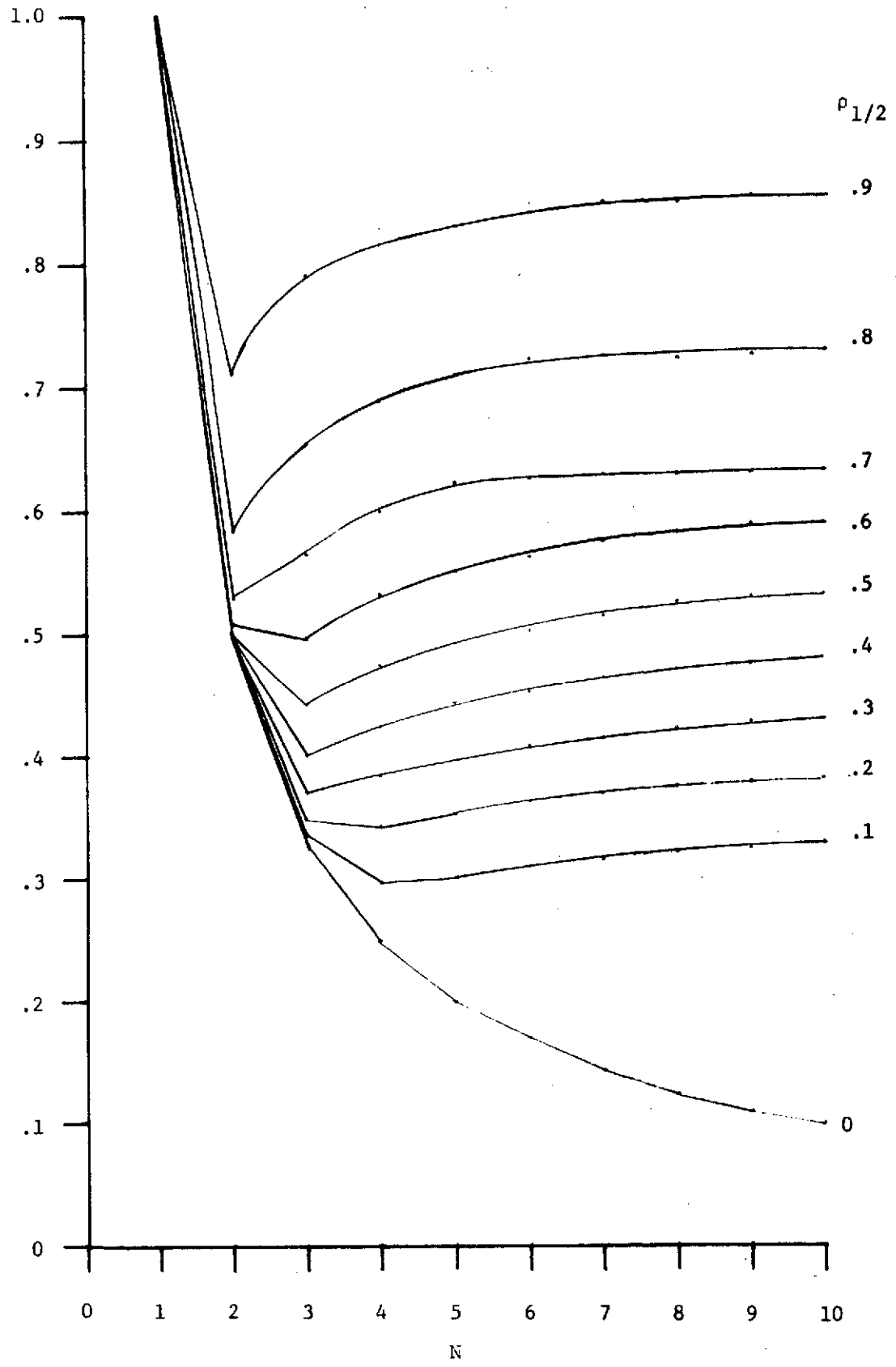


Figure 2.9



$$\frac{1}{N^2} \sum z_i z_j \rho_{ij}^2$$

Versus N and  $\rho_{1/2}$

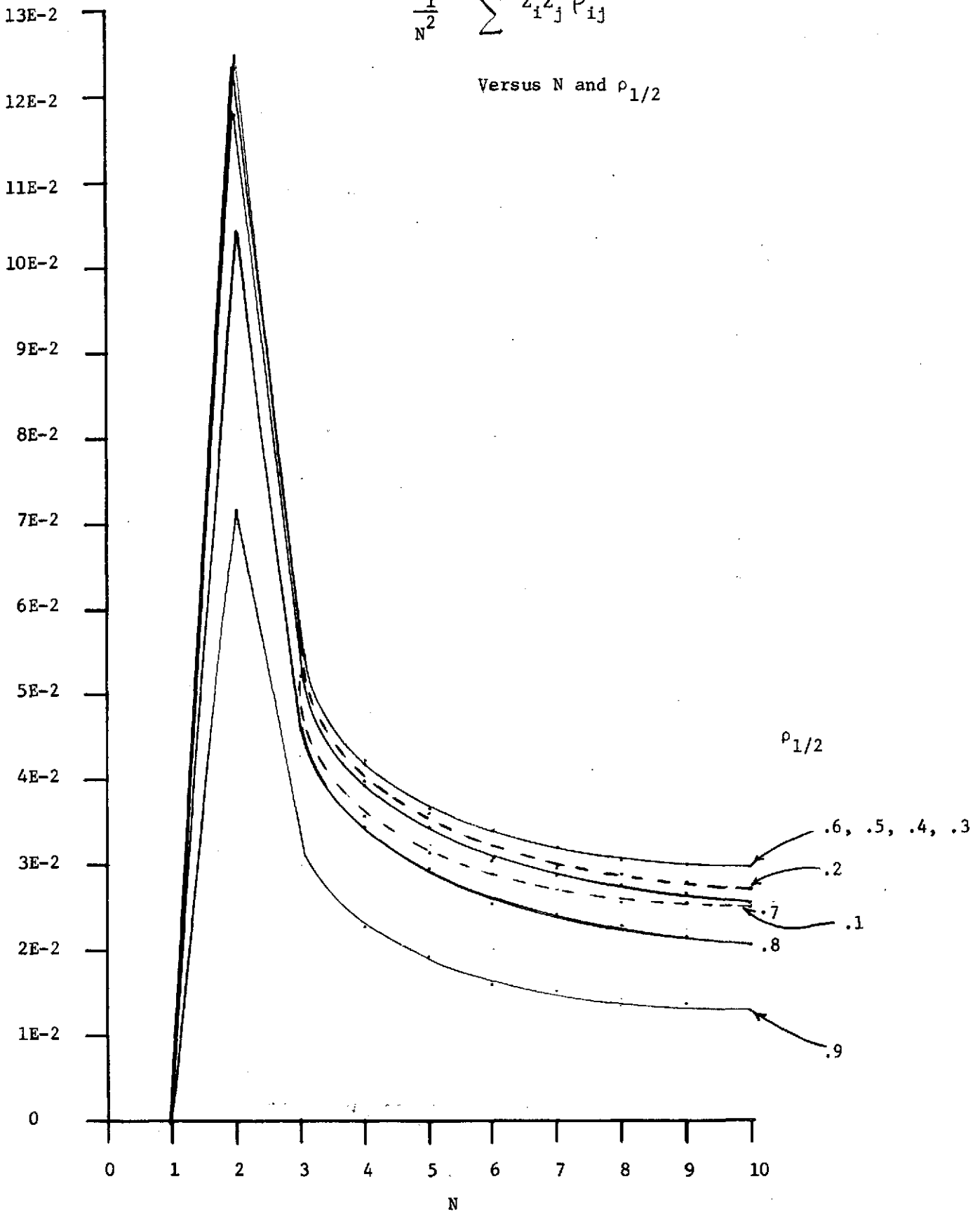


Figure 2.10

## 2.4 Comparison of Tracker Performances

In this section the accuracy expressions derived for the continuous split gate, the discrete split gate, and the MLE trackers are evaluated and compared.

The continuous split-gate tracker accuracy expression of equation (2.88) requires a correlation function,  $\rho_{ij}$ , between adjacent samples in the IF filter output. (It is assumed for simplicity that no pulse compression is performed). The correlation function for the output process of the IF filter is given by the convolution of the correlation function of the input process with the autocorrelation function of the filter impulse response. The correlation function of the input process is just the autocorrelation function of the transmit pulse, since the return signal is the transmit pulse convolved with a spatially white distributed target. Thus if the IF filter is matched to a rectangular pulse of width  $1/B$ , the output correlation function is the convolution of four rectangular pulses. This function is approximately Gaussian in shape with variance given by

$$\sigma^2 = 2 \left( \frac{T^2}{12} + 2 \frac{1}{12B^2} \right) \quad (2.89)$$

Thus, the IF filter output correlation,  $\rho(\tau)$ , is approximately given by:

$$\rho(\tau) = \exp \left\{ -3 \frac{(B\tau)^2}{[1+(B\tau)^2]} \right\} \quad (2.90)$$

Using this expression for  $\rho(\tau)$  and  $BT=1$  equation (2.88) is evaluated. The resulting performance is plotted in Figure 2.11 for several tracker configurations.

The discrete split gate tracker variance is computed by substituting  $N_E = 1$  into equation (2.88) and setting  $\rho_{ij} = 0$  for  $i \neq j$ . The performance of this tracker is also presented in Figure 2.11. The discrete time model can be seen to be overly pessimistic relative to the continuous time model.

A MLE tracker accuracy is obtained from equation (2.46) by substituting

$$\beta = \frac{c}{2\sigma_h} \quad (2.91)$$

and converting from time to distance units via

$$d = \frac{c\Delta t}{2} \quad (2.92)$$

and

$$\sigma_R = \frac{c\sigma_t}{2} \quad (2.93)$$

Performing these substitutions yields for the MLE

$$\sigma_R \sqrt{N_p} = \sqrt{d\sigma_h} \left[ K_{t_o t_o}^{-1} \right]^{1/2} \quad (2.94)$$

This is also plotted in Figure 2.11 and compared with the split gate trackers (right ordinate) for  $\sigma_h = 2.5$  m and  $d = .5$  m ( $\tau_c \simeq 3$  nsec). It should be noted that  $\left[ K_{t_o t_o}^{-1} \right]^{1/2}$  also depends on  $\sigma_h$  through  $U_{\max}$  (equation 2.48)

$$\begin{aligned} U_{\max} &= \alpha \beta T_{\max} \\ &= \alpha \beta \Delta t N_{\text{cells}} \end{aligned} \quad (2.95)$$

where  $\alpha = .3227$  and  $N_{\text{cells}}$  equals the number of resolution cells from the half power point of the return to the end of the observation interval. Substituting

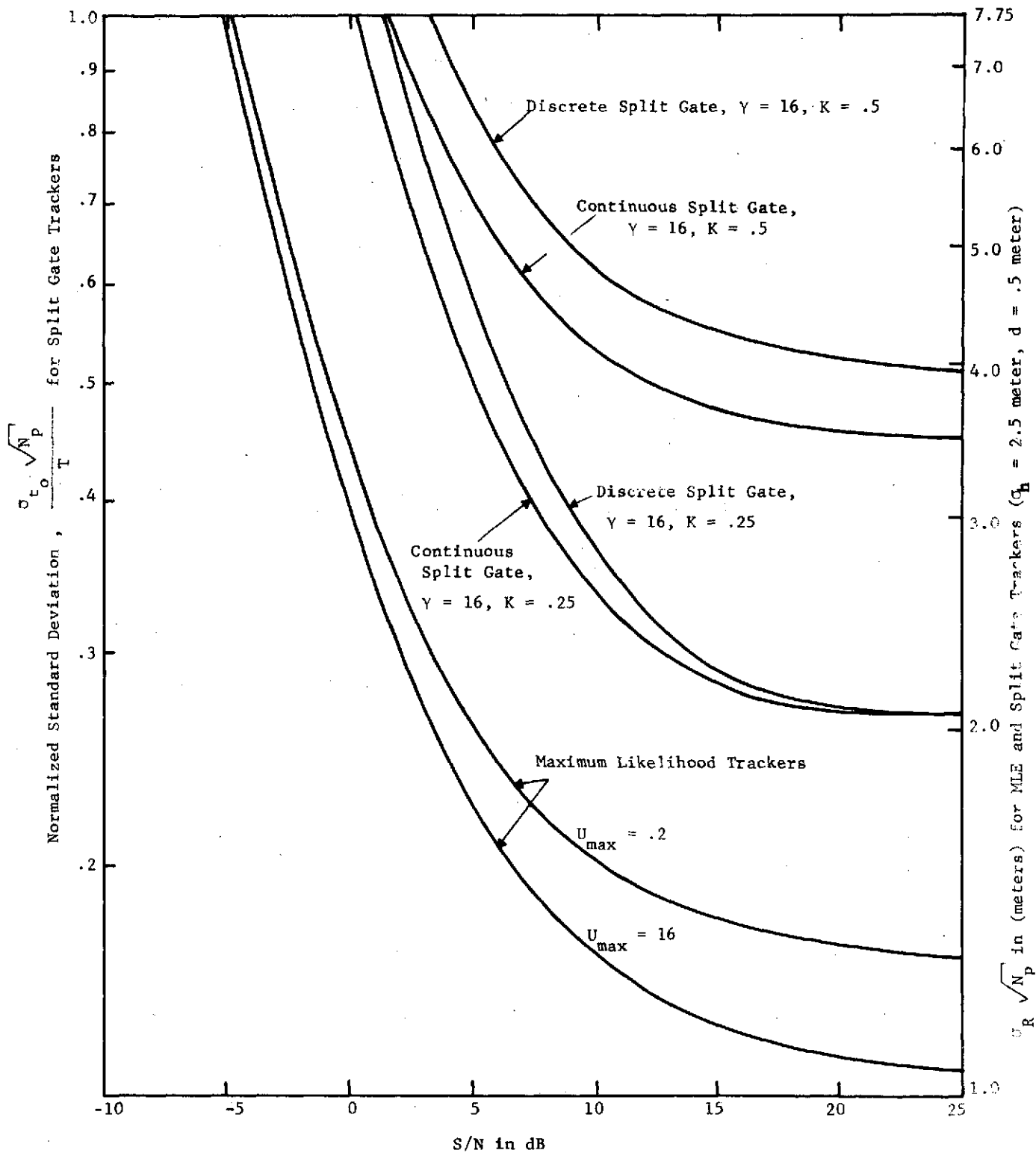


Figure 2.11 . Comparison of Tracker Accuracies

equation 2.91 and  $\Delta t = 3$  nsec yields

$$U_{\max} = .1452 \frac{N_{\text{cells}}}{\sigma_h} \quad (2.96)$$

In Figure 2.11,  $[K_{t_o t_o}^{-1}]^{1/2}$  is computed for  $N_{\text{cells}} = 31$  (corresponding to half the leading edge, 15 cells, plus 16 cells in the equivalent late gate) or  $U_{\max} \approx 2.0$ . A somewhat smaller tracking error can be achieved by the MLE by utilizing more cells on the plateau as illustrated in Figure 2.11 for the case  $U_{\max} = 16$ . To compare the split-gate trackers at a particular waveheight with the MLE, use is made of the relationship between  $\sigma_h$  and T via

$$\sigma_h \approx \frac{c}{2} \frac{T}{3.1} \quad (2.97)$$

which is obtained by a least squares linear fit to the leading edge of the error function. Thus converting the distance units, the error for the split-gate tracker is

$$\sigma_R \sqrt{N} = 3.1 \sigma_h \text{ (NSD)} \quad (2.98)$$

where NSD is the normalized standard deviation for the split-gate trackers (left ordinate) of Figure 2.11.

### References

- [1] Dooley, R.P., "The Effect of Range Sidelobes on Radar Altimeters", TSC-W3.
- [2] Wilkes, S.S., Mathematical Statistics Wiley, 1963.
- [3] Lank, G., "Measurement of Clutter Shape, Position and Amplitude", TSC Project Memo 080-17, 18 December 1972.

### 3.0 BINARY PHASE CODE WITH DIGITAL PROCESSING

#### 3.1 SUMMARY

The practicality of using phase-code and digital processing in a satellite altimeter and wave height analyzer is investigated in this report. It is shown that a multi-bit digital processor (at least 2 bits plus sign) is required due to the distributive nature of the sea surface. Single-bit processing, which has been found effective in many different applications, is found to be unsuitable. Results show that for a compression ratio of 1000:1 and an uncompressed return-to-noise ratio<sup>\*</sup> of -20 dB, the compressed output signal-to-noise ratio is only 4.1 dB which is insufficient to maintain the required tracking accuracy.

#### 3.2 PROBLEM DESCRIPTION

A phase-code altimeter generates a phase-code sequence using feedback shift-registers properly tapped as shown in Fig. 3.1. This sequence modulates the phase of a carrier. The resolution of the phase-code waveform depends on the duration of a bit,  $\tau$ , in the code and the output signal-to-noise ratio depends on the length of the code,  $K$ , as well as the reflected power-to-noise<sup>\*</sup> ratio.  $K$  is equal to the ratio of the duration of the entire waveform,  $T$ , to the resolution  $\tau$  i.e.,

$$T = K\tau \quad (3.1)$$

and it is often called the compression ratio.

---

<sup>\*</sup>As defined here the return power is that from a single range cell. The equivalent peak-power-to-noise ratio is 10 dB for the example shown.

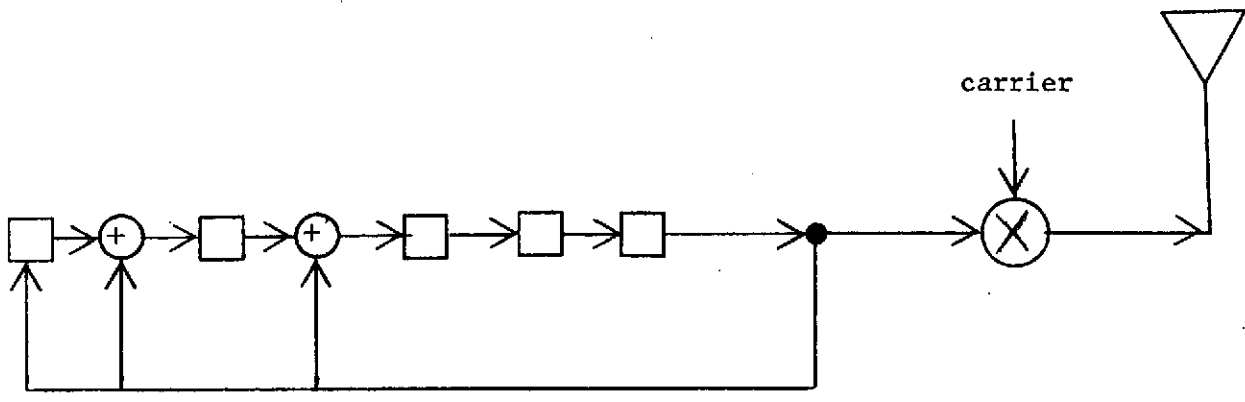


Fig. 3.1 Phase-code generator and transmitter.

The receiver of a phase-code altimeter is shown in Fig. 3.2. As seen, the return

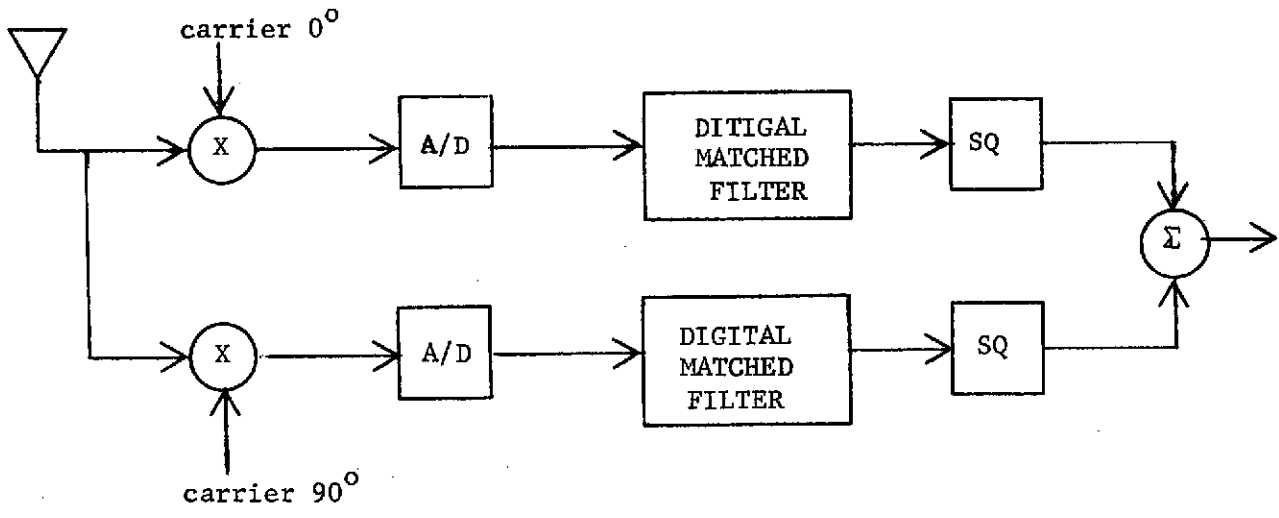


Fig. 3.2 Digital phase-code receiving.

is separated into two channels usually designated by I and Q for in-phase and quadrature. After mixing with the carriers, the video signals are quantized and delivered to a pair of digital-matched-filters, DMF. A DMF is a device which compares the input with the transmitted phase-code sequence

and totals the number of matches and the number of mismatches. The difference of the two numbers is used as an indication of the strength of the signal return. Of course, in the absence of any return, this difference will be zero or nearly zero on the average.

The NASA system requirements indicate that  $\tau$  is on the order of 3 nsec. Since the satellite is far from the target (556 km), the return is likely to be weak. The pre-processed input signal-to-noise ratio for one range cell is expected to be on the order of -20 dB or less. Hence,  $K$  is necessarily long, say on the order of 1000. Together, the two requirements imply that the A/D must be fast enough to sample the input at 300 MHz rate and the DMF must be at least one thousand bits long. Obviously, if high accuracy quantization is also required, the hardware implementation of this receiver will be very difficult involving relatively high risk.

In the following discussion, the performance degradation as compared to a linear system is analyzed as a function of the accuracy of quantization. For simplicity, the analysis has been limited to a smooth sea surface and a pulse-limited situation. The conclusions obtained and the method of analysis can be extended to other situations with a little modification.

### 3.3 Basic Assumptions

As indicated previously, it is assumed that the sea surface is flat. In such a case, the impulse response is a perfect step as shown in Fig. 3.3a. The return from a pulse-code waveform is a ramp as shown in Fig. 3.3b, composed of the returns from the different range cells. For a smooth sea, the power of the return,  $C$ , from the different range cells will be the same on the



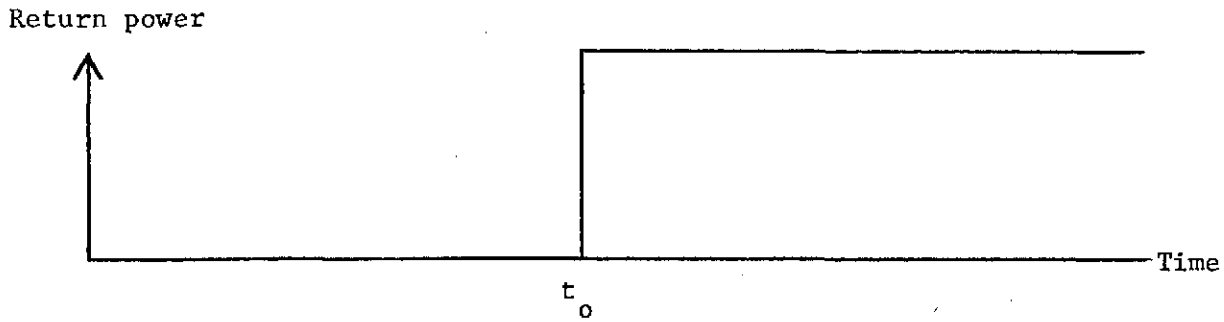


Fig. 3.3a Impulse response of a smooth sea.

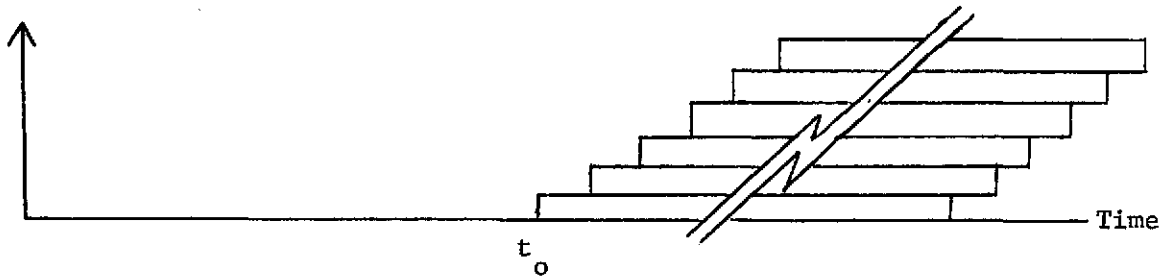


Fig. 3.3b Response of an extended pulse waveform.

average. The receiver, in effect, cross correlates the entire return with a replica of the transmitted pulse-code sequence once every  $\tau$  seconds. The instant such a sequence in phase with the replica appears at the return, the cross correlator output will peak indicating its presence. Since the return is an overlap of many pulse-code sequences with different phase shifts, the cross correlator output will also have smaller peaks due to partial matching between the replica and the return. The power of the subpeaks is proportional to the sidelobes of the auto-correlation function of the phase-code sequence. A typical auto-correlation function of such a sequence is shown in Fig. 3.4.

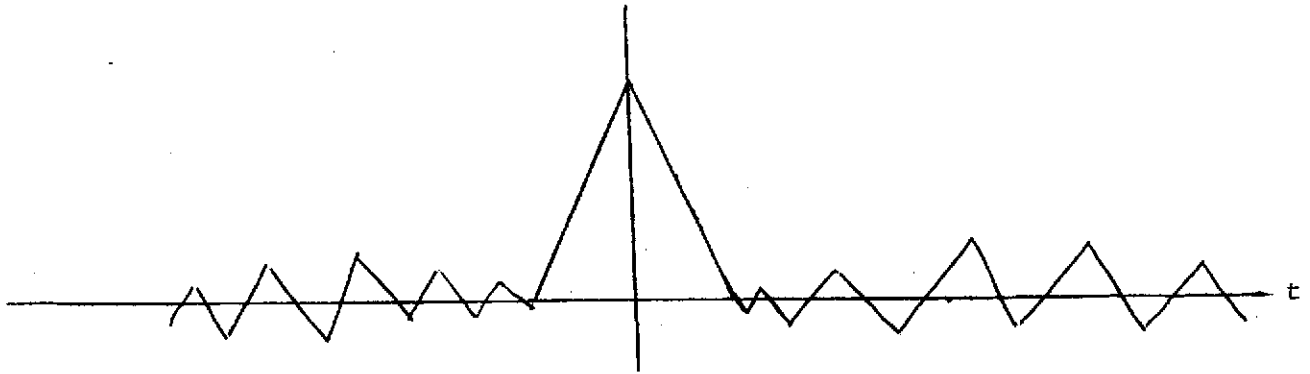


Fig. 3.4 Phase-code auto correlation.

These subpeaks are undesirable and they may be reduced by proper signal design amplitude tapering of the replica. In the present analysis, it is convenient to assume that the sidelobes are identically zero. To a first approximation, this assumption does not affect the conclusions to any large extent.\*

It is assumed that the return from a range cell has the form  $c s(t)$  where  $c$  is a complex Gaussian process and  $s(t)$  is the transmitted signal.  $c$  is independent from range cell to range cell and the amplitude of  $c$  is Rayleigh whose mean power is  $C$ . Due to this assumption, the compressor output signal-to-noise ratio of either branch will be the same as that of the entire processor as shown in Fig. 3.2.

It will also be convenient at this point to define the symbols to be used with the A/D converters. The converters considered here are always odd, uniform, and without any dead zone. The input-output relationship of such a quantizer is shown in Fig. 3.5.

\*Tapering will be more difficult in digital systems especially in single-bit systems. It is expected that larger signal power loss will result in suppressing sidelobes in digital systems.

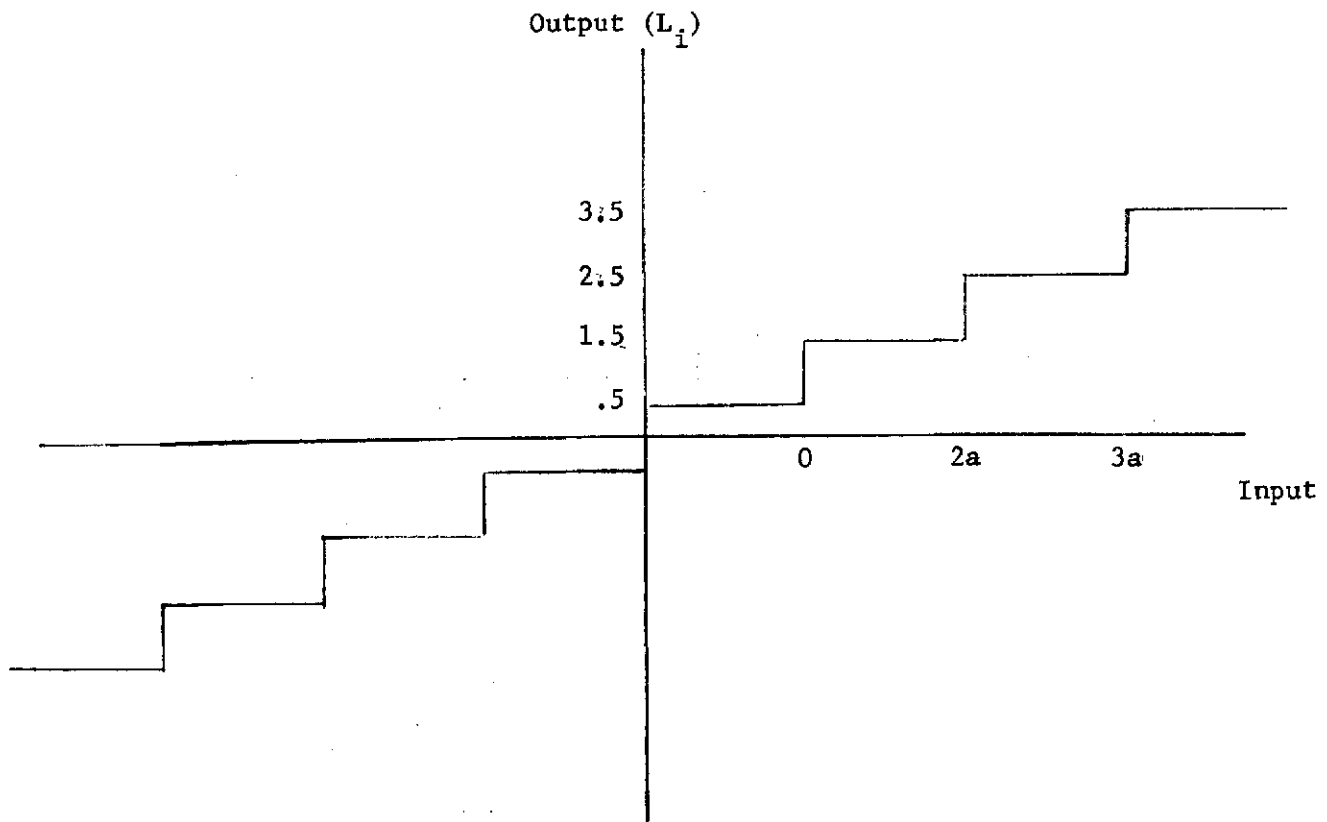


Fig. 3.5 A quantizer.

Shown is a two-bit (plus sign) quantizer with  $M = 4$  output levels on the positive input side. The spacing between two output levels is  $\Delta = 1.0$  and the spacing between any two adjacent input thresholds is "a".

### 3.4 Digital Compressor Output Power

As a measure of the system performance, the output power of the digital processor (one branch) will be computed and compared with the output power of a linear processor using phase-codes. Intuitively, it is expected that a digital or linear compressor restores the return from that shown in Fig. 3.3b to that shown in Fig. 3.3a. The sharpness of the edge and the height of the jump of the reconstructed signal is an indication of the effectiveness of the compressor. As will be shown later, there is a loss of the height of the jump as the quantization error increases.

Let  $s_i$ ,  $i = 1 \dots K$ , denote the phase-code sequence.  $s_i$  may be plus or minus one. Let  $v_i$  denote the video input sequence,  $w_i$  denote the video quantized sequence and  $y_i$  denote the compressed output sequence. Assume the time origin is centered on the instant prior to the arrival of the earliest echo. Then, the video input sequence  $v_j$  is given by

$$v_j = n_j + \sum_{i=1}^{K(j)} c_{j-i+1} s_i \quad (3.2)$$

where  $n_j$  is the Gaussian noise,  $c_i$  is the reflective coefficients and

$$\begin{aligned} K(j) &= 0 & j < 1 \\ &= j & K \geq j \geq 1 \\ &= K & j > K \end{aligned}$$

The compressor output  $y_{j+K}$  is given by

$$y_{j+K} = \sum_{n=1}^K s_n w_{j+n} \quad (3.3)$$

Since both  $n_j$  and  $c_j$  are Gaussian of mean zero, and the quantizer is odd, then  $w_j$  also has mean zero. The compressor output power is equal to the expected value of  $y_{j+K}^2$ . From (3.3), this power is

$$\begin{aligned} E [y_{j+K}]^2 &= \sum_{n,m}^K E [(s_n w_{j+n})(s_m w_{j+m})] \\ &= \sum_{n=1}^K E [w_{j+n}^2] + \sum_{m \neq n}^K E [w_{j+n} w_{j+m}] s_n s_m. \end{aligned} \quad (3.4)$$

The expression on the RHS is split into two sums because it is easier to handle them separately. The terms in the first sum are simply the average quantizer output powers. Each of the  $K$  terms in this sum may be computed by the basic relationship

$$E[w_j^2] = \int_{-\infty}^{\infty} w^2 p_j(w) dw \quad (3.5)$$

where  $p_j(w)$  is the probability density function of  $w_j$ . In the present case,  $w_j$  is discrete so that the integral in (3.5) can be replaced by a finite sum as

$$E [w_j^2] = \sum_{\substack{i=-M \\ i \neq 0}}^M L_i^2 p_j(L_i) = 2 \sum_{i=1}^M L_i^2 p_j(L_i) \quad (3.6)$$

where each  $L_i$  is a quantizer output level (see Fig. 3.5) and the probability  $p_j(L_i)$  is given by the probability that the quantizer input  $v_j$  falls between the  $i$  and  $(i-1)$  threshold. Since  $v_j$  as given in (3.2) is Gaussian of mean zero,  $p_j(L_i)$  is

$$p_j(L_1) = 0.5 - Q(a/\sigma_j)$$

$$p_j(L_i) = Q((i-1)a/\sigma_j) - Q(ia/\sigma_j)$$

$$1 < i < M$$

$$p_j(L_M) = Q((M-1)a/\sigma_j) \quad (3.7)$$

where  $\sigma_j^2$  is the variance of  $v_j$  (see (3.11) below). The function  $Q(x)$  is the tail of the normal probability integral, and is given by:

$$Q(x) = \frac{1}{\sqrt{2\pi}} \int_x^{\infty} e^{-t^2/2} dt \quad (3.8)$$

The terms in the second sum in (3.4) are the cross correlations between pairs of quantized Gaussian random variables. They are related to the input correlations as

$$R(w_m, w_n) = 4 \sum_{\substack{\ell=1 \\ \ell \text{ odd}}}^{\infty} \sum_{u=0}^{M-1} \left( \Delta_u \exp\left(-\frac{u^2 a^2}{2\sigma_m^2}\right) H_{\ell-1}\left(\frac{ua}{\sigma_m}\right) \right) \\ \times \left( \Delta_u \exp\left(-\frac{u^2 a^2}{2\sigma_n^2}\right) H_{\ell-1}\left(\frac{ua}{\sigma_n}\right) \right) \cdot \frac{R^{\ell}(v_m, v_n)}{2\pi \sigma_m \sigma_n \ell!} \quad (3.9)$$

$$\Delta_0 = 0.5$$

$$\Delta_u = 1, u \geq 1$$

where  $H_{\ell-1}(x)$  is the Hermite polynomial of  $(\ell-1)$ th order. This relationship can be derived from the general result given in [1] using the same approach as in [2]. The details are omitted in this report.

At this point, (3.9) can be substituted directly into (3.4) to find the output power of the digital compressor but considerable simplification is possible due to the fact that  $R(v_m, v_n)/\sigma_m \sigma_n$  is small, for  $m \neq n$ . From (3.2)  $R(v_m, v_n)$  is

$$\begin{aligned} R(v_m, v_n) &= E [v_m v_n] + E \left[ \sum_{i=1}^{K(m)} \sum_{k=1}^{K(n)} c_{m-i+1} s_i c_{n-k+1} s_k \right] \\ &= N \delta_{nm} + \sum_{i=1}^{K(m)} \sum_{k=1}^{K(n)} E [c_{m-i+1} c_{n-k+1}] s_i s_k \end{aligned} \quad (3.10)$$

When  $n = m$ ,  $R(v_n, v_n) = \sigma_m^2$ , the variance of  $v_m$ , and is given by:

$$\sigma_m^2 = N + \sum_{i=1}^{K(m)} \sum_{k=1}^{K(m)} c_{m-i+1} c_{m-k+1} = N + K(m) C \quad (3.11)$$

using the fact that  $E[c_i c_j] = 0$ ,  $i \neq j$  and  $E[c_i^2] = C$ . On the other hand, when  $m \neq n$ ,  $R(v_m, v_n)$  is

$$R(v_m, v_n) = C \sum_{k=1}^{K'(m,n)} s_{m-n+k} s_k \quad (3.12)$$

where  $K'(m,n) = \min(K(m), K(n))$

For a well designed code with small sidelobes, the result of the summation in (3.12) will be small but in any case it is always less than  $K(n)$ . Hence,  $R(v_m v_n)/\sigma_m \sigma_n$  is small if  $K(n) \gg 1$  or if  $N \gg K(n)$ . In practice, one of the two conditions is always satisfied.

Since (3.9) is a power series in  $R(v_m v_n)/\sigma_m \sigma_n$ , the first order term in (3.9) will be a good approximation for  $m \neq n$ . Substituting (3.10 and (3.9) into (3.4) it is found that

$$E[y_{j+K}^2] = \sum_{n=1}^K E[w_{j+n}^2] + E \left[ \sum_{m \neq n}^K s_n s_m f(\sigma_{j+n}) f(\sigma_{j+m}) \sum_i^{K(j+m)} \sum_k^{K(j+n)} c_{j+m-i+1} c_{j+n-k+1} s_i s_k \right] \quad (3.13)$$

where

$$f(\sigma) = 2 \sum_{n=0}^{M-1} \Delta_u \exp \left( -\frac{u^2 a^2}{2\sigma^2} \right) / \sqrt{2\pi} \sigma$$

Adding and subtracting the term  $E \left[ \sum_{n=1}^K s_n^2 f^2(\sigma_{j+n}) \sum_{i,k}^{K(j+n)} c_{j+n-i+1} c_{j+n-k+1} s_i s_k \right]$ ,

(4.12) can be put into the form

$$E[y_{j+K}^2] = \sum_{n=1}^K E[w_{j+n}^2] - \sum_{n=1}^K f^2(\sigma_{j+n}) \sum_i^{K(j+n)} c_{j+n-i+1}^2 + E \left( \sum_{n=1}^K s_n f(\sigma_{j+n}) \sum_{i=1}^{K(j+n)} c_{j+n-i+1} s_i \right)^2 \quad (3.14)$$

The first two sums in (3.14) have the following interpretations. The first term is the total quantizer output power in an interval  $T = K\tau$ . The second term is



the output target return power over the same interval. The difference of the two terms is, therefore, the total output noise power.

The third sum, denote it by B, can be simplified considerably. Letting  $\tau = n-i$ , it becomes

$$B = E \left( \sum_{\tau} \sum_{n=1}^K c_{j+\tau+1} f(\sigma_{j+n}) s_n s_{n-\tau} \right)^2 \quad (3.15)$$

The limits on  $\tau$  depends on  $j$  as follows,

$$\begin{aligned} \tau &= -(j-1), \dots, K+j-1 & j \leq 0 \\ &= j, \dots, K+j & j > 0 \end{aligned}$$

The summations  $\sum_{n=1}^K f(\sigma_{j+n}) s_n s_{n-\tau}$  are the sidelobes of the quantized signal when  $\tau \neq 0$ . As a result of the zero sidelobe assumption, B is reduced to

$$\begin{aligned} B &= E \left( \sum_{n=1}^K c_{j+1} f(\sigma_{j+n}) \right)^2 \\ &= C \left( \sum_{n=1}^K f(\sigma_{j+n}) \right)^2 \end{aligned} \quad (3.16)$$

for  $j > 0$  and is zero for  $j \leq 0$ . Thus, the third sum in (3.14) is a measure of the compressor output due to the return which is in-phase with the local signal-replica.

In the next section, the response of a hard-limiting (one bit I and one bit Q, including sign) system will be analyzed in detail to be followed by the analysis of multi-bit system performances.

### 3.5 Hardlimiting Digital Processor

Since the statistics of the input to the receiver is non-stationary, it will be convenient to compute the compressor output for different time intervals separately. Again, as above,  $j=1$  corresponds to the instant prior to the earliest return reaching the compressor. Fig. 3.6 shows the breakdown of the time segments.

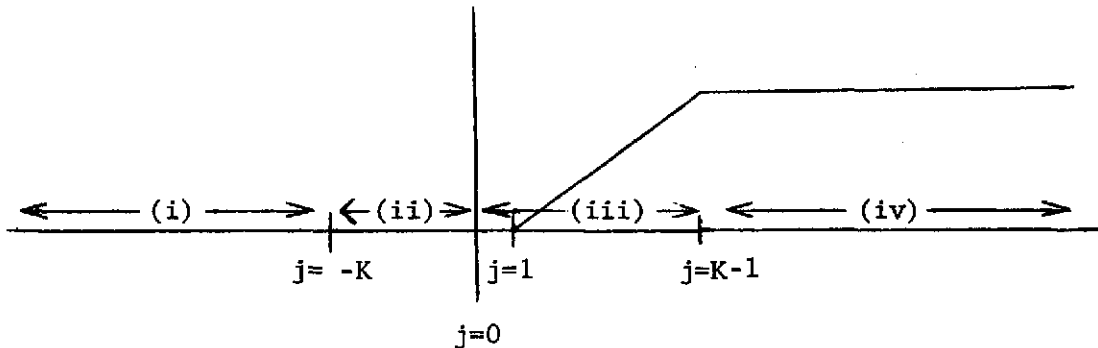


Fig. 3.6 Breakdown of time segments.

Case (i)  $j+K \leq 0$

Prior to the instant  $j = -K$ , the input in the compressor is entirely Gaussian noise generated by the front-end of the receiver. Since this noise is uncorrelated with the transmitted signal, the second and third term in (3.6) are zero. The compressor output is given by the first term only, which may be computed using (3.6), (3.7) and (2.8). For a hardlimiting system, this is quite simple since all positive input is mapped into  $(+0.5)$  and all negative input is mapped into  $(-0.5)$ . The output power is, on the average

$$E[y_{j+K}^2] = K(0.5)^2 = K/4, \quad j \leq -K \quad (3.17)$$

For a hardlimiter, the first term in (3.14) is always  $K/4$ .

Case (ii)  $0 < j+K < K-1$

During this time interval, the target return is growing as  $j$  increases and is competing with the Gaussian noise for quantizer power. There is as yet no coherent output power at the compressor and the third term in (3.14) is still zero. The terms in the second sum are, however, growing linearly as a function of  $j$ . The average compressor output is

$$E[y_{j+K}^2] = K/4 - \sum_{i=1}^{j+K} i C f^2(\sigma_i) \quad (3.18)$$

where some simplification has been made based on (3.14) and the definition of the upper limit  $K(j+n)$ .  $\sigma_i$  is given by (3.11) as

$$\sigma_i^2 = i C + N \quad (3.19)$$

$f(\sigma_i)$  is

$$f(\sigma_i) = \frac{1}{\sqrt{2\pi} \sigma_i} = \frac{1}{\sqrt{2\pi (i C + N)}} \quad (3.20)$$

Consequently,

$$E [y_{j+K}^2] = K/4 - \frac{1}{2} \sum_{i=1}^{j+K} \frac{2iC}{\pi(iC+N)} \quad (3.21)$$

Case (iii)  $K \leq j+K < 2K-1$

From the time  $j=1$  on,  $E[y_{j+K}]^2$  will always be a return component which is matched to the transmitted-signal-replica. However, the share of the quantizer power devoted to this particular component is gradually changing from a peak at  $j=1$  to a constant level at  $j=K$ . The total input power is

$$\begin{aligned} \sigma_j^2 &= N + jC & j \leq K \\ &= N + KC & j > K \end{aligned} \quad (3.22)$$

so that

$$f(\sigma_j) = \frac{1}{\sqrt{2\pi(jC+N)}} \quad j \leq K-1 \quad (3.23)$$

The output compressor power is

$$\begin{aligned} E [y_{j+K}^2] &= K/4 - \frac{1}{2} \left[ \left( \sum_{i=j}^K \frac{2iC}{\pi(jC+N)} \right) + \frac{2KC(j-1)}{\pi(KC+N)} \right] \\ &+ \frac{1}{2} \left[ \frac{2(j-1)\sqrt{C}}{\sqrt{2\pi(KC+N)}} + \sum_{i=j}^K \frac{2\sqrt{C}}{\sqrt{2\pi(iC+N)}} \right]^2 \end{aligned} \quad (3.24)$$

Case (iv)  $j + K \geq 2K-1$

Beyond  $j = K$ , the return from the sea surface has reached a maximum and the average power will remain constant.  $E[y_{j+K}^2]$  is simply

$$E[y_{j+K}^2] = K/4 - \frac{1}{4} \left( \frac{2K K C}{\pi(K C + N)} \right) + \frac{1}{2} \left( \frac{2K/C}{\sqrt{2\pi (K C + N)}} \right)^2 = K/4 \quad (3.25)$$

Let  $K = 1000$ . The digital compressor output as a function of time is shown in Fig. 3.7.

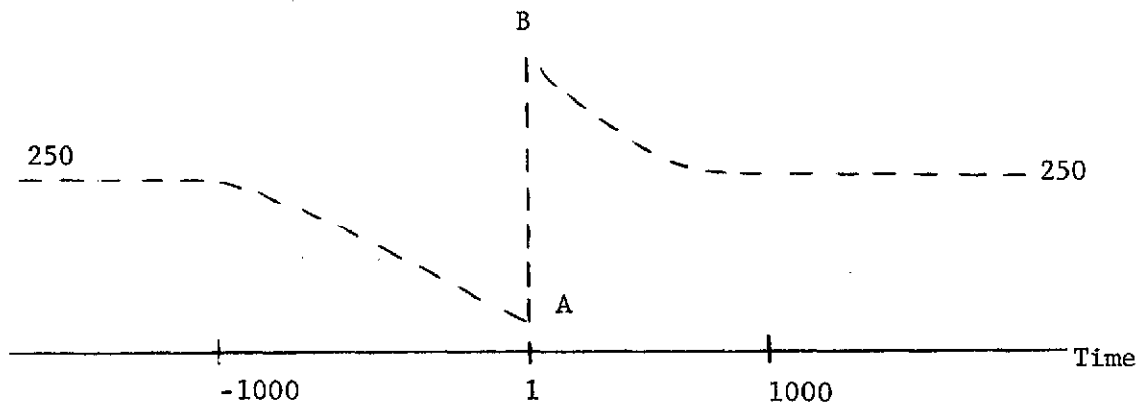


Fig. 3.7 Average compressor output.

The power levels reached in Fig. 3.7 depend on the ratio  $C/N$ . For different values of  $(C/N)^{-1}$  these levels are tabulated in Table I.

TABLE I. Average Compressor Output Levels

$(C/N)^{-1}$	A	B	Coherent Power (B-A)
10	98	616	518
30	108	557	449
50	115	522	407
100	129	470	341
200	147	415	268
300	160	384	224
500	178	348	170
1000	201	310	109

For a given K, a linear compressor output will be

$$\begin{aligned}
 E [y_{j+K}^2] &= KN & j < 1 \\
 &= KN + K^2 C & j \geq 1
 \end{aligned}
 \tag{3.26}$$

To compare various system performances, it will be convenient to define a 'jump' ratio as

$$Y = \frac{E [y_{K+1}^2] - E [y_K^2]}{E [y_K^2]}
 \tag{3.27}$$

For the linear case, this ratio is simply

$$\gamma_{\text{Linear}} = K \frac{C}{N} \quad (3.28)$$

For the hardlimiting case,  $\gamma_{\text{HL}}$  is tabulated in Table II for various values of  $N/C$  with  $K = 1000$

TABLE II.  $\gamma_{\text{Linear}}$  And  $\gamma_{\text{HL}}$  For  $K = 1000$

<u><math>(C/N)^{-1}</math></u>	<u><math>\gamma_{\text{Linear}}</math></u>	<u><math>\gamma_{\text{HL}}</math></u>	<u>Loss (dB)</u>
10	100.0	5.29	12.77
30	33.3	4.18	8.95
50	20.0	3.54	7.52
100	10.0	2.65	5.77
200	5.0	1.81	4.41
300	3.3	1.38	3.77
500	2.0	.96	3.18

The degradation defined as  $\gamma_{\text{Linear}}/\gamma_{\text{HL}}$  of  $\gamma_{\text{HL}}$  is plotted in Fig. 3.8 as a function of  $N/C$ . It should be noted that this loss in performance cannot be compensated for by raising the transmitter power by a factor equal to the ratio  $\gamma_{\text{Linear}}/\gamma_{\text{HL}}$ . As seen, even though a system with  $N/C = 100$  and  $K = 1000$  has a loss of 5.77 dB, an  $N/C$  ten times smaller can only bring the hard-limiting system performance to about half that of the linear system. In fact, for large  $K$  it may be shown that  $\gamma_{\text{HL}}$  is approximately

$$\gamma_{HL} = \frac{\frac{8}{\pi} [(K+\beta)^{\frac{1}{2}} - (1+\beta)^{\frac{1}{2}}]^2}{K(1 - \frac{2}{\pi}) + \beta(\ln(K+\beta) - \ln(1+\beta))} \quad (3.29)$$

$$K \gg 1$$

$$\beta = N/C$$

Therefore, even if  $\beta = 0$

$$\gamma_{HL} = \frac{8}{\pi} / (1 - \frac{2}{\pi}) = 7.07 \quad \beta \rightarrow 0 \quad (3.30)$$

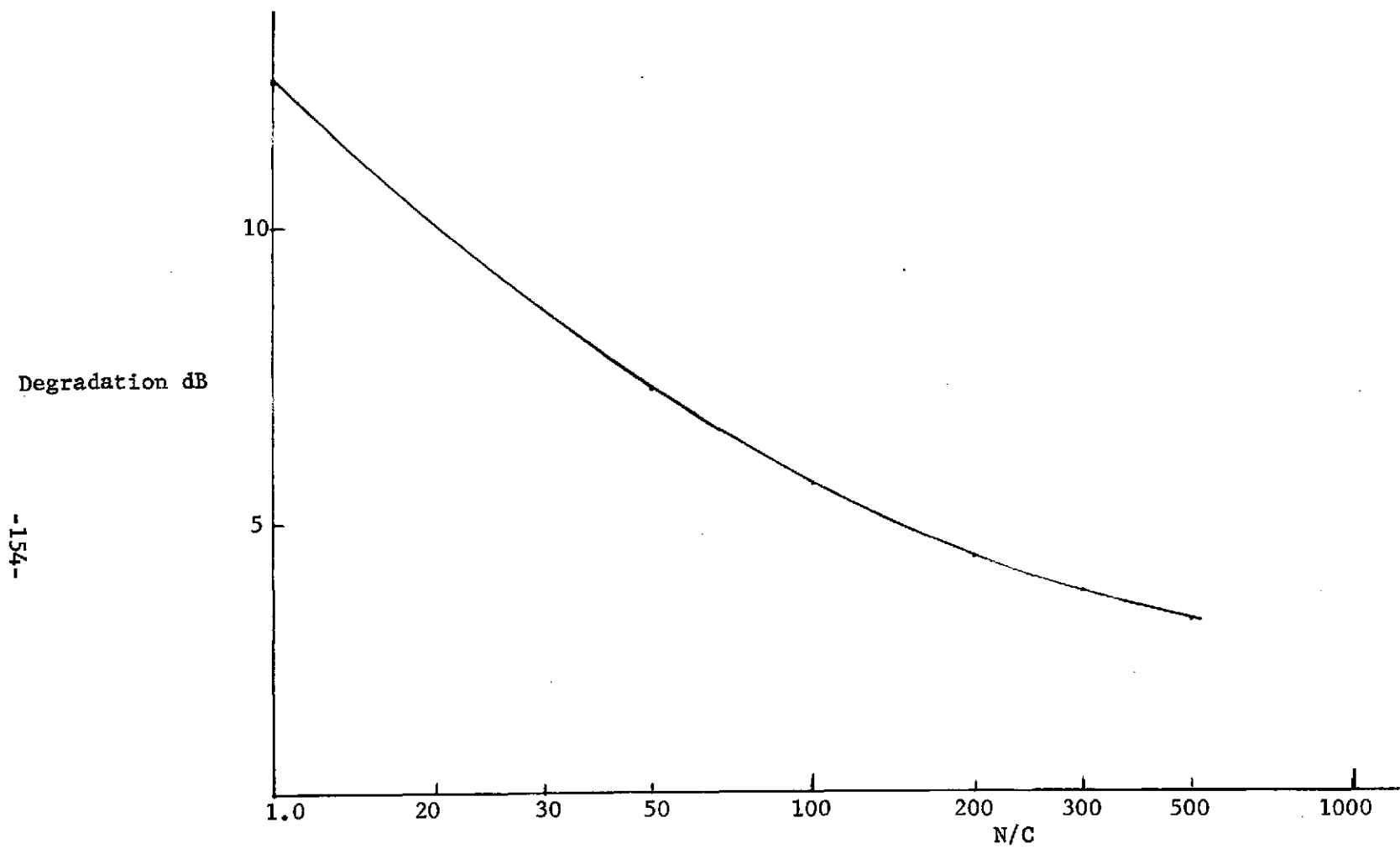
Thus, the degradation as compared to a linear system is inversely proportional to  $\beta$  as  $\beta \rightarrow 0$ . On the other hand, (3.29) also shows that as  $\beta \rightarrow \infty$ ,  $\gamma_{HL}$  is

$$\gamma_{HL} = \frac{2}{\pi} \frac{K-1}{\beta} \quad \beta \rightarrow \infty \quad (3.31)$$

so that the degradation approaches  $\frac{2}{\pi}$  (2 dB).

In view of the present NASA requirements,  $\gamma$  must be close to 10 dB to achieve the necessary tracking accuracy. A hardlimiting system is, therefore, inadequate. In the next section, multi-bit systems will be considered.





-154-

Fig. 3.8 Degradation in dB.

### 3.6 Multibit Digital Processor

Since in the present application the compressor output at the 'jump' is the most important, the ratio  $\gamma$  as defined in Section 3.5 is the only quantity being considered in detail here. Generally, the compressor output will resemble that shown in Fig. 3.7 for 1 or 2-bit systems and will approach the ideal step function as more bits are added.

The equations needed are (3.14 and (3.16). They are evaluated numerically on a UNIVAC 1108 computer. The results are shown in Figs. 3.9 and 3.10 for one to five-bit\* processors. The  $K$  and  $N/C$  assumed in these computations are 1000 and 100 respectively so that a linear system will have a  $\gamma_{\text{Linear}} = 10$ . In these figures,  $\gamma$  is plotted as a function of the normalized threshold spacing  $a/\sqrt{C}$ . As seen, there is an optimum spacing for each of the five processors. Generally, the optimum is quite broad. The best that an  $M$ -bit system can obtain is shown in Table III.

TABLE III. Digital Processor Performance,  $\gamma$  ( $K = 1000$ ,  $N/C = 100$ )

HL	2.65
1-bit	5.40
2-bit	7.85
3-bit	9.11
4-bit	9.70
5-bit	9.92
Linear	10.0

---

\* Sign bit is extra.

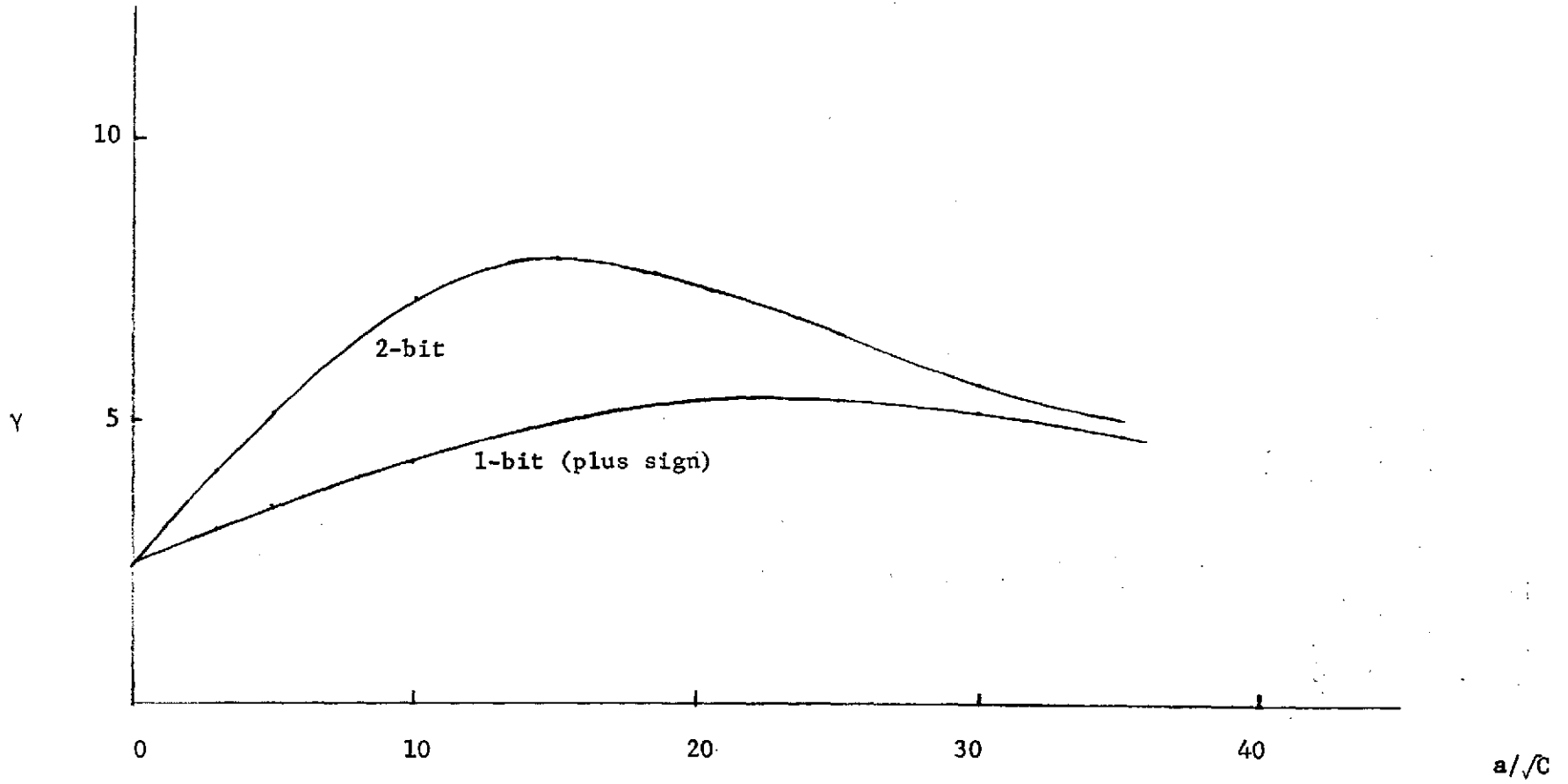


Fig. 3.9 Performance of 1- and 2-bit (plus sign) processor.

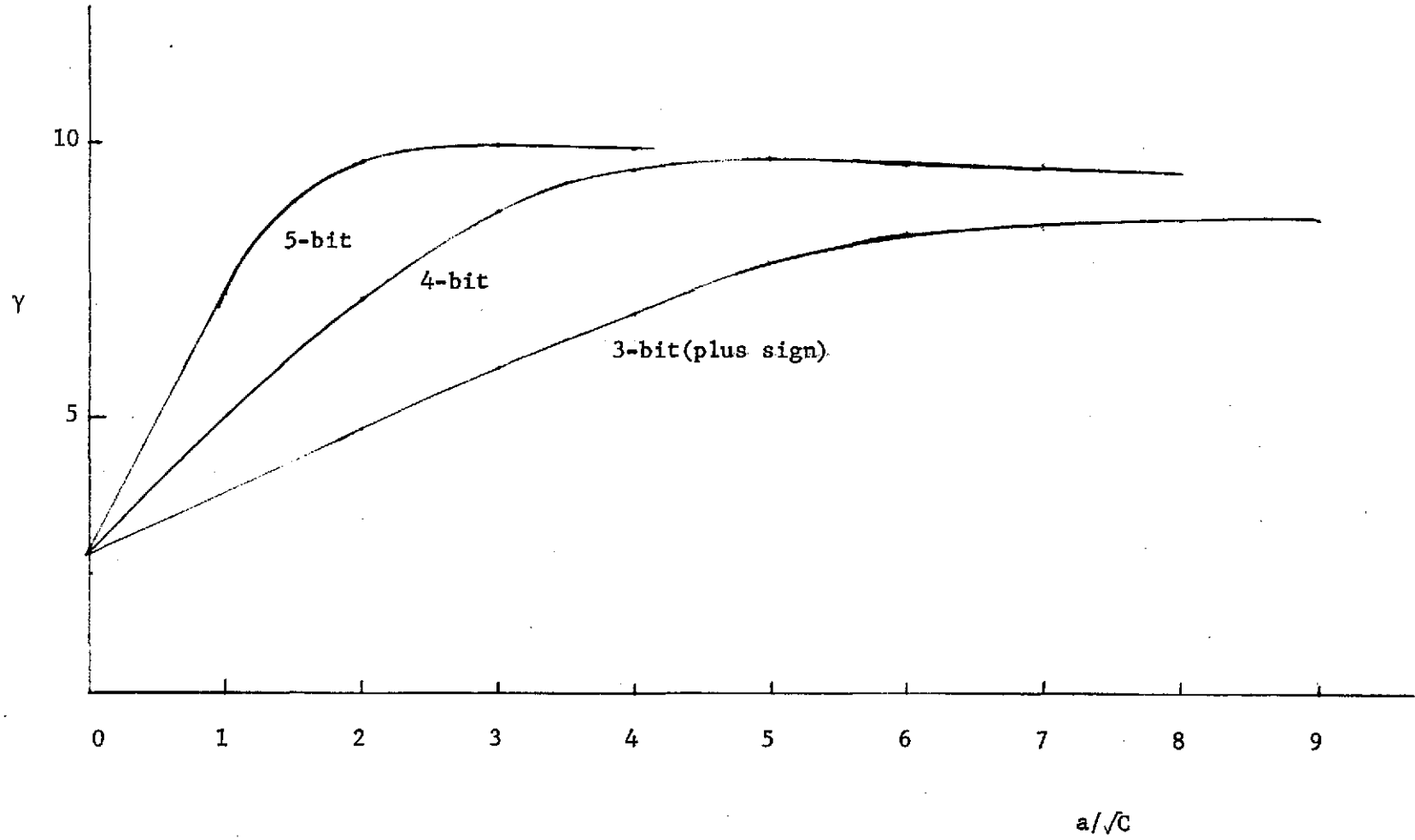


Fig. 3.10 Performance of 3, 4 and 5-bit processor.

It was shown in the previous sections that there is a significant loss (6 dB) associated with hard limiting processing. The model used to arrive at this result assumed that the altimeter - uncompressed return is pulse limited. In practice, the occurrence of this situation depends on the choices of pulse duration and antenna beam width. Very often, the system parameters are so chosen that the return is only partially pulse-limited. As a result, the system loss will depend on the pulse limiting factor  $\beta$  defined on the ratio of the number of range cells in a single pulse versus the number of range cells being illuminated by the antenna at the sea surface. For compression ratio  $K = 1000$  and noise-to-single cell return of 100, the loss as a function of  $\beta$  is plotted in Fig 3.11. As seen, the loss is above 5 dB when  $\beta$  is larger than .3. Thus, this new result does not affect previous conclusions significantly.

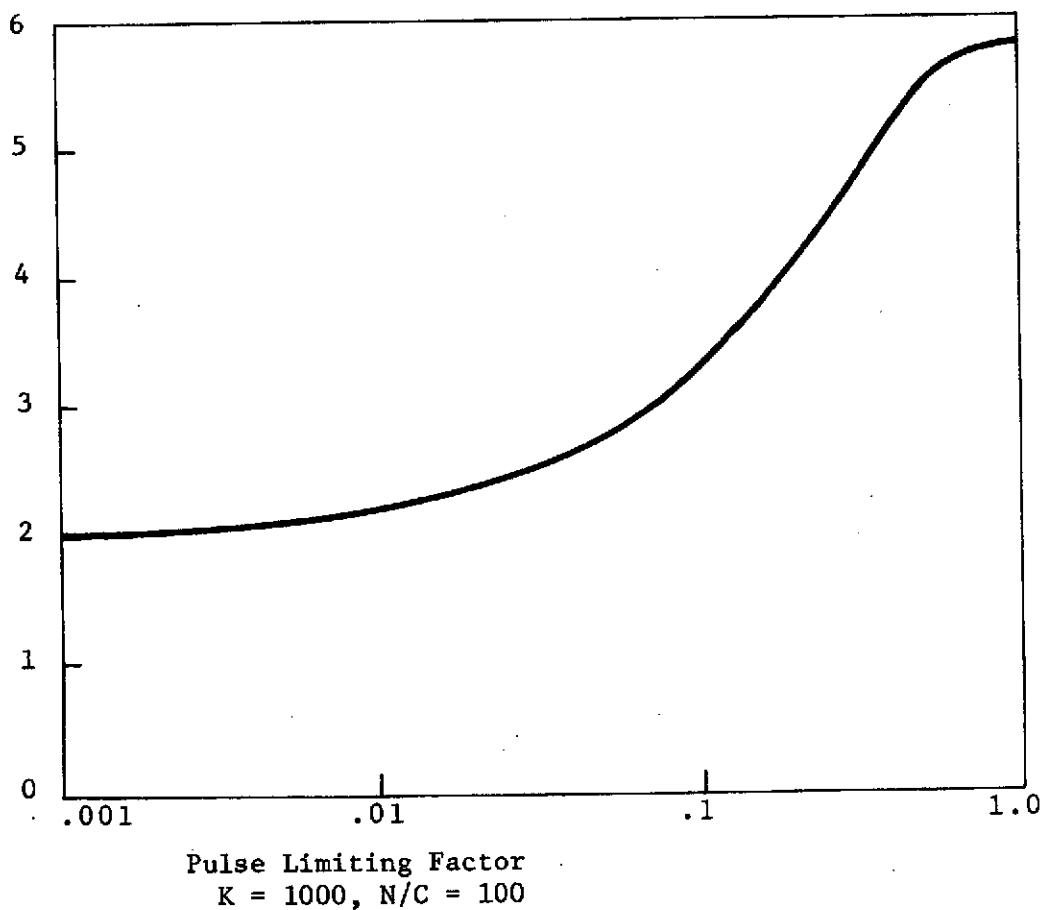


Fig. 3.11 Loss as a function of pulse limiting factor.

Based on these results a 2-bit (plus sign) digital processor seems adequate for the present application and the optimum threshold spacing is  $a/\sqrt{C} = 15$ . The compressor output power for the entire time interval of interest is shown in Fig. 3.12.

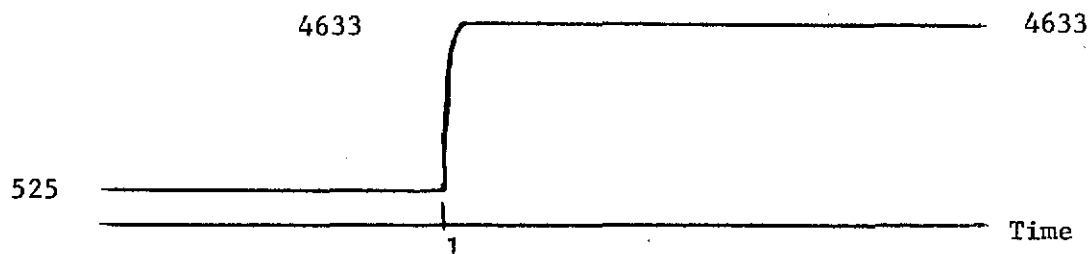


Fig. 3.12 Compressor output of a 2-bit (plus sign) digital processor ( $K = 1000$ ).

### 3.8 Conclusion

Analytical results have been obtained in this report to show that a hardlimiting digital processor operating on a phase-code signal is inadequate in the NASA altimeter and wave height measurement applications. It is shown that because of the distributive nature of the sea surface, the hardlimiting processor output signal-to-noise is bounded at a low value regardless of the compression ratio  $K$  or the return echo-power-to-noise ratio as long as  $K$  is much larger than unity. In the example shown, the output signal-to-noise ratio is only 4.1 dB for  $K = 1000$  and  $C/N = -20$  dB. This is insufficient to maintain the required tracking accuracy.

It is also shown in this report that the digital processor performance improves as the quantization error is reduced. A 2-bit-plus-sign processor seems to be adequate when the threshold spacings are properly set. However,

at the speed of the intended operation and in a satellite environment, there is much risk involved in implementing such a complicated digital processor. The cost, as compared to a linear FM system, is also likely to be much greater.

#### References

- [1] W. B. Davenport and W. L. Root, An Introduction to The Theory of Random Signals and Noise, McGraw-Hill, N.Y., Chapter 13, 1958.
- [2] A. I. Velichkin, "Correlation Function and Spectral Density of a Quantized Process", Telecommunications and Radio Engineering, Part II: Radio Engineering, July 1962, pp 70-77.

## 4.0

COMPARISON OF SEA SURFACE CROSS SECTION MEASUREMENTS AT NORMAL  
INCIDENCE WITH BARRICK'S MODEL

In this appendix, Barrick's model for the normalized sea cross-section is compared with several sets of experimental results. It is found that his model predicts values for the cross-section per unit area which are somewhat higher than the measured values and suggests that reducing Barrick's model by about 6 dB would give a more conservative model.

Barrick [1], [2] gives the cross section per unit area of the sea as:

$$\sigma^0 = \frac{\sec^4 \gamma}{S^2} \left( \exp \left[ \frac{-\tan^2 \gamma}{S^2} \right] \right) \quad (4.1)$$

where

$\gamma$  is the angle of incidence (i.e. angle from vertical)

and

$S$  is the rms sea slope.

Barrick relates the rms sea slope to wind velocity and wave height by:

$$S^2 = 5.5 \times 10^{-3} V \text{ and } \sigma_h^2 = 2.55 \times 10^{-4} V^4 \quad (4.2)$$

where  $V$  is in m/sec. Barrick's model is based on specular scattering, and thus has no frequency dependence. At normal incidence e.g.(4.1 gives:

$$\begin{aligned} \sigma^0(\text{dB}) &= 22.6 - 10 \log V(\text{m/sec}) \\ &= 19.4 - 10 \log V(\text{kt}) \end{aligned} \quad (4.3)$$

or

$$\sigma^0(\text{dB}) = 13.6 - 5 \log \sigma_h \text{ (m)} \quad (4.4)$$



In Figs. 4.1 - 4.6, equation (4.3 is compared with experimental measurements as reported by several references. In Figs. 4.2 - 4.4, the median cross-section was reported. For those figures, eq. (4.3 is reduced by 1.59 dB. This corresponds to the mean-to-median ratio for Rayleigh clutter.

Three comments seem appropriate to Figs. 4.1 - 4.6.

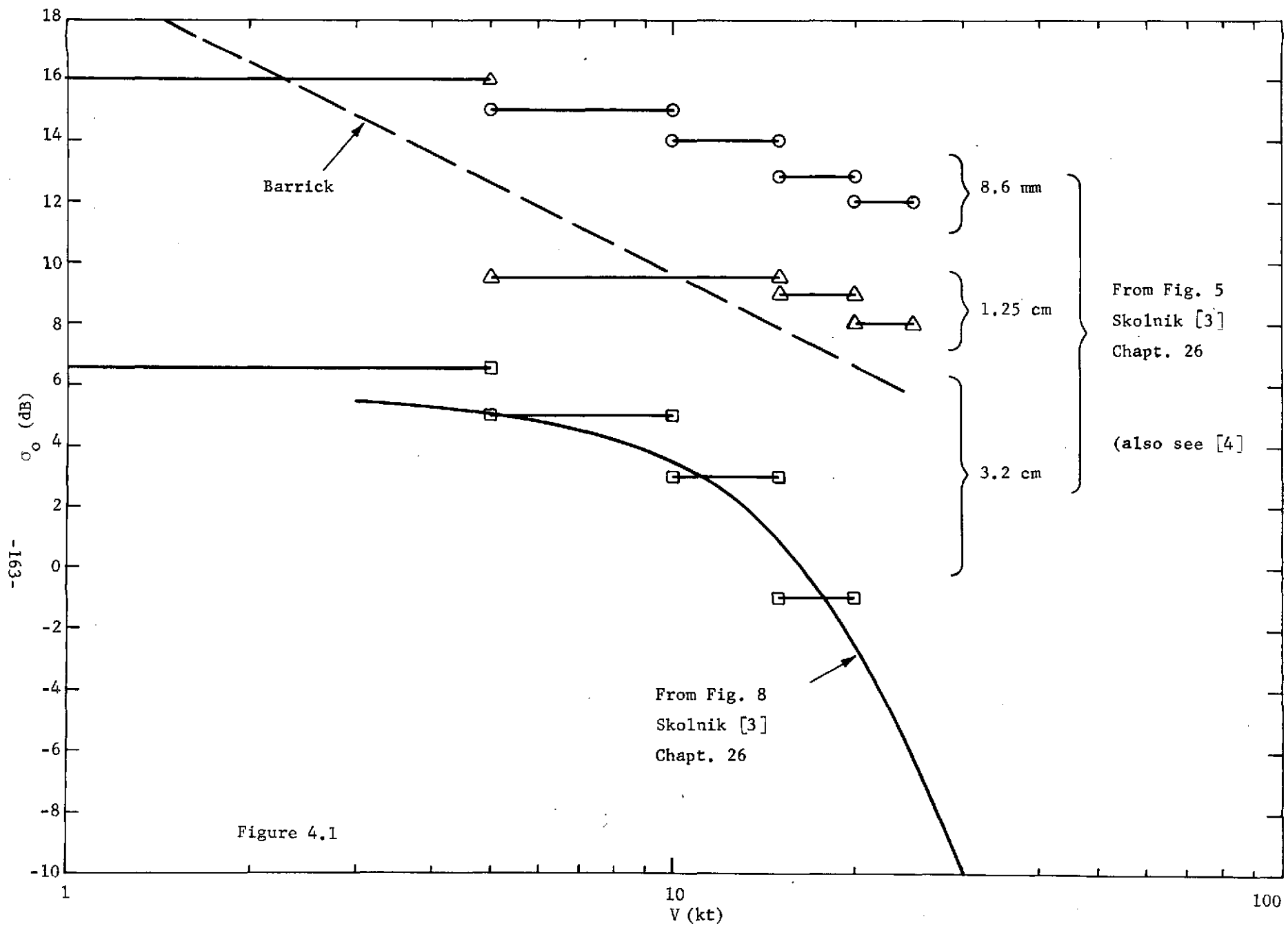
- a) There is a large scatter to the experimental data which is probably not entirely due to experimental error. (e.g. reduction of the measured values due to finite beam width).
- b) There appears to be a trend towards reduced cross-section at higher wind speeds. Further, Barrick's model reflects this trend moderately well.
- c) Barrick's model seems to be somewhat optimistic, particularly when compared to the NRL data on Figs. 4.2 - 4.4.

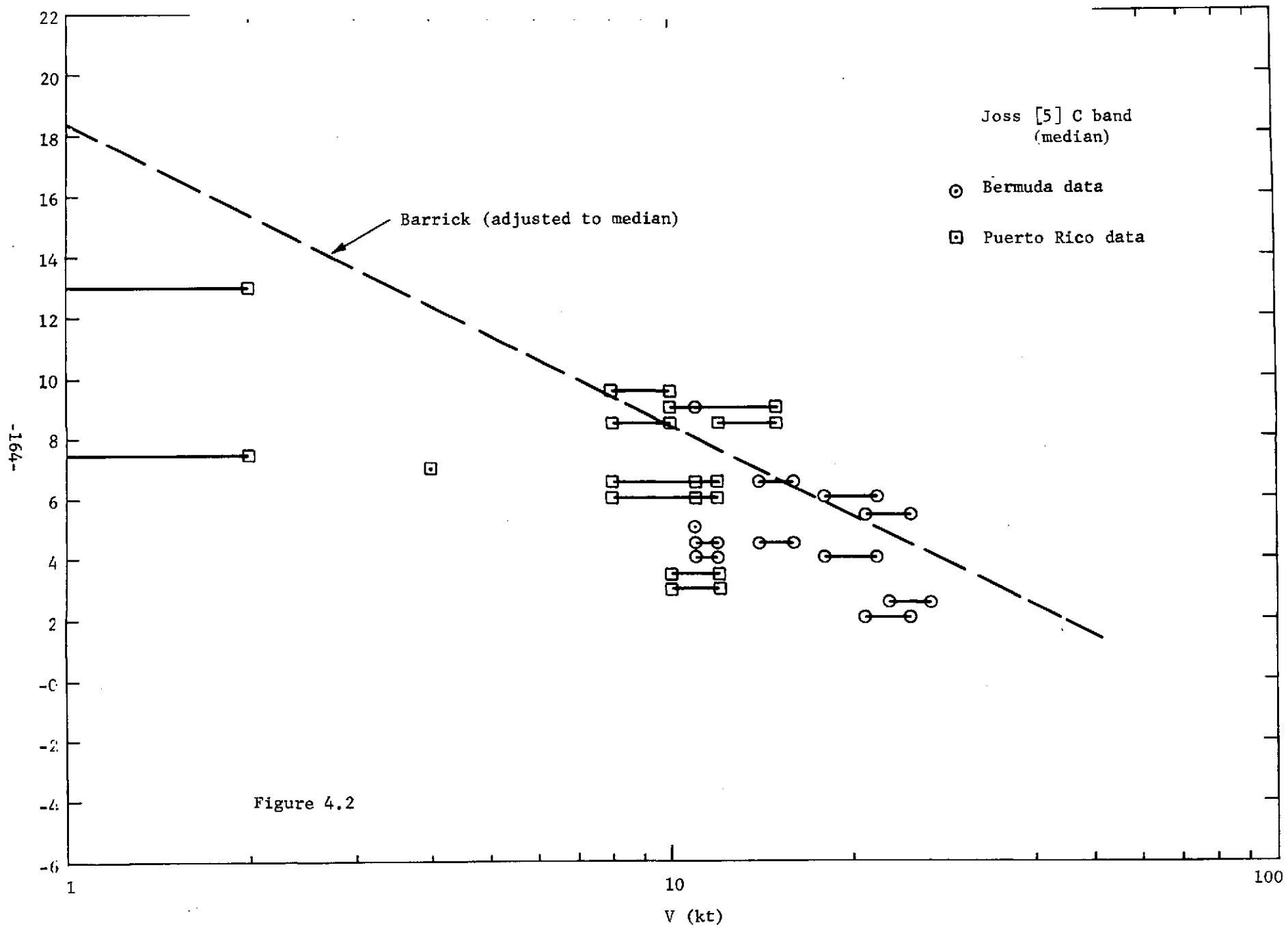
These comments suggest that Barrick's model 4.3 can be taken as a relative optimistic prediction of the mean cross-section at normal incidence.

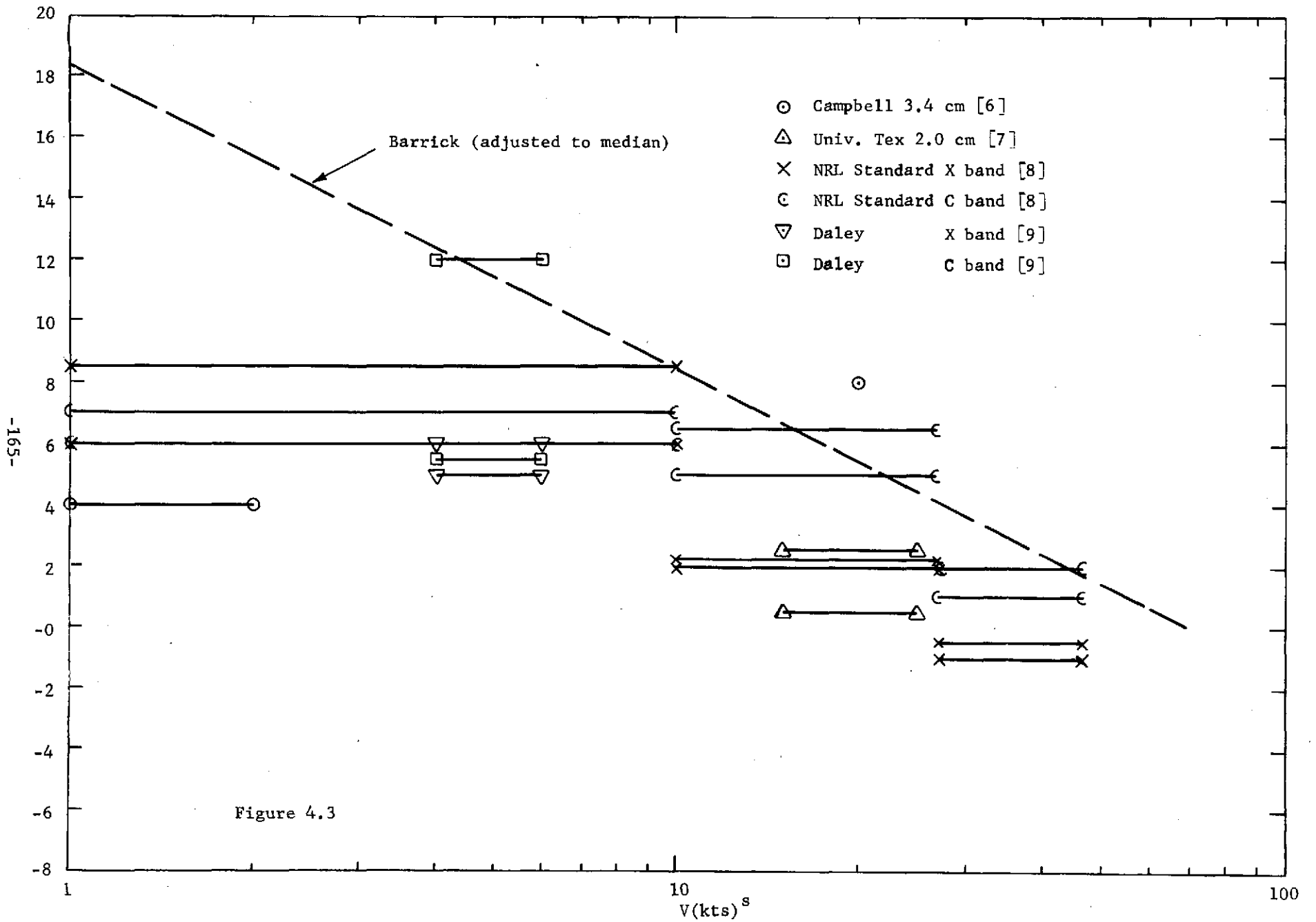
$$\begin{aligned}\sigma^0(\text{dB}) &= 16.6 - 10 \log V \text{ (m/sec)} \\ &= 7.6 - 5 \log \sigma_h \text{ (m)}\end{aligned}$$

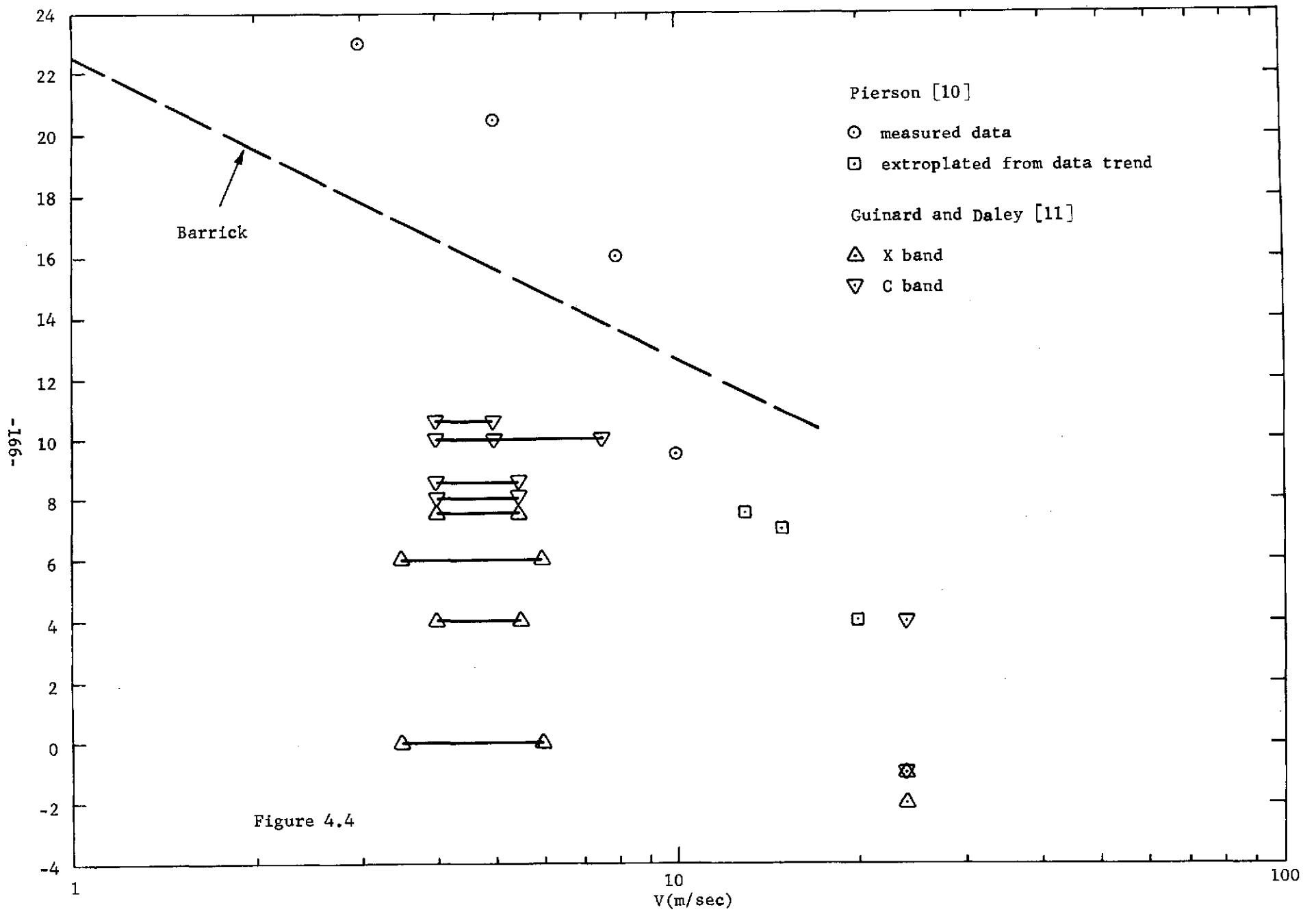
might represent a more conservative estimate.

The scatter of the data strongly suggests that any proposed altimeter design should not be severely degraded by even a 10 to 15 dB reduction of  $\sigma^0$  relative to Barrick's model.

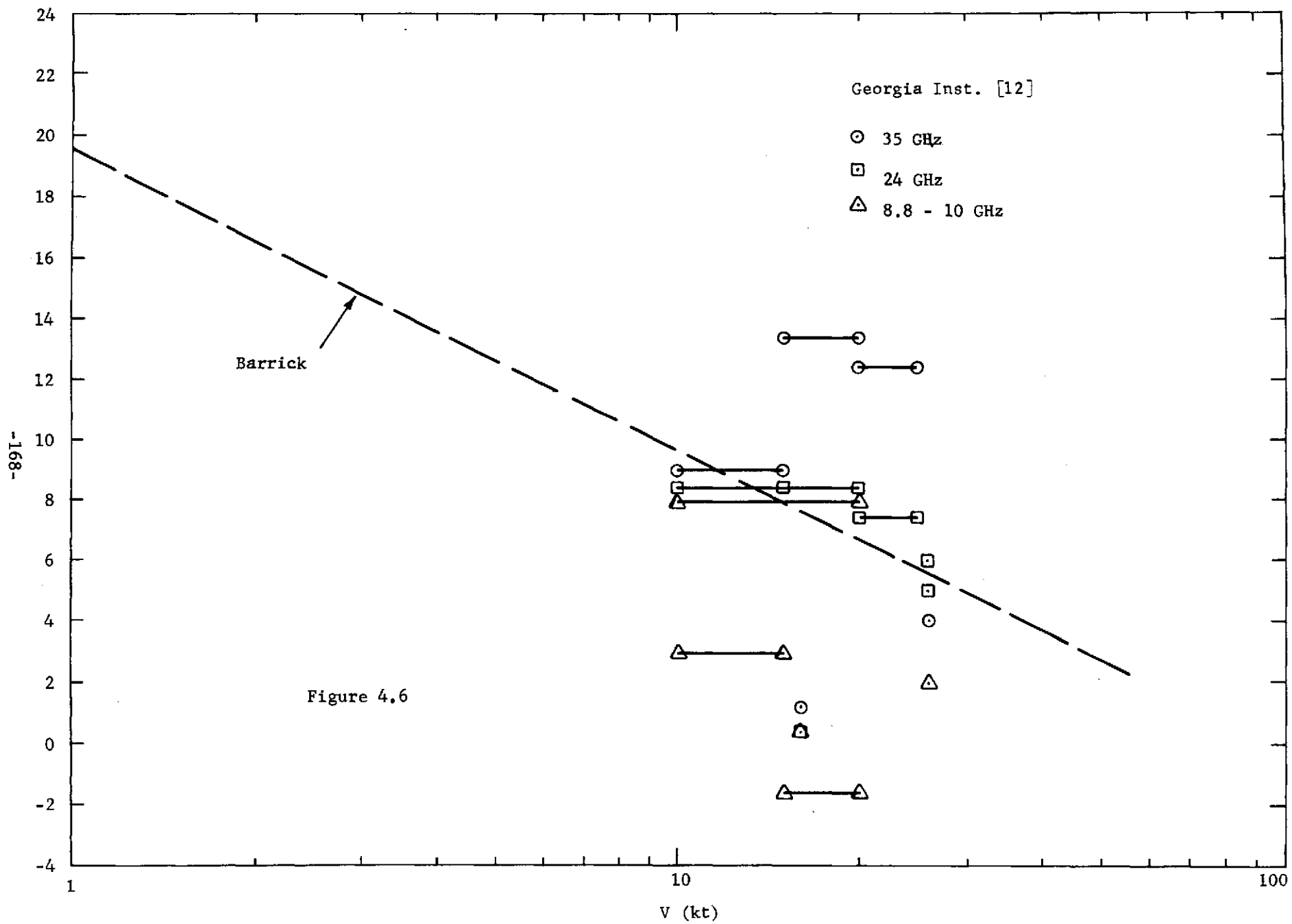












#### 4.1 Effect on Tracker Performance

To determine the effect of sea state and the model used on tracking accuracy, the performance of several split-gate trackers was computed. The results are given versus sea state for Barrick's model, and for Barrick's model minus 6 dB. To make the comparison, a signal-to-noise ratio at some value of  $\sigma^0$  (cross-section) had to be assumed. A design point of S/N = 10 dB at  $\sigma^0 = 6$  dB was used. The results are given in Figure 4.7.

As was expected, the tracking accuracy is affected by the reflectivity model used, however, the effect is not severe. There is about 30% degradation between results using Barrick's model, and results using the more conservative model. As a point of reference, for a significant wave height of 10 m, Barrick's model gives  $\sigma^0 = 11.6$  dB, while the conservative estimate gives  $\sigma^0 = 5.6$  dB. Recall that the design value is  $\sigma^0 = 6$  dB at a 10 meter wave height; thus the conservative model is being used in the altimeter design.

It is interesting to note that if the tracking accuracy is normalized to significant wave height, the results are almost independent of wave height above 3 m. Thus the signal loss at the higher sea states is not significantly affecting the tracking accuracy. The most important effect is simply that the leading edge of the return becomes less distinct at high sea states.



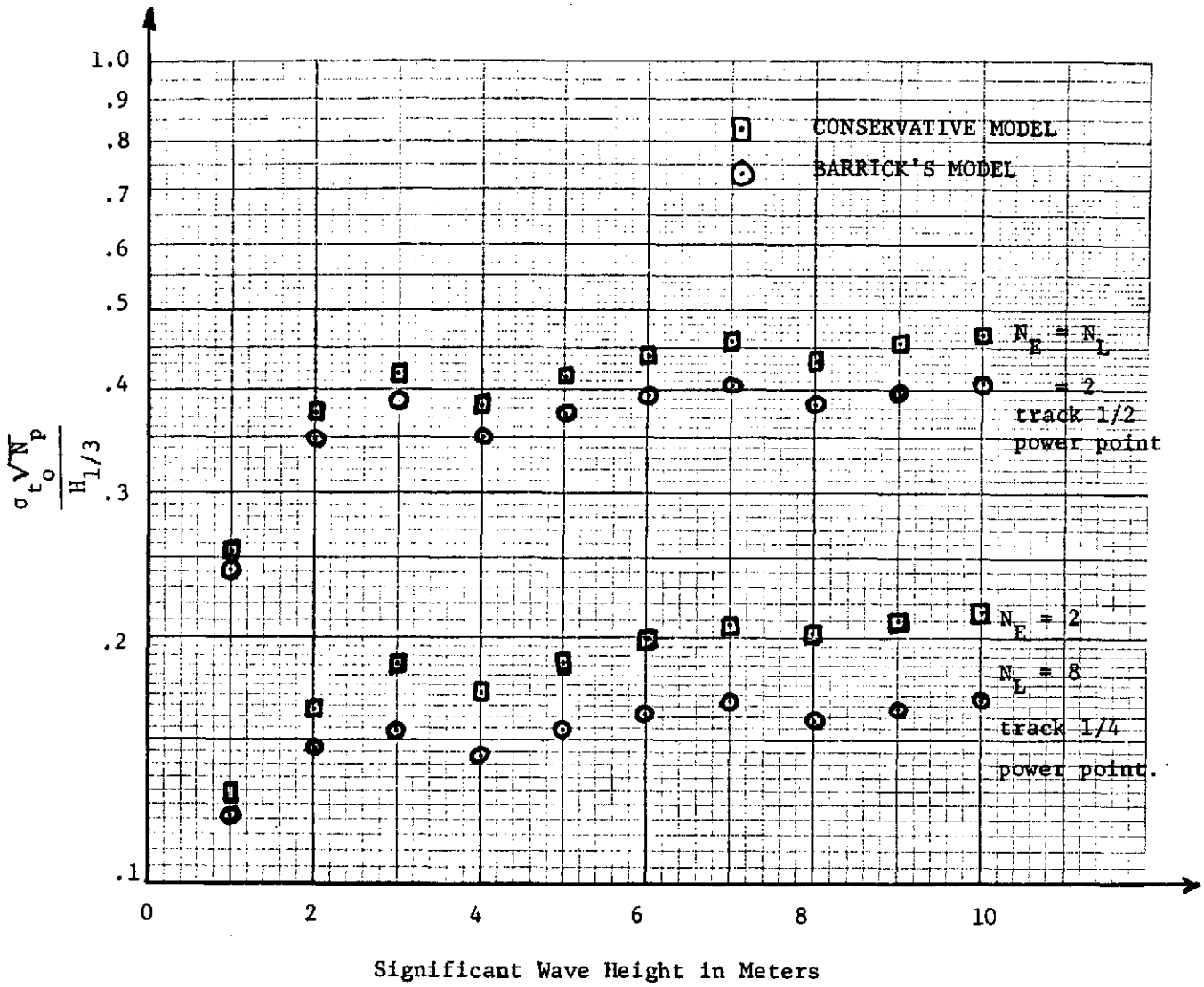


FIGURE 4.7

Comparison of Tracker Performance versus Wave Height for Two Sea Reflectivity Models\*

\*Note: These numbers are normalized to significant wave height rather than the ramp width. ( $H_{1/3} = 1.29 (CT/2)$ ). Further, they do not include the effect of correlation between samples.

References:

- [1] Barrick, D. E. "Determination of Mean Surface Position and Sea State from the Radar Return of a Short-Pulse Satellite Altimeter." Chapter III paper #16, NOAA Technical Report ERL 228-AOML 7 "Sea Surface Topography from Space" Vol. I, J. R. Apel Ed., October 1971
- [2] Barrick, D. E. "Rough Surface Scattering Based on the Specular Point Theory" IEEE Trans. on Antennas and Prop. Vol. AP-16, July 1968, pp. 449-454
- [3] Skolnik, M. I. "Sea Echo" Chapt. 26 of Radar Handbook, M. I. Skolnik Ed. McGraw Hill, N. Y. 1970
- [4] Grant, C. R. and B. S. Yaplee "Back Scattering from Water and Land at Centimeter and Millimeter Wavelengths." Proc. IRE, Vol. 45, pp. 972-982, July 1957
- [5] Daley, J. C., J. T. Ransone, J. A. Burkett, "Radar Sea Return-JOSS I" NRL Report 7268, Naval Research Laboratory, Wash. D. C., May 11, 1971
- [6] Campbell, J. P. "Back Scattering Characteristics of Land and Sea at X-Band" Aeronautical Electronics 1958 National Conference Proc., Dayton, Ohio, May 12-14, 1958
- [7] University of Texas Defense Research Laboratory Report dated 3-21-68
- [8] Daley, J. C., W. T. Davis and N. R. Miles "Sea Return Standard" NRL Memo Report 2066, Naval Research Laboratory, Wash. D. C., Nov. 21, 1969
- [9] Daley, J. C. "Airborne Radar Back Scatter Study at Four Frequencies" NRL memo 5270-20A:JCD:big. NRL Prob. R02-57, Ser 8560, Aug. 23, 1966.
- [10] Pierson New York University June 1967, (See F. E. Nathanson TSC-WO-31, 6 July 1971)
- [11] Guinard, N. W. and J. C. Daley "An Experimental Study of a Sea Clutter Model" Proc. IEEE Vol. 58 No. 4, April 1970 pp. 543-550
- [12] Long, M. W., R. D. Wetherington, J. L. Edwards, A. B. Abeling "Wavelength Dependence of Sea Echo", Final Report Proj. No. A-840, Engin. Exp. Sta. Georgia Inst. Tech., Atlanta, Ga., July 15, 1965

Since the system design was based on orbital parameters and whereas the breadboard unit will actually be tested using an aircraft, it is necessary to modify the selected set of system parameters given in Part I. This section describes the required changes in the system parameters for an aircraft mounted altimeter. It is shown that the reduction in height and velocity from a satellite to an aircraft requires an increase in antenna beamwidth from  $3^{\circ}$  to  $15^{\circ}$  and a reduction in peak power from 2 kw to 1.0 watts. A reduction in the maximum spatial frequency (associated with the Gulf Stream) to .007 Hz enables the tracker bandwidth to be reduced to about .06 Hz. In order to check the validity of the predicted altimeter performance (and for investigative purposes) it is suggested that some of the system parameters be made variable over a range of values. Specifically, a recommended range of values are given for tracking gate widths, compression ratio and pulse length, PRF and bandwidth.

It would be desirable to study, with the aircraft-mounted altimeter, the altitude measurement accuracy and how it is affected by changes in:

1. Tracking gate widths;  
Early gate: 1-8 resolution cells  
Late gate: 1-16 resolution cells
2. Compressed pulse length: 3.0 nsec to 10 nsec
3. PRF: vary from half to twice the inverse decorrelation time
4. Number of uncorrelated pulses averaged by the loop filter

These test objectives require modifications to the orbital values of system parameters as shown in Table 5.0-1 and described in the following sections.

#### 5.1 Beam Width and Tracker Gate Widths

A minimum of 24 resolution cells must be contained within the return beam-limited pulse length,  $t_B$ , in order to test the suggested ranges of gate widths. At the maximum compressed pulse width of 10 nsec, this requires a 240 nsec surface return pulse length. This pulse length is given by

$$t_B = \frac{2h}{c} \left[ \frac{1}{\cos(\theta_B/2)} \right]^{-1}$$

where  $h$  is altitude,  $c$  is speed of light, and  $\theta_B$  is 3 dB beamwidth of the altimeter dish. At an aircraft altitude of 3048 m, a beamwidth of  $17.5^\circ$  is necessary for a 240 nanosecond  $t_B$ . This is in contrast to the satellite case, in which a  $3^\circ$  beamwidth at an altitude of 556 km provides a  $t_B$  of 1.2  $\mu$ sec. Thus the antenna beam must be opened up for the aircraft altimeter, in order to approximate the duration of the satellite sea surface return.

Table 5.0-1 System Parameters (Aircraft Mounted Altimeter)

I.	Radar Parameters	
	Antenna Beamwidth	15°
	Pointing Accuracy	$\sigma_{\theta} = 2.5^{\circ}$
	Antenna Gain	Peak 20.9 dB
		Average 20.25 dB
	Peak Power	200 mw (min) (use 1 watt TWT)
	System losses (other than processing losses in pulse compressor)	5 dB
	Noise Figure	5.5 dB
	Frequency	13.9 GHz
	* Pulse Compression Processing Loss	.55 dB
	* Main Lobe Broadening Due to Tapering	23%
	* Compressed Pulse Length (after tapering)	3 to 10 nsec
	Tracker Bandwidth	$\geq .06$ Hz
	PRF	100 to 1000 Hz
	Number of Samples to be Integrated by Tracker	700 to 3400
	Single Pulse SNR	10 dB
	Compression Ratio	1000 to 100**
	Bandwidth	360 MHz to 120 MHz**
	Uncompressed Pulse Length	2.8 $\mu$ sec to .9 $\mu$ sec**
II.	Ocean Cross-Section	$\sigma^{\circ} = +6$ dB
III.	Maximum Spatial Frequency	SF = .007 Hz
IV.	Aircraft Parameters	
	Height	3.0 km
	Velocity	71 m/sec (140 knots)

\* Modified Taylor weighting, -25 dB peak sidelobe, to be switched in or out.

\*\* Variable compression ratio, bandwidth, and uncompressed pulse length to be obtained by generating maximum linear FM waveform and gating out desired segment.

It should be noted that, at the lowest sea states, the surface shaping function will limit the effective beamwidth to less than  $17.5^\circ$ , so that the full 24 resolution cells will not be available in the aircraft test for all sea states. Consequently, a  $15^\circ$  beam is suggested for use in the aircraft version. The surface shaping function limitations are summarized in Table 5.1-1.

TABLE 5.1-1

SURFACE SHAPING FUNCTION LIMITATIONS

Wind Speed (knots)	Effective 3dB Beamwidth	Surface-Shaping-Limited Pulse Duration at 10,000' (nsec)
7	$13.5^\circ$	140
10	$16.1^\circ$	200
14	$19^\circ$	280
19	$22^\circ$	380
22	$24^\circ$	450

5.2 Compressed Pulse Length

For a surface wave device pulse compressor, the compressed pulse length could be varied by interchanging surface wave devices of differing bandwidths. A simpler and more economical technique, for a linear FM waveform, would be simply to gate out a portion of the transmit pulse, thereby decreasing the dispersion and bandwidth proportionally. This technique has the further advantage of keeping the single pulse signal-to-noise ratio at the pulse compressor output constant as bandwidth is changed. The required compression ratio (CR req'd) for a given signal-to-noise ratio is

$$CR_{req'd} = \frac{K}{\tau_c} = KB^2$$

where  $\tau_c$  is compressed pulse length, B is waveform bandwidth. Thus, as B is varied, a constant signal-to-noise ratio is maintained if CR is varied as  $B^2$ . This variation of CR is realized if the dispersion (uncompressed pulse length) is varied proportional to B, since  $CR = BT$ .

### 5.3 PRF

As a result of the decrease in altimeter velocity, the decorrelation time of the surface return has increased significantly. For a 3.0 nsec compressed pulse, the decorrelation time for a 140 knot aircraft is 4.8 msec<sup>\*</sup>, compared to .6 msec for the same pulse length in a satellite. Thus the decorrelation-limited PRF is about 200 Hz at this pulse length whereas at a 10 nsec pulse length, the decorrelation-limited PRF is 360 Hz. The PRF should therefore be variable from 100 to 1000 Hz, to cover a range of half to twice the inverse decorrelation time at all pulse lengths.

### 5.4 Pulse Averaged by Loop Filter

The number of pulses averaged by the tracking loop filter is roughly the ratio of the PRF to the loop bandwidth. Thus, provision should be made to vary this ratio, as well as the PRF.

### 5.5 Peak Transmitter Power

Even with a 15° beamwidth, the power in the surface return would be 40 dB higher than that for the satellite altimeter with a 3° beam. This is because of the large difference in altitudes, since the return signal strength from the pulse-limited footprint varies as one over the cube of the altitude. Consequently, a savings can be realized in the aircraft breadboard model by eliminating the final TWT in the transmitter and using a 1 watt TWT.

---

\* Wave spray may decrease this number to about 1.8 msec.